Drosophila adipose tissue displays an apicobasal cell polarity and undergoes an epithelial-to-amoeboid transition driving cell dispersal by swimming migration

Jameela Almasoud

A thesis submitted in fulfilment for the degree of Doctor of Philosophy

February 2025

Department of Cell and Developmental Biology

University College London

Declarations

I, Jameela Almasoud, confirm that the work presented in my thesis is my own. Where information has been derived from other sources, I confirm that this has been indicated in the thesis.

UCL Research Paper Declaration Form

referencing the doctoral candidate's own published work(s)

Please use this form to declare if parts of your thesis are already available in another format, e.g. if data, text, or figures:

- *have been uploaded to a preprint server*
- *are in submission to a peer-reviewed publication*
- *have been published in a peer-reviewed publication, e.g. journal, textbook.*

This form should be completed as many times as necessary. For instance, if you have seven thesis chapters, two of which containing material that has already been published, you would complete this form twice.

1. **For a research manuscript that has already been published** (if not yet published, please skip to section 2)

2. **For a research manuscript prepared for publication but that has not yet been published** (if already published, please skip to section 3)

What is the current title of the manuscript?

Apicobasal polarity in the *Drosophila* adipose tissue regulates collagen IV-mediated cell-cell adhesion which gets dissolved during Ecdysone-induced tissue remodelling

a) **Has the manuscript been uploaded to a preprint server?** (e.g. medRxiv; if 'Yes', please give a link or doi)
No

b) **Where is the work intended to be published?** (e.g. journal names)
JCB

c) **List the manuscript's authors in the intended authorship order**

Jameela Almasoud, Cyril Andrieu, Bren Hunyi Lee and Anna Franz

d) **Stage of publication (e.g. in submission)**

Manuscript in preparation with plans to post it on

BioRxiv and submit it to JCB in March 2025

3. **For multi-authored work, please give a statement of contribution covering all authors** (if single-author, please skip to section 4)

In which chapter(s) of your thesis can this material be found?

Jameela Almasoud planned and performed all the experiments and analysis in all chapters. Cyril Andrieu performed a separate experiment and analysis of *in vivo* live imaging of fat body remodeling which is not included in this thesis but which will be included in the publication. Bren Hunyi Lee prepared one fly line used in Chapter VI to study CIVICs when polarity proteins are knocked down. The project was conceptualized and supervised by Anna Franz. Both Jameela Almasoud and Anna Franz wrote the manuscript.

4. **e-Signatures confirming that the information above is accurate** (this form should be co-signed by the supervisor/ senior author unless this is not appropriate, e.g. if the paper was a single-author work)

Candidate

Date:

27/02/2025

Supervisor/ Senior Author (where appropriate)

Anna Franz

Date

27/02/2025

Abstract

The *Drosophila* adipose tissue, called the fat body, plays diverse roles in development including in energy storage, growth regulation, immune responses and wound healing. During embryonic and larval stages, the fat body exists as a flat, single-layered sheet that is surrounded by a basement membrane. As development progresses into the pupal stage, the fat body undergoes fat body remodeling, where fat body cells dissociate from neighboring cells and detach from the basement membrane to initiate amoeboid swimming cell migration. We hypothesize that fat body remodeling is similar to an epithelial-to-mesenchymal/amoeboid transition (EMT/EAT), a process essential for development and cancer metastasis. However, unlike epithelia, the fat body was not previously recognized to exhibit apicobasal polarity, a requisite for EMT.

Surprisingly, my findings revealed that larval fat body cells display apicobasal polarity prior to fat body remodeling, despite being ensheathed by basement membrane. This polarity is shown to be essential for maintaining tissue integrity and supporting Collagen IV mediated cell-cell adhesion. This polarity is lost as remodeling begins. I show that GATA transcription factor, Serpent and Ecdysone signaling are critical regulators of polarity loss, as well as, dissociation of fat body cells and the initiation of swimming migration.

Overall, my study reveals apicobasal polarity as a defining feature of the larval fat body cell, contributing to tissue integrity mediated via an unusual type of Collagen IV-mediated cell-cell adhesion. During metamorphosis, fat body remodeling represents an EMT/EAT-like transition, driven by Ecdysone signaling and Serpent, transforming the fat body tissue from a continuous sheet to individual migrating fat body cells that disperse throughout the pupal body.

Impact statement

My research reveals the unexpected presence of apicobasal cell polarity in the *Drosophila* larval fat body, contradicting the long term thought that *Drosophila* fat body cells lack polarity due to their non-epithelial nature and their unique architecture of having a basement membrane underlying both cell surfaces. This discovery redefines our understanding on *Drosophila* larval fat body structure and function. In this study I demonstrated a role of fat body cell polarity in maintaining tissue integrity by regulating an unusual form of cell-cell adhesion mediated by Collagen IV Intercellular Adhesion Concentrations which may be conserved in other tissues. I showed that similar to EMT, fat body cell polarity is lost early during the process of fat body remodeling. Upon closer examination, my findings suggest that fat body remodeling is mediated by Ecdysone signaling and the GATA transcription factor Serpent, eventually leading to cell-cell dissociation and amoeboid cell migration.

These findings describe fat body remodeling as a process similar to epithelial-to-mesenchymal/amoeboid transition EMT/EAT, with insights into how loss of polarity drives tissue remodeling resulting in dissociated cells with migratory properties. By using a screening assay to screen for key regulators of fat body remodeling, my research establishes a framework for exploring the mechanisms underlying loss of cell-cell adhesion and initiation of cell migration in fat body remodeling. Overall, my findings highlight similarities of fat body remodeling to EMT, thus establishing FBR as a novel model to study EMT/EAT-like transition and tissue remodeling, laying the foundation for future research on cell adhesion, cell migration and potential therapeutic interventions.

Acknowledgment

This PhD journey has been one of the most challenging yet rewarding experience of my life. I am also incredibly proud of the person I have grown up to become in the past four years, as each obstacle has shaped me into the resilient and determined individual, I am today.

I begin by expressing my deepest gratitude to the United Arab Emirates and to His Highness Sheikh Mohammed bin Zayed Al Nahyan, whose visionary leadership and unwavering commitment to education, science, and innovation continue to inspire and empower Emirati youth to pursue excellence and contribute meaningfully to the global scientific community.

First and foremost, I extend my heartfelt gratitude to my Family, with a special appreciation to my mother, Fatima Aldossari, for her unconditional support and belief in me. I am immensely thankful to my father Mr. Mohammed Almasoud, for being my sponsor and my major supporter and for making this journey possible. To my beloved siblings (Dr. Shouq, Eng. Abdulaziz, and Abdulla Almasoud), thank you for your endless love and patience throughout this journey. To my family, your encouragement has been my source of strength during the most challenging times.

I extend my sincere appreciation to my supervisor Dr. Anna Franz for her invaluable guidance and insightful discussions that helped shape my research and academic growth. I would also like to sincerely thank my secondary supervisor, Prof. Yanlan Mao for her expertise that have helped navigate the complexities of my research and my postgraduate tutor Prof. Susan Evans, for her constant advice throughout my PhD journey. To my lab colleagues, Cyril, Ioanna, Bren and Rouxu thank you for your camaraderie throughout this journey.

A special thank you goes to Mahum Shaikh, who’s presence and support have been my anchor through all the ups and downs. Her constant reassurance and companionship have made all the difference. I am truly grateful to have had her by my side the past 4 years.

From the bottom of my heart, thank you to all my dear friends, especially Mariam Al Zarooni, for being a part of this journey. Your encouragement means the world and I am forever grateful.

Table of Contents

List of Figures

Chapter I. Introduction

1.1. Tissue remodeling

1.1.1. Overview of tissue remodeling

Biological cells, tissues, organs and organisms undergo constant remodeling to preserve their architecture during growth, both in normal physiological conditions and in response to diseases by changing their internal structure (Lange & Ramirez, 2021). This in turn, enables adaptation to changes in external stimuli in order to mediate response to diseases, injuries or even therapeutic interventions, which highly depends on mechanical factors and biological responses at the cellular level (Ambrosi et al., 2019). Tissue remodeling involves the reorganization and reorientation of existing tissues and can be categorized as either physiological or pathological tissue remodeling (Pinet & McLaughlin, 2019). The natural endogenous process that is essential for normal development, growth, and maintenance of tissues, organs and the overall organism is referred to as physiological tissue remodeling (Bonnans et al., 2014; Pinet & McLaughlin, 2019). For instance, metamorphosis in *Xenopus laevis* involves craniofacial tissues such as cartilage, bone, nerves and muscles to undergo remodeling, resulting in morphological changes like repositioning the eyes from lateral to a dorsal forward-facing position (Figure 1.1). Similarly, *Drosophila melanogaster* is also required to undergo tissue remodeling during metamorphosis to transform the larvae into an adult with features such as the eyes, antennae and mouth (Figure 1.1) (Pinet & McLaughlin, 2019).

Xenopus laevis

Drosophila melanogaster

Figure 1.1: Tissue remodeling alters head morphology during maturation.

During metamorphosis in *Xenopus laevis*, the cartilage, bone muscle and nerve tissue within the craniofacial region undergoes remodeling and leads to morphological changes such as repositioning of the eyes from a lateral position to a dorsal forward-facing position, reformation of the jaw, structural changes of the brain, etc. During metamorphosis in *Drosophila melanogaster*, tissue breakdown, growth and remodeling transforms the larvae into an adult fly with sensory features such as (antennae, mouse and compound eyes). Adapted from Pinet & McLaughlin, 2019.

Pathological tissue remodeling, on the other hand, is described as the uncontrolled remodeling that is caused by congenital defects and pathological processes like tissue fibrosis and cancer (Lu et al., 2011). The process of tissue remodeling generally involves the controlled remodeling of the extracellular matrix (ECM), that is present in all tissues such as the lungs, intestines, etc. (Bonnans et al., 2014). The ECM is a three-dimensional, non-cellular structure that is essential for life since it provides the supporting framework that holds cells together (Bonnans et al., 2014). Additionally, it plays a key role in initiating the crucial biochemical and biomechanical signals necessary for tissue differentiation, morphogenesis and homeostasis (Frantz et al., 2010). During embryonic development and organ homeostasis, the ECM is tightly controlled (J. Huang et al., 2021). However, in case of diseases like cancer, the ECM is frequently deregulated and becomes disorganized. The abnormal architecture of the ECM in diseases like cancer, can directly affect the disease progression by stimulating cellular transformations and metastasis (Lu et al., 2012).

1.2 Overview of EMT

Epithelial to mesenchymal transition (EMT) is a subtype of tissue remodeling. At the cellular level, EMT is described as a process that converts epithelial cells into mesenchymal cells with migratory and invasive properties (Kalluri & Weinberg, 2009; Nistico et al., 2012). Classically, EMT has been described as a binary decision, involving the transition of a complete epithelial state to a complete mesenchymal state (Campbell, 2018). EMT is a process that is known to be vital for embryogenesis, wound healing and malignant progression (Kalluri & Weinberg, 2009; Nieto, 2009; Thiery et al., 2009). According to the classic definition of EMT, cells that form the epithelial sheets in tissues exhibit apico-basal polarity and are interconnected by cell-cell

junctions, as shown in Figure 1.2 (Campbell, 2018). Although it is possible for some cells to undergo rearrangement, movement of epithelial cells are controlled by the confines of the epithelial sheet (Nistico et al., 2012). The function and integrity of epithelial cells depends on intercellular junctions (Chanson et al., 2011; LaBarge et al., 2009; Perez-Moreno & Fuchs, 2006). The main intercellular junction in the epithelial tissue includes E-cadherin (Figure 1.2), which is a transmembrane molecule that connects neighboring cells extracellularly, and β-catenin, that connects E-cadherin to the actin cytoskeleton intracellularly at adherens junctions. Controlled regulation of E-cadherin and β-catenin is vital for the epithelial phenotype. This is because E-cadherin and β-catenin do not only play a role in maintaining cellular adhesion between epithelial cells, but also organize cellular arrangement, transfer signals from the microenvironment to the cells and also regulate phenotypic changes of epithelial cells (Nistico et al., 2012). During EMT, loss of apico-basal polarity is followed by the remodeling of both cell-cell and cell-basement membrane interactions, which then causes epithelial cells to detach from each other and from the underlying basement membrane. Moreover, a new transcriptional cascade is activated to promote mesenchymal fate (Dongre & Weinberg, 2019). One of the first steps in the metastatic cascade is the invasion of cells into the extracellular matrix (Tsai & Yang, 2013).

I will next take a step back and provide a general overview of apico-basal polarity and the extracellular matrix, two hallmarks of epithelia that get lost during EMT, before discussing the various aspects of EMT in much more detail later on.

Epithelial cells

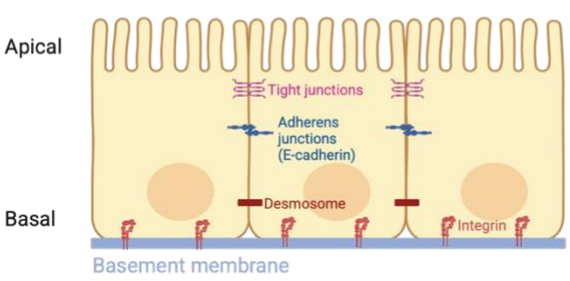

-Polygonal/columnar shape

-Apico-basal polarity

-Cell-cell adhesion

-Non-motile

EMT

MET

Mesenchymal cells

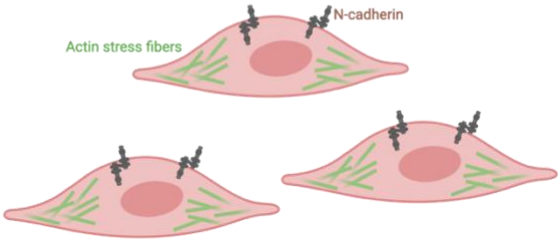

-Spindle shape

-Loss of apico-basal polarity

-loss of cell-cell adhesion

-Migratory (actin stress fibers)

Figure 1.2: Schematic representation of epithelial-to-mesenchymal transition.

Epithelial-to-Mesenchymal transition (EMT) is a process where epithelial cells lose polarity and cell-cell adhesion and acquire a mesenchymal phenotype with migratory and invasive properties. This Figure illustrates the key features of EMT, such as the loss of epithelial properties (e.g. tight junctions and E-cadherin) and the acquisition of mesenchymal traits (e.g. spindle shaped cells, increased motility and expression of mesenchymal markers such as N-cadherin). Created in https://BioRender.com

1.3 Apicobasal cell polarity

1.3.1 Mechanism of polarity in *Drosophila* epithelium

Cell polarity is essential for many biological processes, since it contributes to development and helps maintain normal tissue integrity (Ellenbroek et al., 2012). The phenomenon of cell polarity is defined as the asymmetric distribution of proteins in cells, thus resulting in an asymmetric distribution of functions (Nelson, 2003). The well-known type of cell polarity is the apico-basal polarity of epithelial cells, which is important for regulating cell-cell adhesion (Gibson & Perrimon, 2003). The maintenance of apical-basal polarity in epithelial cells is crucial since an altered polarity may contribute to developmental or pathological EMT (Shin et al., 2006). Loss of cell polarity especially in epithelial cells may result in tissue disorganization which can facilitate the initiation and progression of cancer (Ellenbroek et al., 2012). There are three polarity complexes that are conserved throughout several cell types and species. These complexes are the Par, Crumbs, and Scribble complexes (Ellenbroek et al., 2012).

The Par complex is apically localized and consists of Par3/Bazooka, Par6 and atypical protein kinase C (aPKC). The first Par protein homolog that was discovered was Par3, which was identified in *Drosophila* (Kuchinke et al., 1998). These apical polarity regulators are needed for the initial formation of adherens junctions, since they facilitate the separation of the apical membrane from the adhesion belt. The initial formation of adherens junctions occurs during cellularization of blastoderm epithelium (Tepass & Hartenstein, 1994). Prior to cellularization, the egg membrane is divided into two distinct regions, the supranuclear region that corresponds to the apical domain and the internuclear regions that corresponds to the basolateral domain

(Mavrakis et al., 2009). During the process of cellularization, Par3 gets concentrated in the upper third of the lateral membrane, which is required for the formation of spot adherens junctions on the apicolateral membrane (Harris & Peifer, 2004). During gastrulation, the spot adherens junctions will form the zonula adherens. Zonula adherens is a cell-cell adherens junction that forms a belt in the apical region, defining the border between the lateral and apical membrane and helps link cells into a continuous sheet (Woichansky et al., 2016). When the blastoderm epithelium is fully formed, apical polarity reporters (Par6, aPKC, and Par3) get recruited to the apical domain (Harris & Peifer, 2005, 2007; Hutterer et al., 2004).

Proteins in the Par complex, specifically Par6 and aPKC were first identified in *Caenorhabditis elegans* where knockdown of any of the proteins in the par complex resulted in abnormal symmetrical division of the fertilized zygote (Kemphues et al., 1988). The initial recruitment of Par6/aPKC to the apical membrane of epithelia requires an interaction with Par3 in order to form the Par complex (Harris & Peifer, 2005; Horikoshi et al., 2009). However, this interaction must then be resolved in order to position Par3 to the adherens junction and Par6/aPKC to the apical membrane. aPKC- dependent phosphorylation expels Par-3 from the aPKC/Par-6 complex (Horikoshi et al., 2009; Morais-de-Sá et al., 2010), and resolves the interaction between Par3 and Stardust, to allow the formation of the Crumbs/Stardust complex (Krahn et al., 2010). The serine/threonine kinase activity of aPKC is evolutionary conserved and is vital for establishing apical polarity in epithelial cells (Goldstein & Macara, 2007; St Johnston & Ahringer, 2010; Suzuki & Ohno, 2006). While Par3 remains enriched at adherens junctions, Par6 and aPKC together with Crumbs get localized in the marginal zone, which lies apical to the adherens junctions. Crumbs is considered an important regulator and determinant of epithelial

polarity, since loss of crumbs results in defects in epithelial membrane polarity and the integrity of adherens junctions (Tepass et al., 2001). However, not all epithelial in *Drosophila* express Crumbs, such as the intestinal epithelia (Tepaß & Knust, 1990). Moreover, not all epithelia that express Crumbs require Crumbs to maintain epithelial polarity, such as the epithelia in the larval imaginal disc (Pellikka et al., 2002). In addition, other apical polarity regulators, particularly Par3 can compensate for the function of Crumbs (Tanentzapf & Tepass, 2003). This suggests that epithelial polarity is maintained through multiple pathways and is regulated through overlapping mechanisms to ensure the robustness of tissue development.

The basal polarity complex consists of Scribble, Dlg, and Lgl which were first discovered in *Drosophila*. In order to sustain cell polarity, the apical and basal polarity complexes must interact in an antagonistic manner. Both Dlg and Lgl were initially classified as tumor suppressor genes, since disruption of Dlg or Lgl results in excessive tissue growth during the larval stage (Bilder, 2004; Woods & Bryant, 1991). The apical polarity regulator aPKC, plays an important role in the localization of basal polarity proteins. This is because aPKC phosphorylates the basolateral protein Lgl to prevent it from accumulating in the apical membrane (Betschinger et al., 2003). Thus, aPKC phosphorylation of other polarity proteins is vital for epithelial polarity. An example of the polarity pathway for the follicle cell epithelium in the *Drosophila* ovariole is shown in Figure 1.3. First, aPKC phosphorylates Par3, preventing it from accumulating apically from the adherens junction and phosphorylates Lgl to prevent it from being localized in the apical domain. In addition, aPKC also recruits the apical determinant PatJ to the apical membrane. In turn, the basolateral protein Lgl prevents aPKC from being localized in the basolateral domain (Schmidt & Peifer, 2020). Basolateral proteins Dlg and Scribble inhibit the movement of aPKC to the

basolateral domain, thus protecting Lgl from being phosphorylated by aPKC. Moreover, Dlg and Scribble recruit other unknown basolateral effectors to define the basolateral domain (Schmidt & Peifer, 2020). This polarity pathway is essential for normal development of the *Drosophila* ovariole, since cells that are mutant for Dlg and/or Scribble lack of protection of Lgl, where aPKC spreads into the basolateral domain, phosphorylating Lgl and displacing it into the cytoplasm (Figure 1.3, Schmidt & Peifer, 2020). Basolateral aPKC then recruits PatJ, an apically localized polarity protein, into the basal domain, thus specifying the basolateral domain to an apical domain. Although aPKC, Par3, Crumbs and Scribble seem to be key players for polarity, this is not the case in all types of epithelia. For instance, in the *Drosophila* adult midgut aPKC, Crumbs, Par3 and Scribble modules are not essential for polarity (Chen et al., 2018).

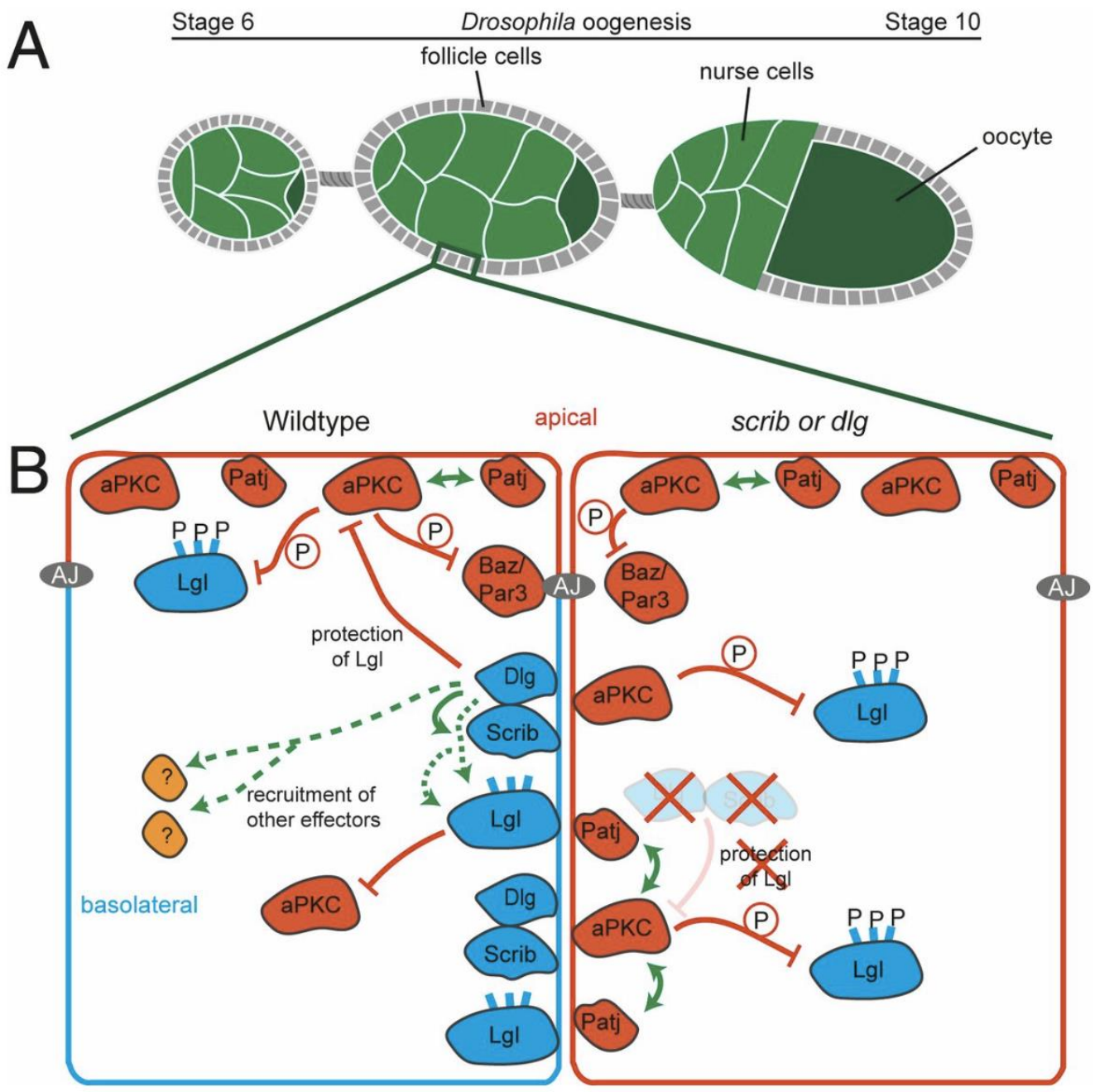
A
Stage 6
Drosophila oogenesis
Stage 10
follicle cells
nurse cells
oocyte
B
Wildtype
apical
scrib or dlg
aPKC
Patj
Lgl
Baz/
Par3
AJ
P
protection
of Lgl
Dlg
Scrib
recruitment of
other effectors
basolateral

Figure 1.3: Polarity pathway in the *Drosophila* follicle cells.

This schematic illustrated the polarity pathway in the follicle cells that form an epithelium in the *Drosophila* ovariole. In the wild type condition, aPKC phosphorylates Par3 and Lgl, to ensure proper apical-basolateral domain segregation. Basolateral proteins Dlg and Scribble inhibit aPKC from spreading into the basolateral domain. Loss of Dlg or Scribble disrupts the polarity pathway, leading to the mislocalization of polarity proteins and loss of epithelial polarity. Adapted from Schmidt et al., 2020.

1.3.2 Primary and Secondary Epithelia

In *Drosophila*, epithelial tissues are classified either as primary or secondary epithelia, depending on their developmental origins and the molecular processes they undergo to establish apicobasal polarity and form junctional organizations. Primary epithelia derive from the blastoderm during early embryogenesis particularly during cellularization and gives rise to tissues such as the epidermis, salivary glands and trachea (Tepass et al., 2001). In contrast, secondary epithelia form later in development through mesenchymal-to-epithelial transition (MET) and include structures like the midgut and glial sheets (Tepass et al., 2001). Despite their distinct origins, primary and secondary epithelia also differ in the way they establish polarity and junctional complexes (Tepass, 1997; Tepass & Hartenstein, 1994). Primary epithelia develop a well-defined apicobasal polarity driven by the apical localization of the Crumbs complex, which includes Crumbs and Stardust. Crumbs is essential not only in defining the apical identity, but also stabilizing zonula adherens. In fact, loss of Crumbs disrupts epithelial integrity (Hong et al., 2001). Secondary epithelia on the other hand, establish apicobasal polarity more gradually and display low or variable Crumbs expression. In these tissues, polarity relies on an apically localized polarity protein complex, specifically the Bazooka complex, which also contributes to junctional formation even if Crumbs expression is reduced. Consequently, unlike primary epithelia that develop junctional structures early during development, secondary epithelia acquire these features progressively, particularly after mesenchymal-to-epithelial transition (MET). These differences highlight the flexibility of epithelial polarity programs which depends on the tissue's origin and developmental timing.

1.3.3 The extracellular matrix

The basement membrane (BM) is a specialized ECM that is made of sheet-like extracellular matrix located at the basal surface of epithelial cells. The ECM surrounds muscle and fat cells and provides structural support for epithelial and endothelial cells growth (Jia et al., 2014). In *Drosophila*, the core basement membrane components, Collagen IV and laminin, are reinforced by Nidogen and Perlecan (Isabella & Horne-Badovinac, 2015). Collagen IV is a heterotrimeric molecule that is made of two alpha1-like chains and one alpha2-like chain. Two genes, *viking* and *collagen at 25C (Cg25C),* are encoded within the alpha chains of Collagen IV. Although the core BM proteins, Collagen IV and laminin, are well conserved between fruit flies and humans, the basement membrane of fruit flies is considered the simpler version of mammalian BM. For instance, humans produce three types of collagen trimers and sixteen types of laminin trimers, while fruit flies only produce one type of collagen trimer and two types of laminin trimers (Isabella & Horne-Badovinac, 2015). In fruit flies, some epithelia synthesize their own BM components, while others rely on other tissues to produce BM components. For instance, in the developing egg chamber, the basement membrane is secreted by follicle cells (Figure 1.4A). However, during embryogenesis, immune cells circulating throughout the body, secrete basement membrane (Figure 1.4B), while in the larvae, the fat body, known as the main metabolic organ in insects, secretes Collagen IV and Laminin into the hemolymph, the body fluid surrounding all organs, which is used by other organs to assemble their BMs (Figure 1.4C) (Isabella & Horne-Badovinac, 2015; Ramos-Lewis & Page-McCaw, 2019). Blocking Collagen IV production in the fat body results in loss of Collagen IV from the BM leading to the complete loss of BM surrounding the imaginal wing disc epithelium, which is the precursor of adult fly wing (Pastor-Pareja & Xu, 2011).

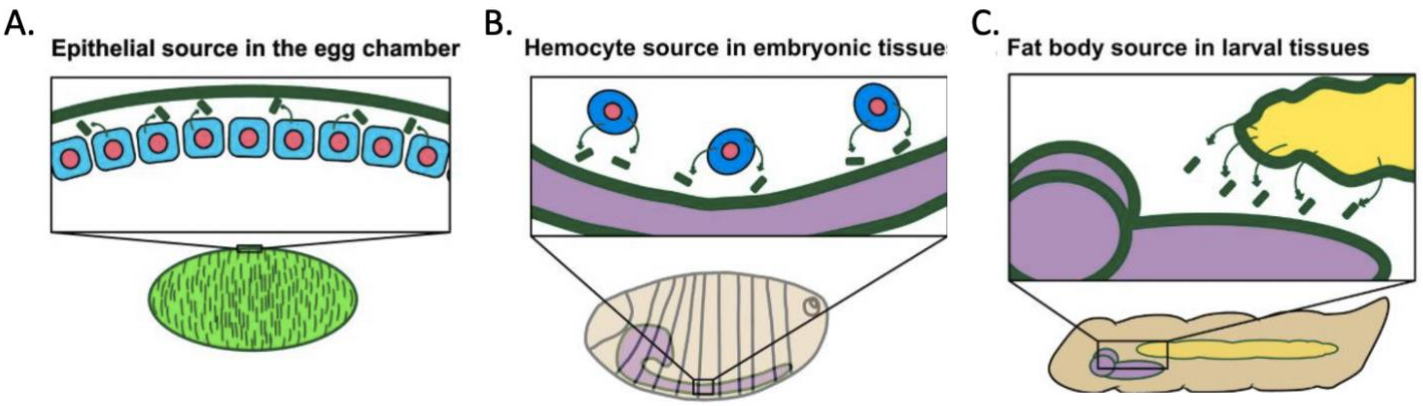
A.
Epithelial source in the egg chamber
B.
Hemocyte source in embryonic tissue
C.
Fat body source in larval tissues

Figure 1.4: During *Drosophila* development, the basement membrane is secreted from several different types of cells.

(A) During developing egg chamber, the basement membrane (green), is secreted by follicle cells (blue).
(B) During embryogenesis, the basement membrane (green) is secreted by hemocytes (blue) onto developing organs such as the ventral nerve cord (purple).
(C) During larvae, basement membrane proteins (green) are secreted by the fat body (yellow) into the extracellular space, which will then diffuse to their target tissues such as the ventral nerve cord (purple). Adapted from Ramos-Lewis & Page-McCaw, 2019.

The composition of the BM is highly dynamic, diverse and tissue specific, varying according to the tissue's physiological or pathological state. This heterogeneity is dependent on the amount of BM composition and its constituents (Isabella & Horne-Badovinac, 2015). For instance, in tumors, the composition of the BM and its constituents differ significantly from the normal physiological BM (Frantz et al., 2010). The expression of ECM remodeling enzymes is tightly controlled, thus being produced in specific cells at specific timings. For example, in *Drosophila*, MMPs are specifically expressed in early embryos to facilitate tracheal branching morphogenesis. Furthermore, alterations in the composition and architecture of the ECM, during tissue remodeling often results in changes in tissue morphology. For instance, tracheal development in *Drosophila* begins with the formation of a tracheal sac that generates 6 primary branches. These branches undergo cell rearrangements from being side-by-side to an end-to-end localization (Ehrhardt et al., 2022). Wing maturation is another example of tissue remodeling in *Drosophila*. As the wing expands, epithelial cells within the folded wing begins to detach from the cuticle. Following expansion, these epithelial cells lose contact with each other through disruption of adherens junctions, resulting in cell shape changes, elongation and migration from the wing to the thorax (Kiger et al., 2007).

1.3.4. Developmental and pathological EMT

It is widely known that EMT normally occurs during development and wound healing in adults, since its critical for the formation of many tissues and organs during development (Hugo et al., 2007). For instance, during the formation of *Drosophila* intestinal tract, epithelial cells in the posterior midgut undergo EMT to adapt mesenchymal behavior and migrate towards the center of the embryo where they re-epithelialize and fuse with the anterior midgut to form a continuous intestinal tract (Campbell et al., 2011). During development, the epithelial cell state ranges from cells acquiring cell-cell junctions (tight junctions, adherens junctions/desmosome) to cells adhering to the basement membrane through hemidesmosomes.

Developmental EMT has been found to undergo a sequence of events. First, the area of tissues that will undergo EMT must be identified temporally and spatially. Tissue morphological rearrangements might take place to aid in moving cells to the site of EMT. Second, a disrupted interaction occurs between epithelial cells and the basement membrane that underlines the epithelial tissue. Third, cells undergoing EMT must detach from the epithelial sheet, this involves actomyosin-based rearrangements of cell shape and crawling of epithelial cells to close the gap. However, despite the detachment of some cells, the remaining epithelial tissue must maintain its structure and identity to ensure its ability to perform its normal function. Lastly, transitioning cells differentiate into a mesenchymal phenotype, modifying the cytoskeletal organization as well as cell-ECM interactions. The process of developmental EMT is shown in Figure 1.5A (Nistico et al., 2012).

Although EMT in embryonic development is a coordinated process, aspects of the EMT program can be activated inappropriately in response to changes in the microenvironmemt and unusual stimuli, which can contribute to disease states including tissue fibrosis and cancer

progression. This is referred to as pathological EMT, which involves the activation of EMT in an uncontrolled and cell-autonomous manner (Figure 1.5B) (Lu et al., 2011), resulting in the disorganization of epithelial tissue and disruption of the epithelial integrity leading to the production of new mesenchymal cells which can propagate to disease (Thiery et al., 2009). The only exception is carcinosarcoma, a rare and extremely aggressive tumor, where epithelial and mesenchymal components can coexist (Thompson et al., 1996). Once EMT is activated, tumor epithelial cells loose epithelial characteristic like cell polarity and cell adhesion and gain invasive and migratory properties to become mesenchymal cells (Ribatti et al., 2020).

A Developmental EMT

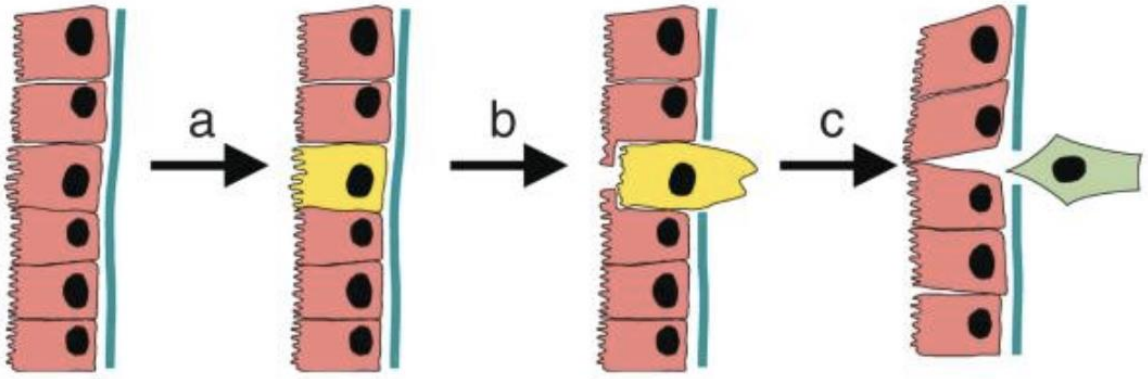

B Pathological EMT

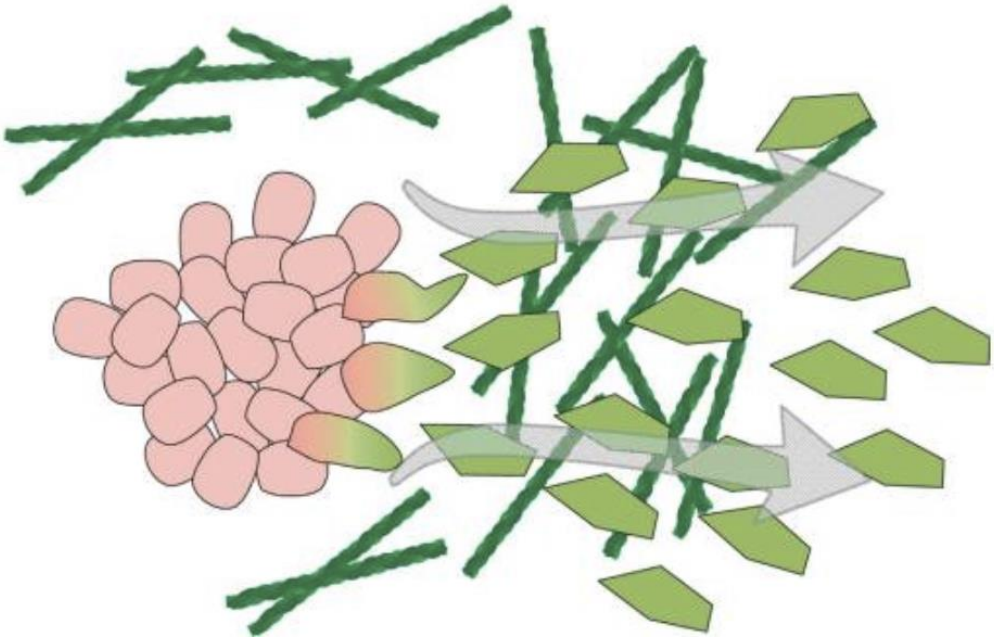

Figure 1.5: Developmental EMT versus Pathological EMT.

(A) Developmental EMT involves the entire epithelial tissue. (a) The first step of developmental EMT involves the specification of cells that will undergo EMT (yellow), which is done through the coordination of cell-cell, cell-BM and soluble signals. (b) The second step involves the degradation of the basement membranewist of the specified cells to facilitate the movement of the specified cell to move inwards (cell ingression). The remaining epithelial cells undergo morphogenesis, where they change their shape and structure to be able to close the space left behind and ensure that the tissue remains intact. (c) In the final step, epithelial cells that have completely detached from the epithelial tissue, undergo changes in its characteristics, adopting a mesenchymal-like phenotype.

(B) Pathological EMT involves the activation of EMT in an uncontrolled and disorganized manner and in a cell-autonomous fashion.

Adapted from Nistico et al., 2012

1.3.5. Regulators of EMT

The process of EMT is generally activated by EMT-inducing transcription factors (EMT-TF's). EMT is mainly controlled by three conserved families of transcription factors, which are Snail, Twist and Zeb. These proteins share a common function which is to repress epithelial genes such as E-cadherin. Repression of E-cadherin causes cells to have a cobblestone spindle-shaped morphology that is observed in a mesenchymal cell (Campbell, 2018). The function of EMT in *Drosophila* varies depending on the type of tissue. For instance, during mesoderm formation both Snail and Twist play a role in repressing E-cadherin expression, thus reducing cell-cell adhesion in order to enable cell invagination during gastrulation (Leptin, 1991). Moreover, Zeb-TF's are also able to repress E-cadherin expression, using a double negative feedback loop (Baranwal & Alahari, 2009; Bracken et al., 2008). Unlike a classic EMT where E-cadherin repression is essential for cells to undergo migration, *Drosophila* mesodermal cells undergo collective cell migration, in other words they migrate while retaining cell-cell adhesion to some extent (Campbell & Casanova, 2016). On the other hand, EMT in the endoderm, specifically the posterior midgut, is regulated by GATA transcription factor Serpent, which downregulates Crumbs, an apical polarity protein determinant, rather than E-cadherin, thus leading to loss of apicobasal polarity and cell detachment (Lim & Thiery, 2011). These findings emphasize that EMT in *Drosophila* can vary depending on the tissue type, thus involving different transcription factors and polarity proteins. Some of the EMT regulators that have been tested in this study are mentioned below:

1.3.5.1. Snail

Snail is an EMT-transcription factor that is part of the Snail family consisting of a conserved zinc finger transcription factor that has been extensively studied revealing its role in development, cell morphogenesis and tumor metastasis (Barrallo-Gimeno & Nieto, 2005). The original identification of Snail was in *Drosophila*, as a key regulator of embryonic mesoderm formation (Grau et al., 1984; Rembold et al., 2014). During the process of gastrulation, snail mutant embryos exhibit impairments in mesoderm development (Simpson, 1983). Moreover, Snail was then reported to play a major role in tumor invasion and metastasis, particularly in epithelial to mesenchymal transition (Muqbil et al., 2014), where it acts as a transcriptional repressor of several genes involved in EMT (Chiang & Ayyanathan, 2013; Saitoh, 2018). Snail has been shown to affect EMT by transcriptionally repressing E-cadherin, which is known to maintain cell-cell adhesion (Campbell et al., 2018). Other studies also reveal the importance of Snail in cell proliferation, cell differentiation, cell death and tissue growth (Tang et al., 2016; C. Wu et al., 2019; Zeng et al., 2020). For instance, the absence of Snail suppresses, while overexpression enhances cell proliferation and tissue growth via hippo signaling (Ding et al., 2022).

1.3.5.2. Twist

The Twist family transcriptional regulators (Twist1 and Twist2) are part of the basic-helix-loop-helix family of proteins (Debnath et al., 2022). In humans, Twist was shown to be upregulated in invasive lobular breast tumors (Yang et al., 2006). Twist1 was first identified in *Drosophila*. Both Twists (Twist1 and Twist2) were shown to play a role in the embryogenesis process. A study showed that twist null embryos revealed abnormal gastrulation without a mesoderm and thus failed to survive (Simpson, 1983). Moreover, Twist was also found to be

important for EMT, where it regulates the transcriptional switch from E-cadherin to N-cadherin (Oda et al., 1998) and the acquisition of other mesenchymal markers like fibronectin and vimentin (Soo et al., 2002). The expression of Twist was shown to be crucial for the proper migration and differentiation of neural crest cells, since Twist mutant mice failed to develop cranial neural tube closure (Soo et al., 2002).

1.3.5.3. Zeb

Zeb transcription factors are a family that consists of two members: ZEB1 and ZEB2. Although both ZEB1 and ZEB2 (Vandewalle et al., 2009) strongly repress E-cadherin, is it not as powerful as Snail. However, in in vitro assays knocking down Zeb1 has a stronger impact on E-cadherin than Snail (Vandewalle, 2005; Vandewalle et al., 2009; Vega et al., 2004). Both ZEB1 and ZEB2 are involved in physiological, as well as, pathological EMT. For instance, ZEB2 knockout mouse models results in embryonic lethality. Additionally, ZEB2 mutations causes MowatWilson Sydrome, where in addition to other abnormalities, these patients show distinct facial characteristic, suggesting the importance of ZEB2 in the migratory behavior of cranial neural crest cells and in EMT (Vandewalle et al., 2009). ZEB1 also functions as a key regulator of BM synthesis. In cancer cells, ZEB1 promotes BM degradation, and facilitates cancer cell invasion (Vandewalle et al., 2009).

1.3.5.4. Serpent

Serpent is a *Drosophila* GATA transcription factor that induces EMT. Serpent is required for EMT in the *Drosophila* midgut, midgut cell specification (Seifert & Lehmann, 2012), as well as, specification and maturation of hemocytes (Rehorn et al., 1996). Due to the importance of Serpent in development, it is unsurprising that the uncontrolled activation of Serpent beyond the regulatory mechanism of normal development can impact signaling pathways in addition to EMT,

which may lead to the initiation and development of primary tumors, instead of only being involved in cancer metastasis (Campbell et al., 2018). It was previously known that Serpent represses the polarity regulator Crumbs, thus downregulating junctional E-Cad during EMT of the endoderm in the *Drosophila* embryo (Campbell et al., 2011). Moreover, another study showed that similar to the embryo, Serpent overexpression also represses the transcription of Crumbs in *Drosophila* wing disc (Campbell et al., 2018), but does not affect apico-basal polarity (Richardson & Pichaud, 2010). This indicates that beyond its effect on Crumbs, Serpent is likely to regulate the transcription of other genes that affect polarity, as previously shown in embryonic mesoderm (Sandmann et al., 2007) and midgut development (Campbell et al., 2011). In addition to Serpent's role in affecting apicobasal polarity, a study conducted on *Drosophila* embryos reveled that ectopic expression of Serpent induces the disassembly of adherens junctions in ectodermal cells and might lead to migration of certain cells into the embryo (Campbell & Casanova, 2015). Interestingly, although no proliferation was observed in the embryo, excessive proliferation with minimal cell migration was seen in wing discs. This suggests that EMT transcription factors can stimulate either migration or cell proliferation, prioritizing one process over the other at a given time (Campbell et al., 2018).

1.3.6. Partial EMT

During development, the epithelial cell state is dictated by cells acquiring cell-cell junctions (tight junctions, adherens junctions/desmosome) as well as cells adhering to the basement membrane through hemidesmosomes. In many cases, loss of cell-cell junctions is not essential to be able to classify cells as having mesenchymal characteristics, which explains why some mesenchymal cells exhibit collective cell migration. This phenomenon is referred to as a hybrid epithelial/mesenchymal phenotype which occurs in a process called partial-EMT

(Campbell & Casanova, 2016). Partial EMT has been observed in endodermal and mesodermal cells in *Drosophila melanogaster*, zebrafish, as well as, in neural crest cells of chick and *Xenopus laevis* (Campbell & Casanova, 2016). For instance, studies conducted using live chick mesodermal cells shows cells migrating in a directional manner while maintaining close contact to one another (Chuai et al., 2012).

Despite the significant progress in cancer diagnosis and treatment, metastasis remains the main cause of cancer-related death and remains a major barrier to effective therapy (Fischer et al., 2015). It is believed that some tumors exploit EMT to gain motility and invasive characteristics of mesenchymal cells during early stages of metastasis (Kalluri & Weinberg, 2009). However, similar to partial EMT phenotypes, observed in development, most primary carcinoma cells advance along the epithelial-to-mesenchymal spectrum to different states, thus resulting in extensive phenotypic heterogeneity within tumors. For instance, several different gene expression profiles have been identified in skin and mammary primary tumors (Zhang & Weinberg, 2018). Moreover, not all cancers undergo a complete EMT; also some cancer cells alter their migration mode depending on their environment. For instance, lineage tracing of mesenchymal markers in some cancer models revealed that mesenchymal markers are not expressed in cancer cell metastasis (Fischer et al., 2015; Zheng et al., 2015). However, it remains unclear whether primary carcinoma cells can undergo metastatic dissemination without activating EMT components (Campbell, 2018). Furthermore, cancer cells can adapt various modes of migration, including collective cell migration or individual cell migration via mesenchymal or ameboid mechanisms (Zhu & Mogilner, 2016). Mesenchymal cells exhibit an elongated morphology and generate traction force via cytoskeletal contractility and integrin-mediated ECM-adhesion to move forward. Mesenchymal cells often generate paths for their

migration via ECM degradation (J. Wu et al., 2021). On the other hand, ameboid cells are characterized as round cells that lack adhesion and high cortical contractility (Lorentzen et al., 2011). A study showed that zebrafish primordial germ cells undergo cortical flow-driven amoeboid migration, where the flows are considered to be a specialized response to external stimuli in order to enable rapid and context dependent motility *in vivo* (Ruprecht et al., 2015), similar to what has been observed in *Drosophila* primordial germ cells (Lin et al., 2021). In other words, this mode of migration does not purely rely on external stimuli since it arises from the internal state of the cell (Lin et al., 2021).

Due to the fact that EMT has been described much more as a fluid transition harboring a continuum of phenotypes between the extreme epithelial and mesenchymal states, defining a process as an EMT process remains a debate. In some studies, processes have been classified as an EMT-like process rather than a classic EMT. For instance, fish epithelial cells exhibit distinct apico-basal polarity and adherens junctions but lack a basement membrane (Campbell & Casanova, 2016). However, as they initiate migration, changes in morphology and polarity have been observed, thus being referred to as an EMT-like process. Moreover, neural crest cells in fish, birds and mammals induce breakdown of the basement membrane as they initiate migration, while no changes have been observed in apico-basal polarity throughout the process, yet this process has been referred to as an EMT-like process (Campbell & Casanova, 2016).

1.4 The *Drosophila* fat body

1.4.1. The *Drosophila* fat body: an overview

The fat body in insects, called the adipose tissue in humans, is an organ that consists of fat body cells (adipocytes in humans). In *Drosophila melanogaster*, the fat body arises from the

embryonic mesoderm (Hartenstein & Jan, 1992). The expression of Serpent, a GATA-like transcription factor, is needed for the progression through early stages of fat body cell development (Sam et al., 1996). The larval fat body lies along the larval body cavity, thus being exposed to the hemolymph and also surrounds the reproductive organ and the gut, as shown in Figure 1.6 (Parra-Peralbo et al., 2021). The larval fat body consists of around 2200 cells. During larval stages the fat body, a single layered sheet of polyploid cells, accumulates lipid droplets which in turn increases the size of fat body cells (Parra-Peralbo et al., 2021). The fat body has several functions such as energy storage and release but it also plays a role in regulating metabolism, growth, immunity (Booth et al., 2016) and wound healing (Franz et al., 2018). These functions are controlled by hormones and depend on crosstalk between the fat body and other tissues (Parra-Peralbo et al., 2021). During pupal and early adult stages, the fat body cells act as a source of nutrients for the first 3 days after eclosion, in other words, during the non-feeding stage of adulthood (Aguila et al., 2007). After eclosion, the larval fat body cells get replaced by new adult fat body cells (Johnson & Butterworth, 1985). Although both, the larval and adult fat body, have similar function such as energy storage and release, they show different features. For instance, unlike the larval fat body which increases in size by the accumulation of lipids, the adult fat body increases in size by increasing the number of fat body cells. In this study, all experiments are either done in the larval or pupal fat body cells, meaning the first population group of fat body.

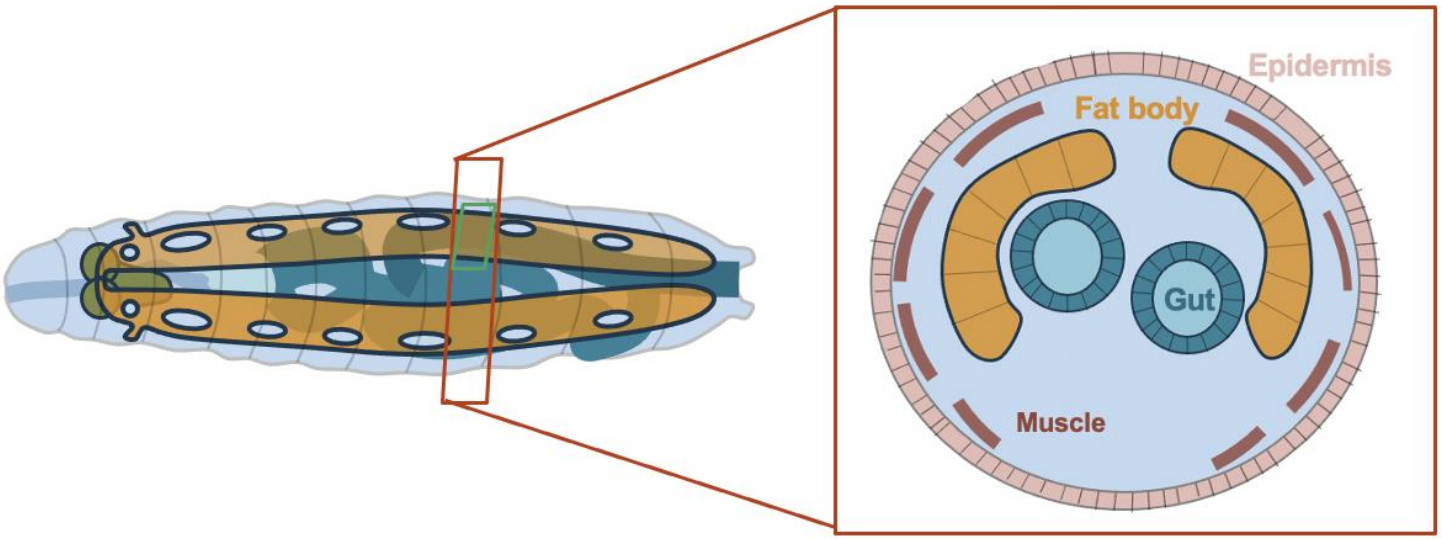

Figure 1.6: *Drosophila* larval fat body tissue.

During late larval stages, the fat body tissue (yellow) lies along the larval fat body surrounding organs such as the gut (dark blue) and is exposed to the hemolymph (light blue).

1.4.2. Fat body remodeling

In *Drosophila melanogaster*, the fat body tissue undergoes a process similar to tissue remodeling called fat body remodeling (FBR), the focus of this study. The process of FBR occurs during early metamorphosis in the young pupa. Throughout the process of FBR, sheets of fat body cells dissociate in three phases: retraction (4-6 hrs after pupa formation (APF), disaggregation (8-10 hrs APF), detachment (12-18 hrs APF) (Bond et al., 2011). During the retraction phase (4-6hr APF), the fat body sheets shift away from the body's posterior region, as shown in Figures 1.7 A1-2. In this stage, the fat body cells do not change their morphology and remain polygonal in shape (Figure 1.7 B2) (Bond et al., 2011). In the disaggregation phase (8-10hr APF), fat body cells begin to detach from each other (Figure 1.7 B4) (Bond et al., 2011). This process is driven by the gradual loss of cell-cell adhesion components (E-cadherin) and cell-basement membrane adhesion components (Collagen IV and Integrin) (Jia et al., 2014). At this point, fat body cells begin to round up. During the detachment phase (12-18hr APF), fat body cells have undergone complete dissociation from neighboring fat body cells and are not spherical in shape. Moreover, during this stage head formation occurs which is accompanied by the spreading of fat body cells into the head and other body parts (Figure 1.7 A5 and B5, Nelliot et al., 2006). Initially it was suggested that by the end of FBR, some of the individual fat body cells get translocated passively to the newly formed head of the pupa by muscular contractions approximately 43 minutes after head eversion is completed (Figure 1.8) (Bond et al., 2011). However, Franz et al. 2018, reported that by the end of FBR, fat body cells become motile and their translocation to the head is at least partly driven by active migration into the head. Figure 1.7 also shows the importance of Ecdysone signaling in the disaggregation and detachment

phases but not in the retraction phase. Disruption Ecdysone signaling inhibits fat body disaggregation, resulting in fat body cells remaining polygonal in shape and staying tightly close to each other, thus inhibiting the detachment phase, and leading to no fat body cells being present in the head of the pupa by the end of FBR (Figure 1.7 A12) (Bond et al., 2011)

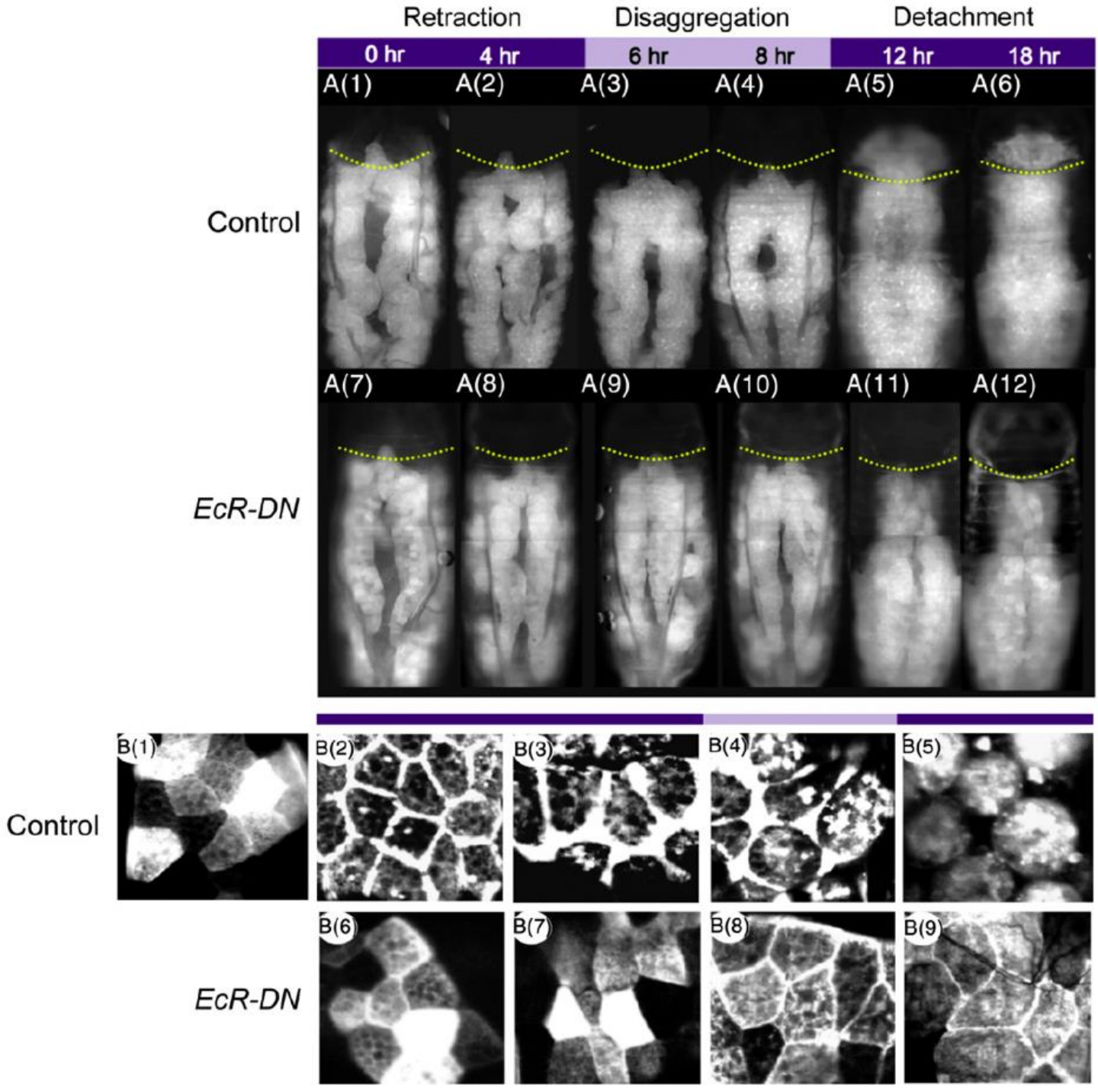
Retraction
Disaggregation
Detachment
0 hr
4 hr
6 hr
8 hr
12 hr
18 hr
A(1)
A(2)
A(3)
A(4)
A(5)
A(6)
Control
A(7)
A(8)
A(9)
A(10)
A(11)
A(12)
EcR-DN
Control
B(1)
B(2)
B(3)
B(4)
B(5)
B(6)
B(7)
B(8)
B(9)
EcR-DN

Figure 1.7: Fat body disaggregation and detachment phases require Ecdysone signaling.

Fat body marked by GFP (UAS-GFP; Lsp2-Gal4). Developmental timepoints marked are after pupal formation.

(A) Animals undergoing the process of FBR. (A1-6) Control animals undergoing FBR. (A 7-12) experimental animals expressing a dominant negative form of ecdysone receptor (EcR-DN).

(B) Confocal images of fat body cells expressing GFP. (B 8-9) During the disaggregation and detachment phases, fat body cells expressing EcR-DN do not change in shape and remain closely attached to each other, when compared to (B 4-5) the control animals at similar timings. Adapted from Bond et al., 2011.

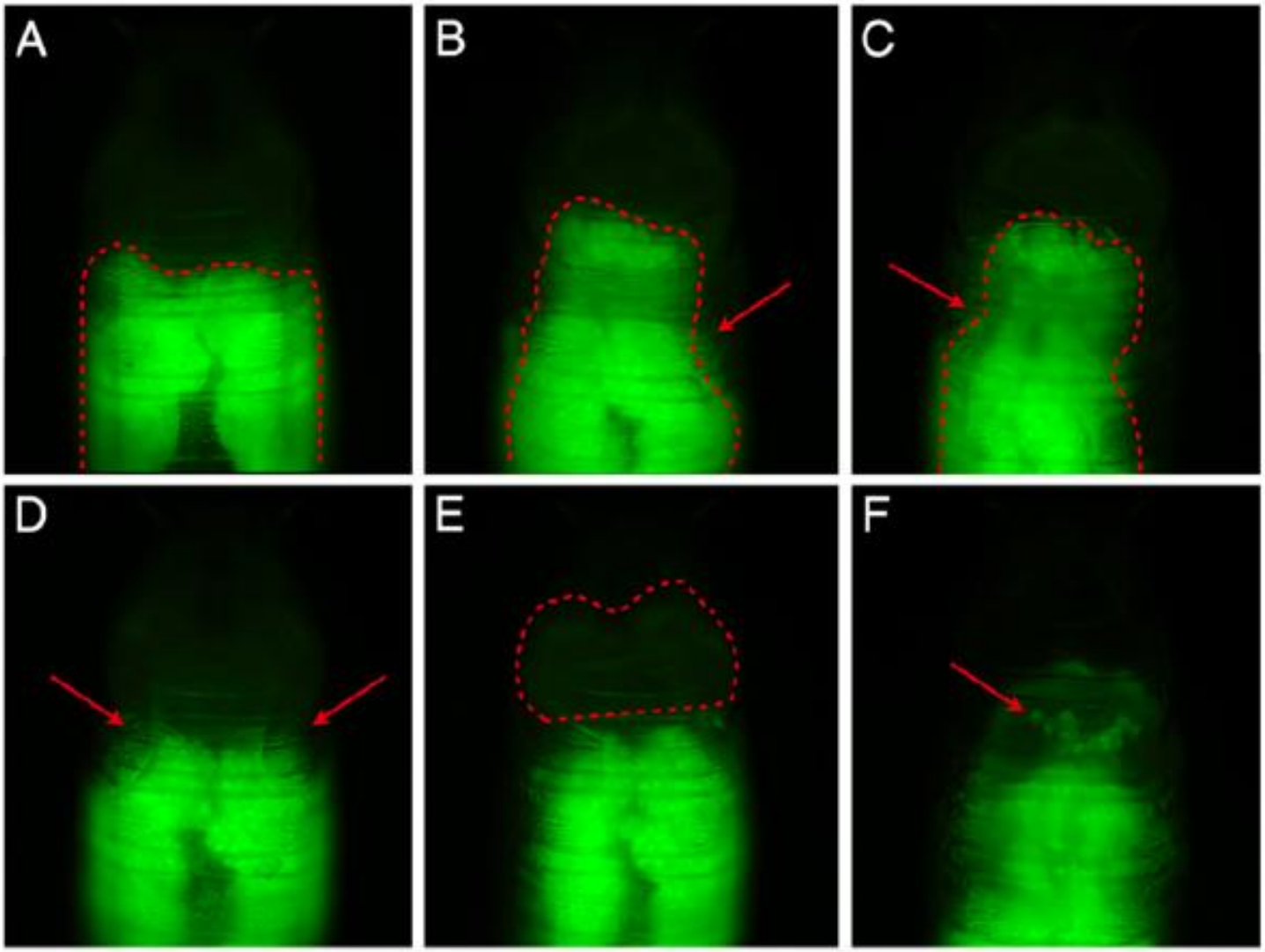
A
B
C
D
E
F

Figure 1.8: Still images of a time-lapse movie of a prepupa expressing GFP in the fat body. Fat body marked by GFP (Lsp2-Gal4+UAS-GFP).

(A-D) Intact fat body before head eversion. (E) Shows head eversion. (F) Shows FBCs being pushed into the head by muscle contractions, individual FBC indicated by a (red arrow). Adapted from Bond et al., 2011.

1.4.3. *Drosophila* fat body vs. Primary and Secondary Epithelia

Drosophila fat body differ from both primary and secondary epithelia in terms of developmental origin and structural arrangement. Unlike primary epithelia that originates from the blastoderm during early embryogenesis and secondary epithelia that develop later in development through MET and develops progressively (Tepass et al., 2001), the *Drosophila* fat body originates from the mesoderm (Hartenstein & Jan, 1992). Additionally, primary epithelia form well-defined apical and basal domains with Crumbs being a classic apical domain determinant (Tepass et al., 2001) while secondary epithelia rely less on the canonical polarity regulator Crumbs (Campbell et al., 2018); the fat body, on the other hand, is not thought to exhibit apicobasal polarity due to its unique structure where the basement membrane is present on both sides of the tissue.

1.4.4. Vertebrate adipocytes

Vertebrates adipose tissue is a specialized connective tissue that functions in energy storage, metabolic regulation and hormonal signaling. Unlike *Drosophila* fat body, the adipose tissue in vertebrates exist in various forms primarily while adipose tissue (WAT) and brown adipose tissue (BAT), each contributing to different physiological roles (S. K. Verma et al., 2017). For instance, WAT plays a role in storing and releasing energy, while also acting as an endocrine organ which regulates appetite, insulin signaling and response to inflammation (Kershaw & Flier, 2004; Rosen & Spiegelman, 2006). BAT, on the other hand, is densely packed with mitochondria and helps generate body heat without shivering, especially in newborns and animals that hibernate (Lumeng & Saltiel, 2011). Beyond its metabolic function, the adipose tissue undergoes structural and functional remodeling in response to nutrition, hormones and

environmental factors. It also helps regulate the immune system, since it contains immune cells that influence inflammatory processes under both, normal physiological and pathological states, such as obesity (Cristancho & Lazar, 2011). Despite the morphological differences between *Drosophila* fat body and vertebrate adipose tissue; vertebrate adipose tissue recapitulates several analogous functions, mainly in metabolic and hormonal regulation.

At the developmental level, vertebrate adipose tissue originates from mesenchymal stem cells and undergoes differentiation to become adipocytes (Cristancho & Lazar, 2011). Studies have shown that pathways involved in EMT and adipogenesis overlap. For instance, transforming growth factor-beta (TGF-β), a signaling molecule that triggers EMT in a classic epithelial, also prevent preadipocytes from differentiating to mature adipocytes and instead leads to the development of fibrosis (Choy & Derynck, 2003). Despite the fact that is it yet poorly understood whether apicobasal polarity is present in vertebrate adipocytes, they do display certain forms of functional polarization. For instance, although GLUT4 is evenly distributed across adipocytes at all time, upon insulin stimulation, GLUT4 containing vesicles gets moved to the plasma membrane, specifically to regions with vesicle fusing (Zeigerer et al., 2002).

1.4.5 Known regulators of FBR

To date there have only been a handful of publications on FBR that revealed only a small number of genes regulating this process including Ecdysone signaling and MMPs (MMP1 and MMP2).

1.4.5.1. Ecdysone

Ecdysone, 20-hydroxy-ecdysone, is a steroid hormone that binds to the ecdysone receptor in various cell types including the fat body. Ecdysone signaling is crucial for the process of FBR because it induces cellular changes needed for pupal development (Bond et al., 2011). In *Drosophila*, late larval progression to pupal stages is determined by a pulse of Ecdysone. Ecdysone activates an intracellular hetreodimeric nuclear hormone receptor complex that consists of Ecdysone receptor (EcR) and Ultraspiracle (Usp) and functions as a ligand-regulated transcription factor. Similar to vertebrate steroids, Ecdysone functions as a ligand regulated transcription factor via members of the nuclear receptor superfamily. Once Ecdysone signaling is activated, it induces the transcription of early response genes that are encoded by genes E74, E75, and Broad Complex (BR-C), which are a family of transcription factors (Delanoue et al., 2010). In turn, these early response genes drive the expression of late response genes that are responsible for regulating the biological responses to each ecdysone pulse, thus resulting in specific morphological changes needed in certain developmental stages (Delanoue et al., 2010).

1.4.5.2. Matrix metalloproteinase

Matrix metalloproteinase (MMP), are calcium dependent zinc-containing metalloproteinases that play a major role in cleaving extracellular matrix proteins in *Drosophila* and mammals (Bindhani et al., 2022; Verma & Hansch, 2007). In addition to the removal of the ECM molecules, MMPS also plays a role in several biological processes inside the organism such as cell proliferation and differentiation (Cui et al., 2017), cell migration (Amălinei et al., 2007), and cancer cell invasion (metastasis, Verma & Hansch, 2007). Unlike humans and mice which have 23 and 24 members of MMPs respectively (Jia et al., 2014), in *Drosophila*

melanogaster, there are only two MMPs found, MMP1 and MMP2 (Llano et al., 2002; Page-McCaw et al., 2003). MMP1 is a secreted protein while MMP2 is a plasma membrane-bound glycosylphosphatidylinositol (GPI) anchored protein (Page-McCaw et al., 2003b; Stevens & Page-McCaw, 2012). Both MMP1 and MMP2 are shown to take part in common and discrete functions. For instance, both MMP1 and MMP2 are needed to induce migration in cardioblasts during collective cell migration (Raza et al., 2017). However, in *Drosophila* fat body MMP1 and MMP2 have discrete functions. In other words, MMP1 was reported to cleave E-cadherin at cell-cell-cell junctions during fat body remodeling when cells undergo dissociation, while MMP2 is needed to sever cell-basement membrane adhesion (Jia et al., 2014). Despite the distinct roles of MMPs in the fat body of *Drosophila*, this study also showed that the simultaneous reduction of both MMP1 and MMP2 expression by RNAi resulted in a more significant delay in dissociation when compared to individual reduction of either MMP1 or MMP2 (Jia et al., 2014).

1.4.6 Similarities between FBR and EMT

FBR has, until now, been considered to be a type of tissue remodeling process rather than EMT, since it was only recently discovered that these cells become motile following FBR (Franz et al., 2018). Taking this new discovery into account, we couldn't help but notice, that FBR and EMT are similar in many ways: Both processes involve the cleavage of cell-cell and cell-basement membrane adhesion proteins (E-cadherin and integrin, respectively), as well as, basement membrane components (e.g. collagen), both are regulated by matrix metalloproteinases (MMPs) and result in cell migration. Although EMT and FBR share certain characteristics such as the downregulation of E-cadherin expression/E-Cadherin cleavage driving loss of adhesion, FBR also does not resemble a classic EMT for several reasons.

Firstly, the fat body tissue is not an epithelial tissue and even has some key differences to a classic epithelium. Epithelial cells have distinct apical and basolateral domains with a basement membrane exclusively on the basal side (Figure 1.9A). In contrast, the fat body sheet is surrounded by a basement membrane on both sides and have not been reported to have an apico-basal polarity (Figure 1.9B). However, it could hypothetically still be that the fat body exhibit apicobasal polarity despite the presence of basement membranes on both sides.

Secondly, while EMT results in mesenchymal cells that migrate using a mesenchymal mode of migration (Figure 1.9 A), fat body cells, on the other hand, migrate via amoeboid migration mode following FBR (Figure 1.9 B). However, although classic EMT is defined by epithelial cells transitioning into mesenchymal cells, there are some cases where epithelial cells transition to ameboid migration, also called epithelial to ameboid transition (EAT), such as in hepatocellular carcinoma and breast cancer (Graziani et al., 2022).

Hence, it is important to investigate whether polarity proteins are asymmetrically distributed in the fat body tissue during larval stages, if so, whether that fat body becomes depolarized during the process of FBR, similar to the epithelium undergoing EMT.

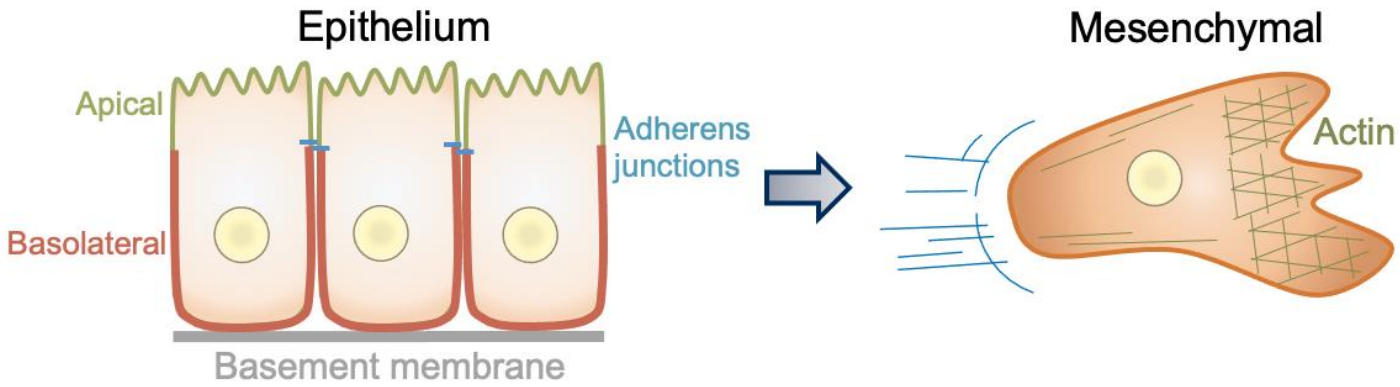
Epithelium
Apical
Basolateral
Adherens junctions
Basement membrane
Mesenchymal
Actin

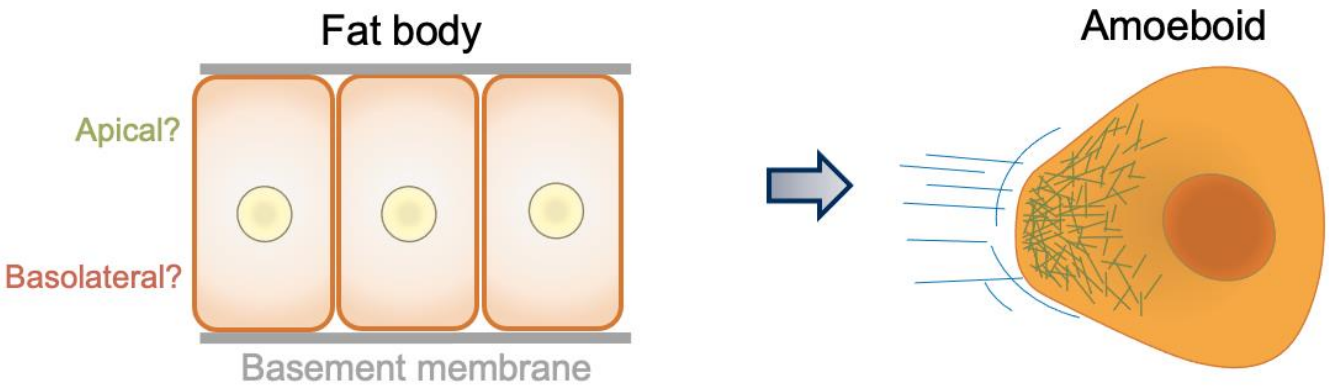
Fat body
Apical?
Basolateral?
Basement membrane
Amoeboid

Figure 1.9: Schematic representation comparing epithelial cells to fat body cells in *Drosophila*.

(A) Epithelial cells exhibit apicobasal polarity, with a basement membrane only on the basal side. Epithelial cells that undergo EMT result in cells that migrate in a mesenchymal mode of migration using actin stress fibers.

(B) Fat body cells, on the other hand, have a basement membrane on both sides, thus it is currently unknown, if fat body cells exhibit apicobasal polarity. After remodeling, fat body cells migrate by swimming in hemolymph using an ameboid mode of migration (Franz et al., 2018).

1.5. Aims and Objectives

In this study we propose that FBR may be classified as an EMT/EAT-like process. Indeed, during FBR, the fat body transitions from being a sheet of connected cells to becoming migratory cells by losing cell-cell and cell-basement membrane adhesion. Yet the cells in the fat body are not known to have an apicobasal cell polarity, a prerequisite of EMT.

The overall aim of this project is to characterize the process of fat body remodeling by:

1. Trying several approaches to live image fat body remodeling. This has previously never been done and would be a valuable approach to characterize the morphological changes happening during fat body remodeling in much more detail than previously described.

2. Assess if there is apicobasal polarity in the *Drosophila* larval fat body before the onset of FBR. I will use immunostainings to classic polarity proteins to assess for a potential asymmetric localization in the fat body.

3. Investigate how cell-cell adhesion is mediated in the larval fat body. Two different mechanisms of cell-cell adhesion have been proposed to mediate cell-cell adhesion in the larval fat body, one via E-Cadherin and one via Collagen IV. I will assess the subcellular localization of both and look at the effects of E-Cadherin knockdown in the larval fat body.

4. Test the effects of knocking down apicobasal cell polarity proteins in the larval fat body. I will knock down aPKC, Crumbs, Scribble and Lgl and assess for cell-cell adhesion defects.

5. Study how the loss of cell-cell adhesion is regulated during FBR and whether it involves loss of apicobasal polarity. I will assess whether apicobasal cell polarity and Collagen IV-based cell-cell adhesion gets lost as cells dissociate during FBR. Moreover, I will perform a candidate-based small screen to identify new regulators of FBR. Finally, I will assess how the positive candidates regulate loss of cell-cell adhesion during FBR.

Chapter II. Materials and methods

2.1 Fly husbandry

Drosophila melanogaster stocks were maintained on cornmeal molasses food in vials or bottles at 25°C and all crosses were performed at 25°C unless otherwise stated.

2.2 *In-vivo* delaying the process of FBR

I have attempted to delay FBR by around 10 hours when it would be possible to dissect the pupa out of the pupal case to live image the process of FBR. A dominant negative Ecdysone receptor (UAS-EcR-DN) was expressed using the fat body specific Lpp-Gal4 driver and temporally controlled the expression using the temperature sensitive repressor of the UAS-Gal4 system, Tub-Gal80(ts). Tub-Gal80(ts) is expressed under the tubulin promoter and at 18°C it acts as a negative regulator of the Gal4 transcriptional activator. At 18°C the Gal80 dimer binds to the Gal4 dimer and blocks the activation domain. In other words, Gal4 can still bind to the UAS sequence, but it can no longer activate transcription of the gene of interest. Deactivation of Tub-Gal80(ts) at 29°C, blocks the Gal80 dimer from binding to Gal4, thus allowing Gal4 to bind to the UAS enhancer sequence and initiate transcription of the downstream gene of interest.

;;Lpp-Gal4+UAS-GFP/ TM6C (balancer chromosome with tubby body shape) was crossed to ;UAS-EcR-B1/UAS-EcR-B1;Tub-Gal80(ts) / TM6C or crossed to ;Tub-Gal80(ts) / TM6C as a control. Initially, the vials were in 29°C for 8 days to deactivate the Tub-Gal80(ts) repressor, thus allowing Gal4 to activate expression of Ecdysone dominant negative to block FBR initiation at timings when it usually happens (~0-4 hours APF). This vial was flipped every

day to amplify the number of offspring being produced. Once third-instar larvae were visible in the vials, wandering L3-larvae were picked and placed into a new vial and stored it at 18°C to block expression of EcR and initiate the process of FBR with a delay. Because development takes twice as long at 18°C compared to 25°C, 0hr old pupa APF (WPP) were marked 16 hours (equivalent to 8hr at 25°C) after moving the non-tubby 3rd instar larvae into 18°C. The marked WPP were kept for another 32hr at 18°C (equivalent to 16hr at 25°C) before being dissected. A schematic of the experimental plan is shown in Figure 3.1 A. A quick identification of whether FBR has taken place is by looking to see if FBCs are now visible in the head, which is the case for the control pupa and not the Ecdysone dominant negative pupa. If fat body cells are not visible in the head of pupa that express Ecdysone dominant negative at the 32hr APF timepoint, then live imaging of a delayed FBR process using a confocal microscope should be attainable.

An alternative approach was used to only block Ecdysone signaling during late larval stages (3rd instar larvae). This was done by first placing the animals at 18°C for 8 days to activate the expression of EcR-DN during early developmental stages until the animals were young 3rd instar larvae, then at 29°C for 24 hours to allow the expression of EcR-DN to block initiation of FBR. Lastly, once the animals were wandering 3rd instar larvae, they were placed back at 18°C to block the expression of EcR-DN and allow FBR to take place within the animal but with a delay.

2.3 *Ex-vivo* live imaging

2.3.1 Approach currently used in Vilaiwan Fernandes' lab for culturing and imaging *Drosophila* larval brains.

2% low temperature gelling agarose in sterile water was made and stored at 4°C. 800µl of media containing Schneider's insect media, human insulin, PennStrap, Ecdysone hormone, and

foetal bovine serum was added into an Eppendorf tube and heated to 42°C on a portable heating block. 200µL of melted agarose solution was added into the Eppendorf tube containing media to a final concentration of 0.4% and the incubator was directly set to 34°C. A small “x” mark was made at the center of a 35x10mm petri dish and the dissected fat body was gently transferred on the “x” mark. 1ml of the media containing agarose was transferred gently starting from the edge of the dish until the fat body tissue is fully covered. The fat body tissue had to immediately and gently be oriented before the agarose solidifies. 15 minutes later, once the agarose had solidified, 3ml of cold media was added on top of the solidified agarose starting from the edge of the dish. Imaging was carried out using a 25x upright water-dipping lens.

2.3.2 Approach currently used in Yanlan Mao’s lab for culturing and imaging *Drosophila* wing discs.

The fat body tissue is first dissected from a L3-larvae, as mentioned above, in media containing Schneider’s insect media, human insulin, PennStrap, Ecdysone hormone, and foetal bovine serum. A hole was punched at the center of a small square sized double sided non-toxic tape. The tape was attached to the center of a fluorodish to create a round “well”. The fat body tissue was then transferred into the well with a small amount of media. The fat body was carefully oriented in a way to avoid tissue folding. Using forceps, a small piece of a Cyclepore Track Etched Membrane was gently laid on top of the well and the sides of the membrane were attached to the double-sided non-toxic tape. 3mls of media was pipetted into the dish, fully covering the fat body tissue. Imaging was then carried out using an inverted lens. The dish was sealed with parafilm to avoid liquid evaporation during long imaging sessions.

2.4 *In vivo* live imaging through the pupal case

White pre-pupae (WPP), (pupae aged 0hr APF) were gently washed in water ensuring no food was attached to the cuticle and kept to dry for 15 mins. A small piece of double-sided tape was attached on the center of a microscope slide and a pupa was placed and oriented at the center of the double-sided tape with the dorsal side facing upwards. The pupa's spiracles on the anterior and posterior ends were gently pushed onto the double-sided tape using the tips of the forceps and a *Drosophila* sorting brush was used to brush over the pupa carefully to attach the ventral side of the pupa to the double-sided tape. Using a syringe, 0.20ml of petroleum jelly was equally spread on each side of the double-sided tape. A 35mm glass-bottom dish was placed on the pupa ensuring the pupa is at the center of the observation area. The dish was then carefully pushed down until the cover slip touches the abdomen of the pupa and contractions can still be visualized under the stereo microscope. 5ml of water was then pipetted into the dish. Imaging was carried out using a 20x upright water dipping lens on a Zeiss multiphoton microscope.

2.5 Dissections of *Drosophila* larval and pupal fat body and of pupae from their pupal case

For the initial experiment of investigating whether the fat body tissue of an L3-stage larva is polarized, the fat body tissue from wandering L3-larvae was dissected by removing the posterior end then turning the animal inside-out using fine forceps. The carcass was first removed, followed by the gut then trachea then the brain.

After discovering the symmetry in the structure of the L3-stage larval fat body tissue; wandering L3-stage larva were selected and placed in water to remove excess food, then placed

on a sylgard-coated depression dish. Animals were placed on their dorsal side and pinned by the tail and mouth hooks. Spring-scissors were used to first make a horizontal incision just anterior to the posterior end of the larva, then a vertical cut along the dorsal midline towards the rostral end of the larva. Finally, a horizontal cut was made to the left and right of the pin at the rostrum of the animal. The flaps were pinned in a clockwise order to ensure that the animal's body is stretched both horizontally and vertically. L3-larvae were then fixed in PBS containing 4% Paraformaldehyde for 30 minutes, to allow the organs to float and facilitate organ removal. For fat body dissections, the trachea along with the gut were first removed, ensuring the fat bodies were kept along the sides of the animal. An incision on the anterior end of the "right side" of the fat body was then made. These right halves of fat body tissues were then placed in 96- well plates and washed twice with PBS. The dissected tissues can be stored in PBS for up to 5 days at 4°C. This dissection method was also used to dissect fat body tissues from 3hr APF pupa.

For identifying new regulators of fat body remodeling experiments, white prepupa were marked and placed at 25°C for 16 hours. 16hr APF pupa were then picked and wiped to remove excess food attached to the cuticle, then placed and sticked on double sided tape on a microscope slide. The pigmented cuticle was then peeled carefully to avoid pocking and killing the animal. The animals were then picked using fine forceps and placed on a glass bottom dish with the dorsal side facing upwards for head count imaging using a fluorescent dissecting scope. For confocal imaging, the ventral side of the animals were facing upward to allow inverted confocal imaging on the dorsal thorax.

2.6 Immunohistochemistry

The dissected fat body tissues were fixed in PBS containing 4% Paraformaldehyde for 30 minutes. L3-larval fat body tissue dissections were permeabilized in PBS containing 1% Triton-X-100 in PBS (PBT) at room temperature and blocked in PBT with 4% fetal bovine serum (FBS). The dissected L3-larval fat body tissues were then incubated overnight at 4°C with primary antibodies diluted in PBT. After three washes in PBS, the dissected fat body tissues were incubated with secondary antibody, anti-rat 567nm (1:200; abCAM), anti-mouse 567nm (1:200; abCAM), anti-guinea pig 567nm (1:200; abCAM), anti-rabbit 567nm (1:200; abCAM), for 2 hours at room temperature. Fixed and stained preparations were mounted on DAPI-vectashield and prepared for imaging.

2.7 Electron microscopy

Fat body tissues were dissected from L3-stage larva, fixed in 2% Paraformaldehyde and 1.5% (v/v) glutaraldehyde in 0.1 M cacodylate. After three washes in 0.1M cacodylate, the fat body tissues were post-fixed in 1% osmium tetroxide and 1.5% K3[Fe(CN6)] for 1 hour at room temperature then rinsed three times with ddH_2O. After osmium-ferricyanide staining, fat body tissues were treated with 1% thiocarbohydrazide (TCH) solution for 20 minutes at room temperature. This was followed by a secondary staining with 2% osmium tetroxide for 30 minutes at 4°C to further enhance staining of membranes and lipid-rich structures, thus enhancing contrast. After three washes with ddH_2O, fat body tissues were stained with 1% aqueous uranyl acetate overnight at 4°C. Next, the tissues were incubated with freshly made lead aspartate solution for 30 minutes at 60°C. After being rinsed with buffer and gradually dehydrated with increasing concentrations of ethanol (70%, 90%, 100%), the fat body tissues

were infiltrated with a graded series of EPON (e.g., 50% resin in propylene oxide for 1 hour to 100% resin for 2 hours at room temperature). The tissues were then placed carefully in blocks, polymerized in 100% resin and baked overnight in 60°C.

2.8 Screen to identify new regulators of FBR

I performed a literature search of genes known to be involved in tissue remodeling and EMT-like models in different tissues of *Drosophila melanogaster*. The modENCODE Tissue Expression Data on fly base showing the expression of gene in L3-larvae (before FBR), WPP (0hr APF), and pupae P8 (long after FBR 47hr-57hr APF) provides an indication of expression changes before and during FBR and thereby might indicate whether a gene might play a role in fat body remodeling by showing the expression of the gene in L3-larvae (before FBR), WPP (0hr APF), and pupae P8 (after FBR 47hr-57hr APF). Two different approaches can be used to test the requirement of a gene in FBR: (1) crossing the RNAi line to "*Lsp2-Gal4+UAS-NLS-mCherry*" to assess whether the RNAi leads to a reduction in the number of fat body cells in the head in a 16hr old APF pupae, when remodeling is usually complete and when some FBCs would have normally moved into the head in the control. (2) crossing the RNAi line to "*Lpp-Gal4+UAS-myr-td-tomato*" to assess whether fat body cells in the dorsal abdomen and thorax failed to dissociate at 16hr old APF or had undergone partial dissociation (delay in FBR).

2.9 Imaging and Analysis

Microscope images were created by Leica SP8, Zeiss-vis and Zeiss multiphoton using 63x objectives. All analysis was done using Fiji-ImageJ (Schindelin et al., 2012)..

For quantification, orthogonal (X/Z) views were generated from the central plane of each Z-stack. Fluorescence intensities were measured using ROIs. All data analysis and graphs are created in Prism 9.

2.9.1 Analysis of CIVICs

CIVICs quantifications were performed on the maximum projection of the top 10 layers within the z-stack. Since CIVICs are not visible on the surface layers of the tissue, the 10 layers (step size: 2.5 micrometer) that were quantified were selected starting from the 10^{th} layer below the surface of the z-stack. A threshold rage of 43-255 was applied in Fiji and particles with sizes from 0.2-infinity (pixel^2) were identified and analyzed.

2.9.2 Analysis of polarity proteins knockdowns

Quantifications of dissociation caused by polarity protein knockdowns were performed from 30 layers into the z-stack from the surface of the tissue, continuing to the final layer of the z-stack. Tricellular and bicellular gaps were counted manually using the cell counter plugin on FiJI-ImageJ (Schindelin et al., 2012).

2.10 Statistical analysis

Graphpad Prism software was used to analyze data and generate graphs. For statistical analysis, I used parametric paired t-test, to compare the average mean intensities of polarity proteins at wandering L3-stage larva and 3hr APF, basement membrane surface intensities and

the number of CIVICs in the first 10 layers of the z-stack between the two sides of the fat body tissue (side a and b). Parametric One-Way ANOVA, followed by Dunnett's multiple comparison test was used to compare tricellular and bicellular gaps and the number of CIVICs of the polarity proteins knockdowns to the control, as well as, average mean intensities of Dlg, Par-3, and Crumbs when UAS-EcR-B1-DN or UAS-Srp-RNAi are expressed on either side a or b. One-way ANOVA (Kruskal-Wallis test) followed by Dunn's multiple comparison test was used to analyze the number of fat body cells in the heads of 16hr APF pupa in several genotypes. Statistical tests used in each experiment are indicated in the relevant figure legends.

2.11 Fly strains

Genotype	**Source**	**Identifier**
Lpp-Gal4	Gift from Pierre Leopold	N/A
Lsp2-Gal4	Bloomington *Drosophila* Stock Center (BDSC)	6357
Ubi-Caax-GFP	*Drosophila* Genomics Research Center	109824
Tub-Gal80ts	Gift from Paul Martin's Lab	N/A
UAS-EcR-B1-DN	BDSC	6869

UAS-GFP	BDSC	6658
UAS-Serpent-RNAi	VDRC	109521
UAS-Serpent-RNAi	VDRC	35578
UAS-lifeactin-GFP	Gift from Stramer Lab	N/A
UAS-Myr-td-Tom	BDSC	32221
UAS-NLS-mCherry	BDSC	38424
w67	Lab stock AF	508
UAS-Broad-complex-RNAi	VDRC	104648
UAS-Twist-RNAi	VDRC	37092
UAS-Pebble-RNAi	VDRC	109305
UAS-Pebble-RNAi	VDRC	35350
UAS-Snail-RNAi	VDRC	50004
UAS-Snail-RNAi	VDRC	50003
Lgl-GFP	BDSC	63183
UAS-aPKC-RNAi	BDSC	34332
UAS-aPKC-RNAi	VDRC	105624
UAS-Scribble-RNAi	BDSC	35748
UAS-Scribble-RNAi	VDRC	105412
UAS-Crumbs-RNAi	BDSC	34999

UAS-Crumbs-RNAi	VDRC	39177
UAS-Crumbs-RNAi	VDRC	330135
UAS-Crumbs-RNAi	BDSC	40869
UAS-Lgl-RNAi	VDRC	109604
UAS-Ecad-RNAi	VDRC	103962
UAS-Ecad-RNAi	VDRC	27082
UAS-Ecad-RNAi	BDSC	32904
Vkg-GFP	*Drosophila* Genomics Resource Center	110626

2.12 Antibodies and reagents

Antibodies	**Source**	**Identifier/RRID**
Mouse monoclonal anti-crb (1:50)	Developmental Studies Hybridoma Bank (DSHB)	Cat# Cq4 RRID: AB_528181
Guinea pig monoclonal anti-Lgl (1:50)	Pichaud Lab	N/A
Mouse monoclonal anti-dlg1 (1:20)	DSHB	Cat# 4F3 anti-discs large RRID: AB_528181
Rabbit monoclonal anti-par-3 /Bazooka (1:2000)	Pichaud Lab	N/A

Guinea pig monoclonal anti-par-6 (1:500)	Pichaud Lab	N/A
Rabbit monoclonal anti-aPKC (1:500)	Pichaud Lab	N/A
Rat monoclonal anti-De-cad (1:20)	DSHB	Cat# DCAD2 RRID: AB_528120
Mouse monoclonal anti-mys (1:20)	DSHB	Cat# CF.6G11 RRID: AB_528310
Chemicals and Reagents		
Schneider's *Drosophila* medium	ThermoFisher Scientific	Cat# 21720024
Growth factor insulin	Mao Lab	N/A
Antibiotic PennStrap	Fernandes Lab	N/A
Bovine Serum Albumin	Merck	12352202

Results

Chapter III. Testing different approaches to live image fat body remodeling

3.1 *In-vivo* delaying the process of Fat Body Remodeling

Up to date, only two papers have studied the process of FBR, giving a brief description of the process by imaging fat body isolated from the animal at different stages. Their results suggested that during the process of FBR, FBCs appear to first be polygonal in shape which then round up and undergo dissociation from neighboring FBCs (Bond et al., 2011). The reason for this rough description is because live imaging is not thought to be possible at early pupal stages since the opaque pupa case cannot be peeled off, thus the only way previous studies have studied FBR was by squeezing out the interior of the animal along with the labelled fat body tissue onto a microscope slide prior to imaging.

For my project, I first wanted to study the morphological changes occurring during the process of FBR in more detail and with higher spatiotemporal resolution in the wild type condition. The process of FBR has been reported to occur from 4-12hr After Puparium Formation (APF, at 25°C) (Bond et al., 2011), when it's not possible to dissect the pupa out of the pupal case for *in vivo* live imaging. Moreover, during this stage there are many muscle contractions leading to the frequent movement of the fat body within the animal's body. Thus, I attempted to delay the process of FBR by ~10hr, when the pupa can be dissected and there are more muscle contractions. I tried this by temporarily expressing EcR-DN to block initiation of FBR at the time when it would normally happen and then releasing this block in order for the delayed FBR to

happen at around ~14-22hr APF. This rationale was as follows: In WT, FBR is induced by Ecdysone binding to its receptor EcR in the fat body around the wandering third instar stage. FBR is then complete when the cells are fully dissociated around 12hAPF. This is also when the individual FBCs translocate into the head and other body parts following head eversion which happens at 12hr APF (at 25°C). When UAS-EcR-DN is expressed in the fat body with the fat body specific driver Lpp-Gal4, FBR is blocked and the tissue remains as a sheet and hence no FBCs are found in the head, apart from the area near the thorax, after head eversion from 12hAPF onwards. I thought that if I initially allowed expression of EcR-DN in the fat body up to the wandering third instar stage, I would block FBR when it would normally get induced. But if I then blocked the expression of EcR-DN from late wandering instar stage onwards, FBR would then be induced with a delay, assuming that there would still be sufficient Ecdysone in circulation. If the timing was right, this would ideally lead to FBR to only start just after head eversion and I would then not see any FBCs in the head at the equivalent time of 16hr APF (at 25°C) since the cells would still be in a sheet; while if I checked the same pupae later at the equivalent time of 24hr APF (at 25°C), there would be individual FBCs found in the head. However, it could also happen that this protocol permanently blocked FBR and no cells would be seen in the head at the later stage or that it didn't delay FBR enough and individual cells would be seen in the head already following head eversion.

To try whether this protocol could work, I expressed UAS-GFP (to label FBCs) either alone (control) or with UAS-EcR-DN using an early fat body specific "Lpp-Gal4" driver which drives expression starting from the first instar larval stage and temporally controlled its expression using Tub-Gal80(ts), the temperature sensitive repressor of the UAS-Gal4 system. I initially kept the animals at 29°C to deactivate the repressor and allow the expression of EcR-DN

in the fat body to block Ecdysone signaling, thus blocking the initiation of FBR at normal timing (~4-12hr APF at 25°C). I then removed the block of Ecdysone signaling by moving animals to 18°C during the late larval stage to activate the repressor and block the expression of EcR-DN (Figure 3.1 A). To ensure that I have successfully delayed the process of FBR with my temperature regime, I dissected and inspected FBCs at the 32hr APF timepoint (at 18°C), which due to the slower rate of development at this lower temperature is equivalent to 16hr APF (at 25°C) when I expected to see no FBCs in the head of the pupa expressing EcR-DN in contrast to the control. I then reassessed the same pupae later at 56h APF (at 18°C) which is equivalent to 32h APF at 25°C. This is when I expected to see some or many individual FBCs present in the head of the pupa expressing EcR-DN. However, my results showed that only 3/9 pupae had successfully delayed FBR. In these three pupae expressing EcR-DN no individual FBCs were seen in the head of the pupa at the 32hr APF (at 18°C) while several individual FBCs (9-36 cells) were seen at 56h APF (at 18°C; Figure 3.1 C at the top), in comparison to the control where more than 30 FBCs were visualized in the head at both time points (Figure 3.1 B). Furthermore, the remaining 6 out of 9 pupae expressing EcR-DN have undergone a partial delay in FBR, where few FBCs were present in the head at the 32hr timepoint and the number of FBCs increased at the 56hr timepoint, indicating that FBR had been partially delayed (Figure 3.1 C at bottom). Figure 3.1 D shows a summary table of the results.

Because only a few pupae managed to partially delay FBR, figuring out the exact timing at which animal pupate at 18°C is essential to have a higher N number. Since, animals have pupated at different timings; troubleshooting was done to try to age animals using embryo cages in order to have the majority of the animals pupating at the same time. Flies were placed in a cage and onto an apple juice agar plate with yeast to induce egg laying. Initially flies were left to

lay eggs onto the apple juice agar plates for 24 hours before starting the experiment where the flies would be flipped onto a new apple juice agar plate with yeast every hour to have pupae aged within a smaller range and expected to pupate within the same timing. However, this is not successful since the number of embryos laid on each plate were low, leading to slime accumulation in the vials and lethality before pupal stages.

A

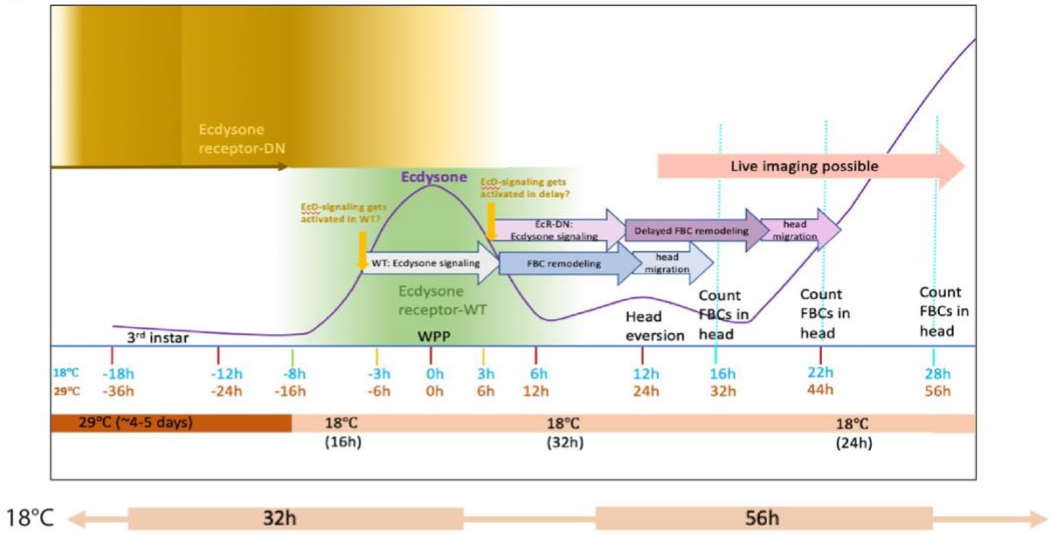

B

Control (N=10)

(Lpp-Gal4+UAS-GFP x w67 + Tubgal80^{ts})

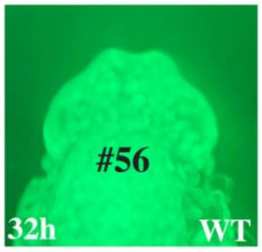

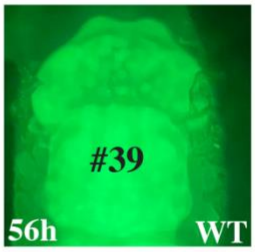

C

UAS-EcR-DN (N=9)

(Lpp-Gal4+UAS-GFP x UAS-EcR-DN + Tubgal80^{ts})

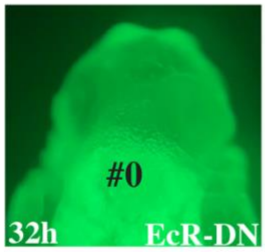

Successful delay of FBR

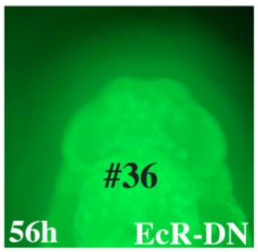

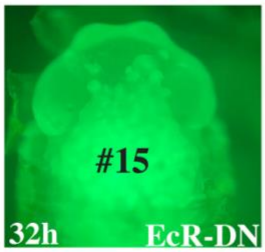

Partial delay of FBR

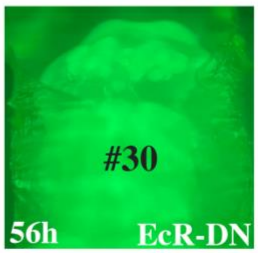

D

Summary of Results

	N number	WT timing of FBR (# 30-56 → #↓)	Successful delay of FBR (#0 → # 9-36)	Permanent block of FBR (# 0 → # 0)	"Partial delay" of FBR (# 10-26 → #↑)
Control	10	10	0	0	0
UAS-EcR-DN	9	0	3	0	6

F

Figure 3.1: Delaying FBR by blocking Ecdysone signaling all throughout early developmental stage.

(A) Schematic of the experimental plan to delay FBR by blocking Ecdysone signaling early on in development.
(B) Shows FBCs present in the head of the control pupa (Lpp-Gal4+UAS-GFP+tubGal80ts) at the 32h timepoint and with a decrease in the number of FBCs in the head 24hrs later.
(C) Pupa that expressed EcR-DN (Lpp-Gal4+UAS-GFP+UAS-EcR-DN+tubGal80ts) varied in results where only 3/9 had successfully delayed FBR (0 FBCs in the head at the 32h timepoint and few FBCs present in the head 24hr later, example at top) while the majority had a “partial” delay (few FBCs in the head at the 32h timepoint and the number of FBCs increased 24hr later, example at bottom). All animals were marked 16hr after being transferred to from 29 to 18°C during wandering third instar stage, dissected and imaged using a fluorescent dissecting microscope. Number of FBCs counted in head shown inside pictures.
(D) Summary table of the results.

Although there is no evidence in the literature for the earlier role of Ecdysone signaling in the fat body tissue during early developmental stages, it is known that Ecdysone signaling is important in directing developmental transitions such as larval molting and metamorphosis (Ishimoto et al., 2009). Therefore, to avoid any potential negative effects of blocking Ecdysone signaling in the fat body before the third instar larval stage, I adjusted the protocol to only block Ecdysone signaling starting from early 3rd instar larvae. For this purpose, the animals were first kept at 18°C for about 8 days, to activate the repressor and block the expression of EcR-DN during early developmental stages. Once the animals were young 3rd instar larvae, they were placed at 29°C for 24 hours to deactivate the repressor and allow the expression of EcR-DN in order to block the initiation of FBR (Figure 3.2 A). Lastly, the animals were placed back at 18°C during the wandering third instar stage (followed by marking newly formed 0hAPF pupae 16h later) to block the expression of EcR-DN and allow FBR to take place within the animal with a delay. Since very low numbers of pupae newly pupated 16hr after switching the temperature from 29 to 18°C, new pupae that pupated 14-18hr were marked instead. My results revealed that 5/35 pupa expressing EcR-DN had successfully delayed FBR, while 3/35 had a permanent block of FBR where no FBCs were seen at the 32h timepoint and 44h timepoint (Figure 3.2 C). In addition, 11/35 have failed to delay FBR (Figure 3.2 C), since they were similar to the control (Figure 3.2 B) with large numbers of FBCs being present in the head of pupa expressing EcR-DN at the 32h timepoint and the number of FBCs slightly decreased at the 44h timepoint. Overall, the majority of the pupa (16/35) expressing EcR-DN exhibited a partial delay where small numbers of FBCs were present at 32h which then increased by 44h (Figure 3.2 C). Figure 3.2 D shows a summary table of the results.

Overall, the attempt of setting up a protocol to delay FBR was only partially successful. I decided not to proceed with it by optimizing it, since we worried, that this approach might have other negative side effects. During metamorphosis, some tissues such as the fat body undergo changes needed to promote pupal development and to meet the needs of the adult fly. The fat body is known to release lipids following Ecdysone-induced FBR needed to support pupal growth (H. Zheng et al., 2017). Indeed, inhibition of FBR is associated with late pupal lethality, suggesting the importance of FBR for development (Nelliot et al., 2006). Thus, delaying FBR might not be ideal since it may lead to developmental abnormalities.

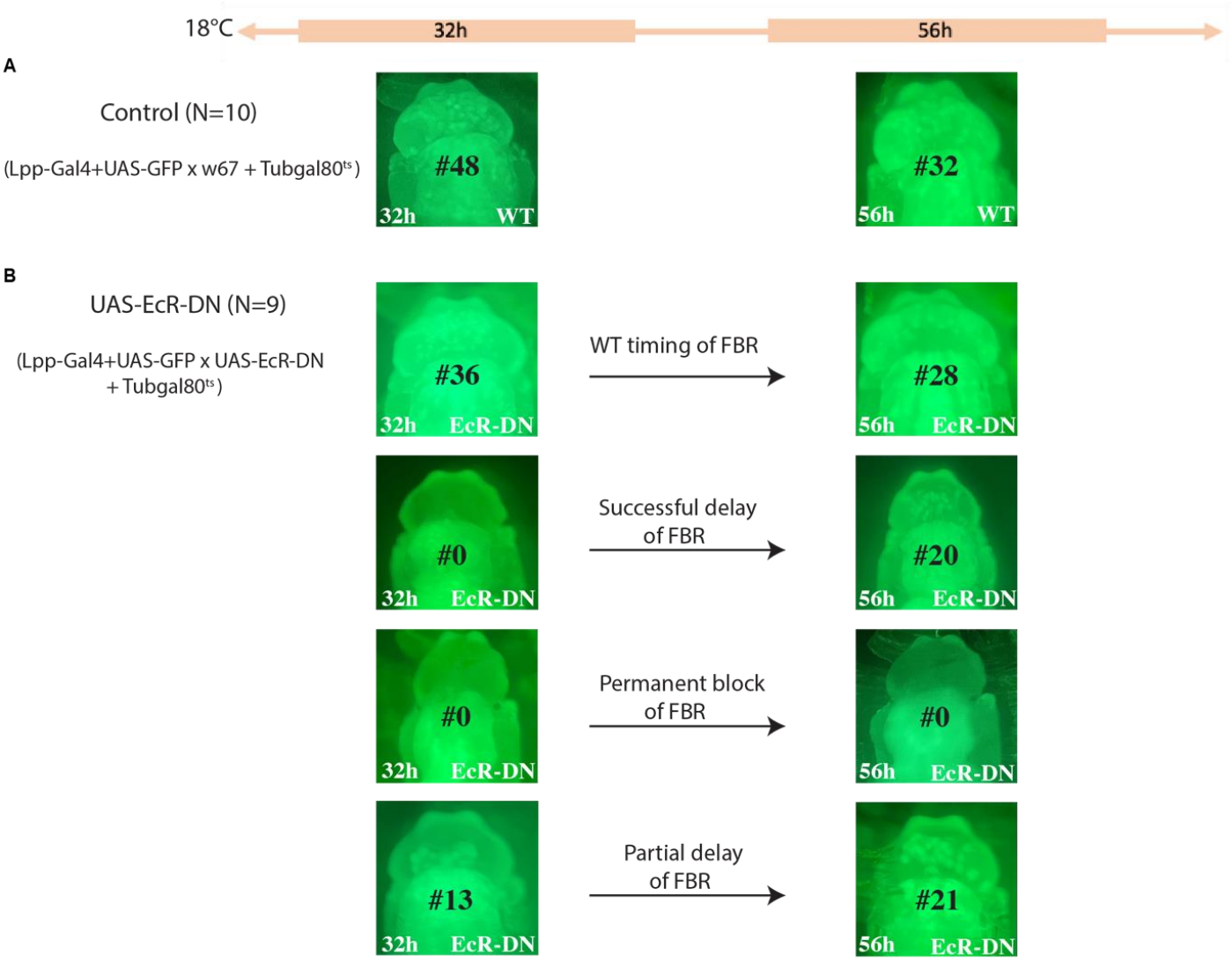

C

Summary of Results					
	N number	WT timing of FBR (# 26-46 → #↓)	Successful delay of FBR (#0 → # 5-20)	Permanent block of FBR (# 0 → # 0)	"Partial delay" of FBR (# 6-30 → #↑)
Control	10	10	0	0	0
UAS-EcR-DN	35	11	5	3	16

Figure 3.2: Delaying FBR by blocking Ecdysone signaling only during early L3-stage larvae.

(A) Shows FBCs present in the head of the control pupa (Lpp-Gal4+UAS-GFP+tubGal80ts) at the 32h timepoint and with a decrease in the number of FBCs in the head 24hrs later.

(B) Pupa that expressed EcR-DN (Lpp-Gal4+UAS-GFP+UAS-EcR-DN+tubGal80ts) varied in results where only 5/35 have successfully delayed FBR (0 FBCs in the head at the 32h timepoint and few FBCs present in the head 24hr later) while the majority has a “partial” delay (few FBCs in the head at the 32h timepoint and the number of FBCs increase 24hr later). Animals were first kept for 5 days at 18°C, then during third instar stage for 24h at 29°C and then kept again at 18°C. Control animals that had just pupated were marked 16hr, while EcR-DN animals were marked from 14-18hrs after being transferred from 29°C to 18°C. Imaged using fluorescent dissecting microscope.

(D) Summary table of the results.

3.2 *Ex-vivo* live imaging

In parallel to the FBR delay experiment, I also tried two different *ex vivo* live imaging approaches. One approach is currently being used in the Fernandes lab to culture and image *Drosophila* larval brains, where the brains are mounted in agarose. The second *ex vivo* approach is currently being used in the Mao lab for culturing and imaging *Drosophila* larval wing discs.

3.2.1 Approach currently used in Vilaiwan Fernandes' lab for culturing and imaging *Drosophila* larval brains.

This approach involved imaging dissected fat body tissue mounted in agar with medium containing added Ecdysone hormone in a petri dish. The idea was to dissect and mount the fat body tissue of an L3-stage larvae, a stage just a few hours before FBR normally starts, in agar to help hold the fat body tissue in place to be able to image the various steps of FBR from morphological changes to dissociation and motility. To test this method, I started by dissecting the fat body tissue from L3-stage larvae expressing Caax-GFP protein. Caax-GFP is a protein that localizes to the plasma membrane as well as, internal membranes. A medium containing Ecdysone, Schneider, growth factor insulin, antibiotic PennStrap and growth promoting fetal bovine serum is added on top of the agar containing the fat body tissue. However, a major issue was then encountered where the fat body tissue tended to float and move away from the field of view several minutes after agarose had solidified and after pouring the cold media on top of the agarose. As a result, this issue made it tricky to image the fat body tissue. It was manageable to take several images on the confocal (Figure 3.3 A) just before the fat body tissue floated away, however imaging for longer hours was not possible. Troubleshooting was done to try to hold the fat body tissue in the agar where I tried increasing the concentration of agarose to 4% rather

than using low gelling agarose. 4% agarose helped hold the fat body tissue for a longer period of time but not long enough to allow imaging for a couple of hours. Initially, forceps were used to help hold the fat body tissue in place until the agar solidifies. However, only the middle region of the fat body tissue was pushed down in the agar using the forceps, thus only the middle region of the fat body tissue was imaged (Figure 3.3 B “blue arrow”), while the sides of the tissue would either be floating (Figure 3.3 B “white arrow”) above the agarose or mounted very deep into the agarose. Moreover, within a couple of minutes the entire fat body tissue mounted close to the surface of the agarose would be floating in the petri dish, limiting the ability to acquire further confocal images.

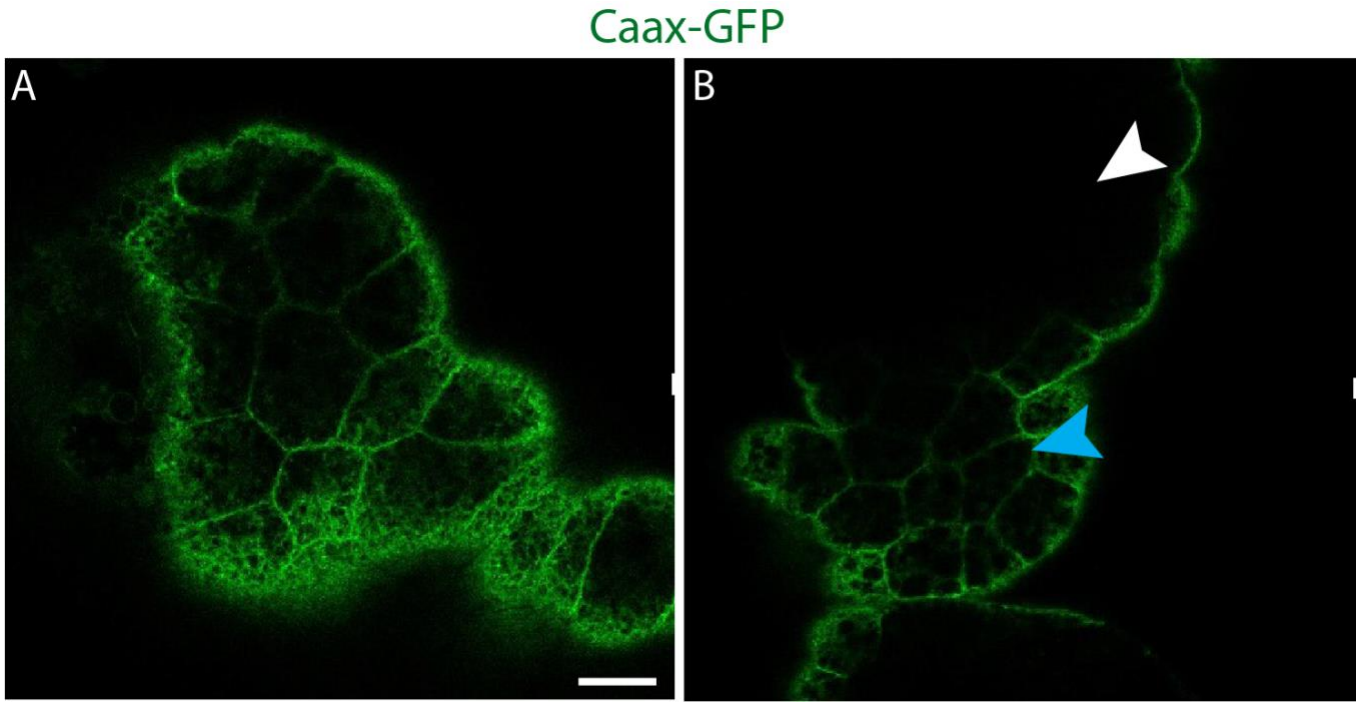
Caax-GFP
A
B

Figure 3.3: Dissected fat body tissue of L3-stage larvae mounted in agarose.

(A) Single focal plane of the fat body tissue for L3-stage larvae expressing Caax-GFP protein that localizes to membranes.

(B) Single focal plane of the fat body tissue from L3-stage larvae expressing Caax-GFP protein, where only the middle area of the fat body tissue can be visualized “blue arrows” while both ends of the tissue are floating above the solidified agarose “white arrow”.

Imaged using Zeiss-vis 40x water immersion lens. Scale bars = 20μm

3.2.2 Approach currently used in Yanlan Mao's lab for culturing and imaging *Drosophila* wing discs

The second approach that was used involved dissecting the fat body tissue from an L3-stage larvae in viscous cellulose media consisting of Schneider, antibiotic PennStrep and growth promoting fetal bovine serum, then mounting the fat body tissue on a fluoro-dish filled with medium containing the hormone Ecdysone and growth factor insulin. A permeable membrane was then placed on top of the fat body tissue to help hold the tissue in place and avoid floating while the tissue was imaged from the bottom. Technical issues like the microscope stage drifting initially limited my results. Once the microscope stage drifting issue was fixed, another issue came up where the tissue floated in the medium, thus going out of focus while taking long movies. However, I managed to get at least one high resolution movie, where the fat body tissue remained close to the glass bottom dish and did not float much. Figure 3.4 shows still images from a timelapse movie of fat body cell-cell dissociation starting at tricellular junctions and then spreading along the length of the junction. Moreover, thread-like structures were observed as two fat body cells began to dissociate (Figure 3.4 A2'). Yet, floating of the fat body tissue in the region between the membrane and the dish remained an issue and limited my results. Therefore, I adjusted the protocol by placing a membrane made of 4% agarose rather than the Cyclepore Track Etched Membrane to help hold the tissue down to the bottom of the glass bottom dish and reduce the risk of the tissue floating. Similar to Figure 3.4, cell-cell separation at a tricellular junction and then spreading along the length of the junction with thread-like structures was observed (Figure 3.5 A2'). Additionally, circular blobs seem to appear in gaps between the dissociated cells (Figure 3.5 A3', A2'' and A3'' "white arrows"). This adapted method using a membrane of agarose was only successfully used a few times, since the piece of agarose often

tended to float in the media, resulting in the fat body tissue not being close to the glass bottom dish, thus going out of focus when imaging.

Lastly, I tried altering the experiment, where the fat body tissue dissected from L3-stage larvae was mounted in the initial way (in a well, made by punching a hole on a non-toxic tape and covered with a membrane), except additionally having the brain, which is the source of Ecdysone, floating in the medium prior to imaging. In this case, interestingly, I observed morphological changes where cells went from polygonal to round (Figure 3.6 A2'). Moreover, I observed blebbing of cells (Figure 3.6 A3'). Since blebbing is one of the defined features of apoptosis (Wickman et al., 2013), I initially thought that the cells were dying. However, I repeated this experiment with the brain floating in media but without adding growth factor insulin in the media which, in contrast to previous experiments, led to tissue shrinkage and FBCs appeared to be dying without any blebbing (Figure 3.7). Although this method still need optimization to try to avoid having the tissue floating in media, it is more promising than previous experiments since it allows to me to image with a higher resolution which led to novel detailed observations on the process of FBR that have never been described before.

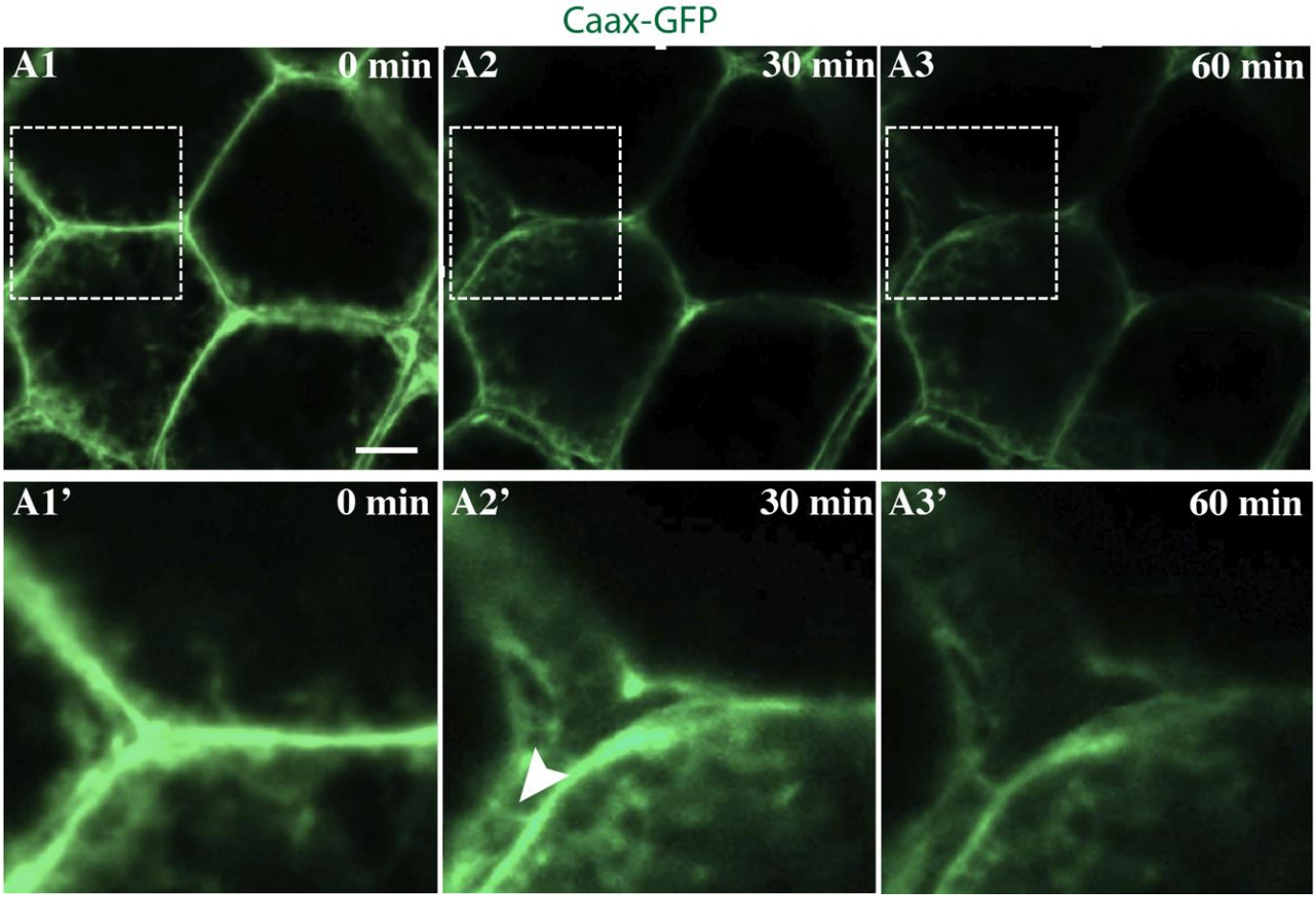
Caax-GFP
A1
0 min
A2
30 min
A3
60 min
A1'
0 min
A2'
30 min
A3'
60 min

Figure 3.4: *Ex-vivo* live imaging of the fat body tissue from L3-stage larvae using the original Mao method.

(A1-A3') Confocal images from time-lapse movie of fat body from L3-stage larva expressing Ubi-Caax-GFP protein to label the plasma membrane.

(A1-A1') At 0 min three fat body cells are closely attached to each other by cell-cell junction (A1), a zoomed in picture is shown in (A1').

(A2-A2') 30 mins later, separation of fat body cells starting from tricellular junctions can be observed (A2). (A2') shows a zoomed in picture where thread-like structures can be observed as the fat body cells are separating.

(A3-A3') Fat body cells continue to separate starting from tricellular junctions and simultaneously along the length of the junction, a zoomed in picture is shown in (A3').

Imaged using Zeiss-vis 63x oil immersion lens. Scale bars = 20μm

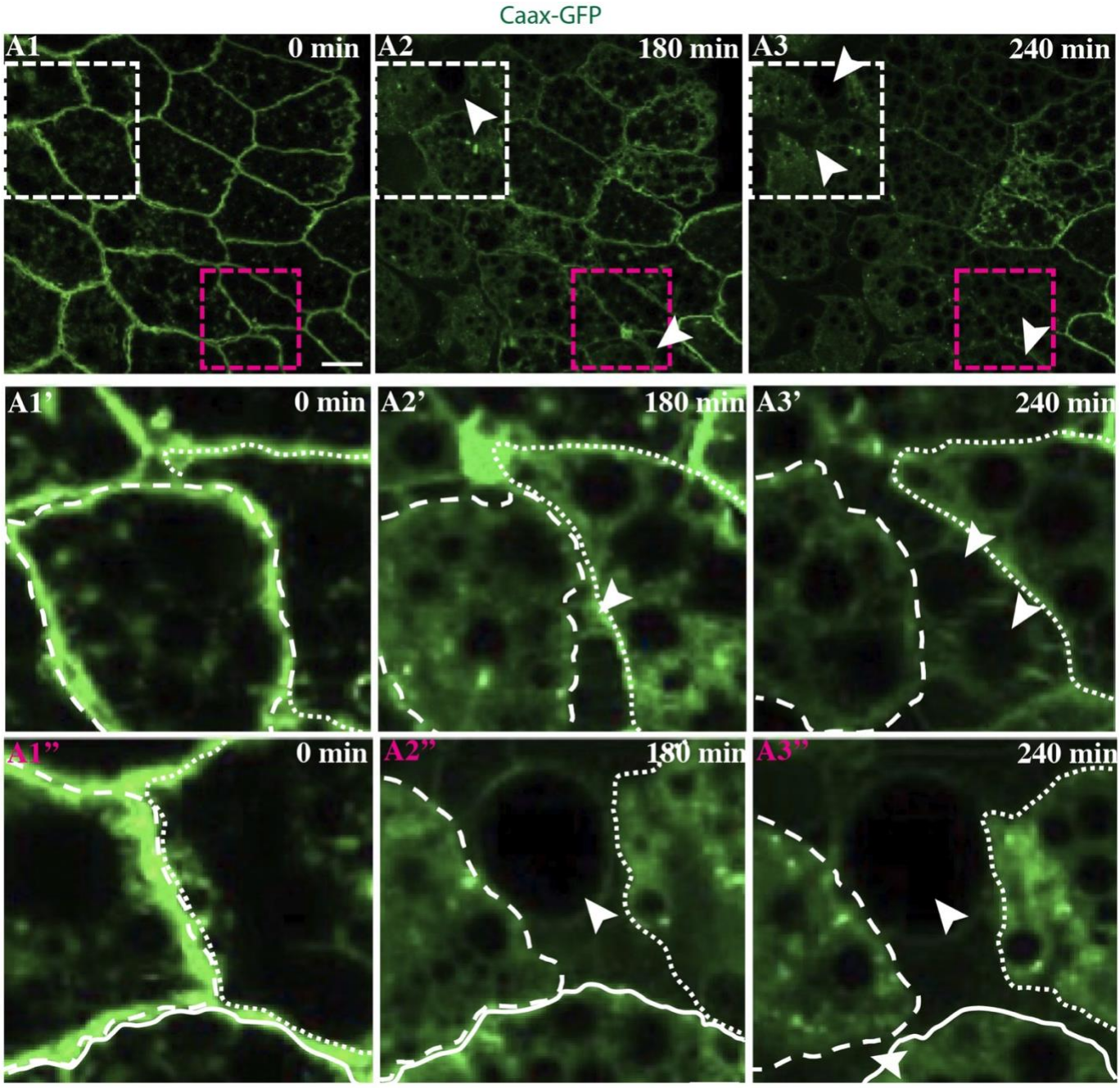
Caax-GFP
A1
0 min
A2
180 min
A3
240 min
A1'
0 min
A2'
180 min
A3'
240 min
A1"
0 min
A2"
180 min
A3"
240 min

Figure 3.5: *Ex-vivo* live imaging of the fat body tissue from L3-stage larvae using the adapted method containing agarose.

(A1-A3'') Confocal images from time-lapse movie of fat body from L3-stage larva expressing Ubi-Caax-GFP protein to label the plasma membrane.

(A1-A1') At 0 min fat body cells are closely attached to each other by cell-cell junction, a zoomed in image is shown in (A1').

(A2-A2'-A2'') 3 hours later, some cells seem to dissociated (A2), a zoomed in image is shown in (A2'); while other cells seem to have dissociated before 3 hours and blobs (arrowhead) seem to appear in gap between two fat body cells once the cells have undergone dissociation (A2); a zoomed in image is shown in (A2'').

(A3-A3') These blobs are also observed 6 hours into FBR in some cells(A3); a zoomed in image is shown in (A3').

Imaged using Zeiss-vis 63x oil immersion lens. Scale bars = 20μm.

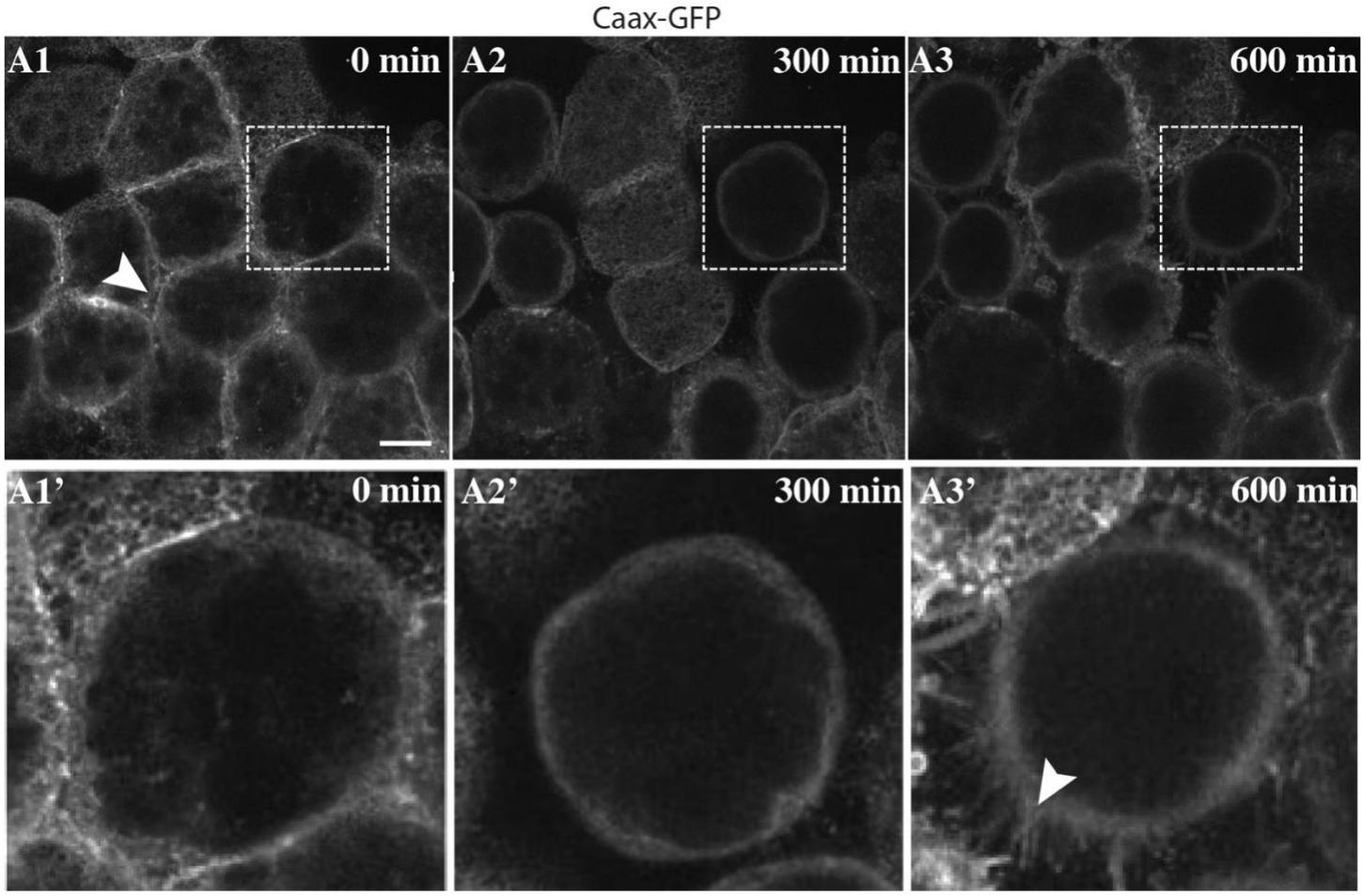
Caax-GFP
A1
0 min
A2
300 min
A3
600 min
A1'
0 min
A2'
300 min
A3'
600 min

Figure 3.6: *Ex-vivo* live imaging of the fat body tissue from L3-stage larvae using the original Mao method, except having the brain, which is the source of Ecdysone, floating in the medium.

(A1-A3') Confocal images from time-lapse movie of fat body from L3-stage larva expressing Ubi-Caax-GFP protein to label the plasma membrane.

(A1-A1') At 0 min fat body cells are closely attached to each other by cell-cell junction, however some fat body cells begin to detach (A1 white arrow); a zoomed in image is shown in (A1').

(A2-A2') 5 hours later, some fat body cells seem to have completely rounded up and detached from neighboring fat body cells (A2); a zoomed in image is shown in (A2').

(A3-A3') Shows fat body cell blebbing (A3); a zoomed in image is shown in (A3', arrowhead).

Imaged using Zeiss-vis 63x oil immersion lens. Scale bars = 20μm.

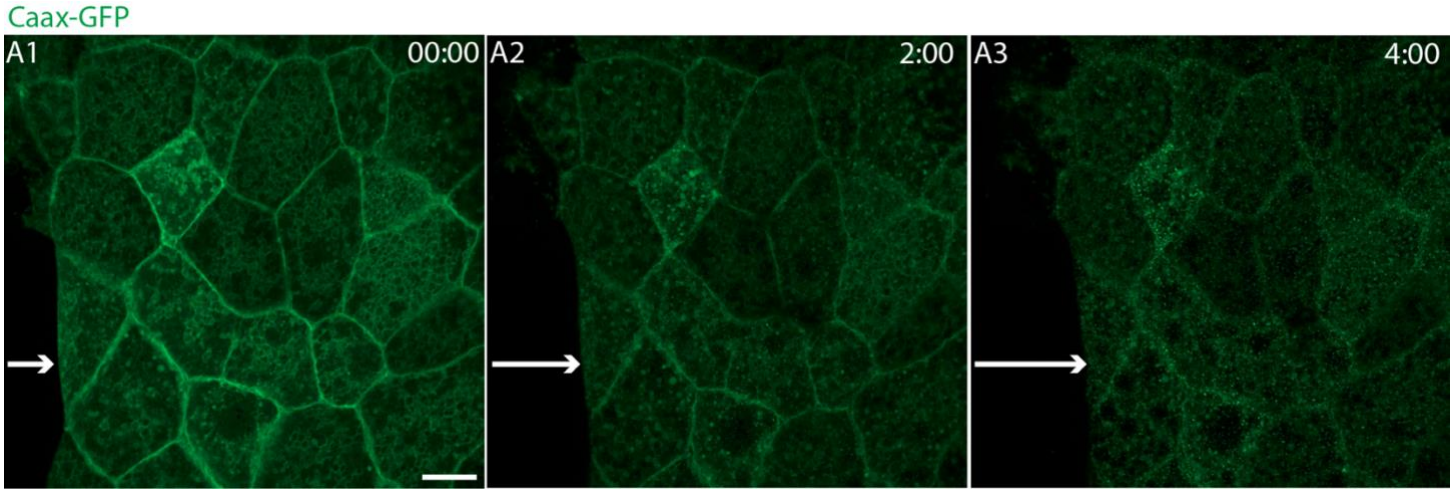
Caax-GFP
A1
00:00
A2
2:00
A3
4:00

Figure 3.7: *Ex-vivo* live imaging of the fat body without adding Ecdysone hormone in the medium.

(A1-A3) Confocal images from time-lapse movie of fat body from L3-stage larva expressing Ubi-Caax-GFP protein to label the plasma membrane.

(A1-A3) At 0hr fat body cells are closely attached to each other via cell-cell junctions (A1), however after 2 hours the fat body tissue appears to shrink as shown in “white arrow” (A2). Further shrinkage of the fat body tissue is shown by 4hr “white arrows” (A3).

Imaged using Zeiss-vis 63x oil immersion lens. Scale bars = 20μm.

3.3 *In vivo* live imaging through the pupal case

In addition to the above mentioned approaches, I tried *in vivo* live imaging of FBR through the pupal case. The process of FBR occurs around 4-12hr APF. During the first hours of pupal development the pupal case begins to harden and becomes darker in color and hence more opaque. Moreover, it is not possible to peel off the pupal case during 0-13hr APF, since the pupal case is too soft and attached to the animal and attempting to peel it off would wound the pupa. Therefore, I came up with a method to image the process of FBR both *in vivo* and without needing to peel off the pupal case. This was done using the Zeiss multiphoton fluorescence microscopy, where I managed to get the right settings on the microscope to avoid overheating of the pupa which leads to lethality. While no one in the field had ever managed to image the process of FBR live, using this method I managed to take several *in vivo* movies at different timepoints to gain a better understanding of the process of FBR in the wild type condition. Despite the fact that imaging is still not perfect due to the frequent muscle contractions moving the fat body tissue around, morphological changes could still be seen. Figure 3.8 shows still images of several time lapse movies. As previously mentioned in the literature, my result also showed that at 0h APF, the fat body cells looked polygonal in shape and remained closely attached to each other (Figure 3.8 A1). Some fat body cells appeared to start rounding up at 2hr APF (Figure 3.8 A2,“ filled arrow”) and separation from neighboring fat body cells was also observed in 2hr APF (Figure 3.8 A2 and A2’). Figure 8B shows still images of a time lapse movie of fat body cells from 5hr-8hr APF. At 5hr APF (Figure 3.8 B1) some fat body cells appear to be rounded, and this was validated by dissecting out the fat body tissue from 4hr APF pupae, stained with polarity protein Dlg and imaged on a confocal microscope (Figure 3.8 C). Additionally, cell-cell dissociation was again observed at 8hr APF, with thread-like structures

between two fat body cells as they detached from each other (Figure 3.8 B2). Moreover, by about 5hr APF, spherical shaped FBCs appeared to be oscillating in place through the X-Z axis (Figure 3.8 B1 and B2, “empty arrow”). To validate that the movement was not migration of FBCs I used a nuclear marker to label the nucleus in FBCs of 4hr APF pupae (Figure 3.9), which shows that FBCs only became migratory ~10h APF. Although some dissociation was observed at 4hr APF, not all FBCs dissociated at the same time. Thus, FBC dissociation was also observed at 8.5hr APF (Figure 3.8 D2). Lastly, *in vivo* live imaging through the pupal case from 12hr-14hr APF show individual free floating FBCs moving in the hemolymph (Figure 3.8 E1 and E2, “empty arrows”).

In conclusion, this method is better than previous methods since it allows me to image the process of FBR under normal conditions, without interfering with ecdysone signaling to artificially induce FBR. Although the images in Figure 3.8 are not clear enough, using a better membrane marker which only labels the FBCs would be essential to acquire better images. So far, Caax-GFP was used, which is not the best marker since it is ubiquitously expressed, meaning it labels the membranes of other tissues such as the epithelium which is near by the fat body tissue, making it harder to only visualize the FBCs. Moreover, live imaging over longer periods is very limited due to the frequent muscle twitching.

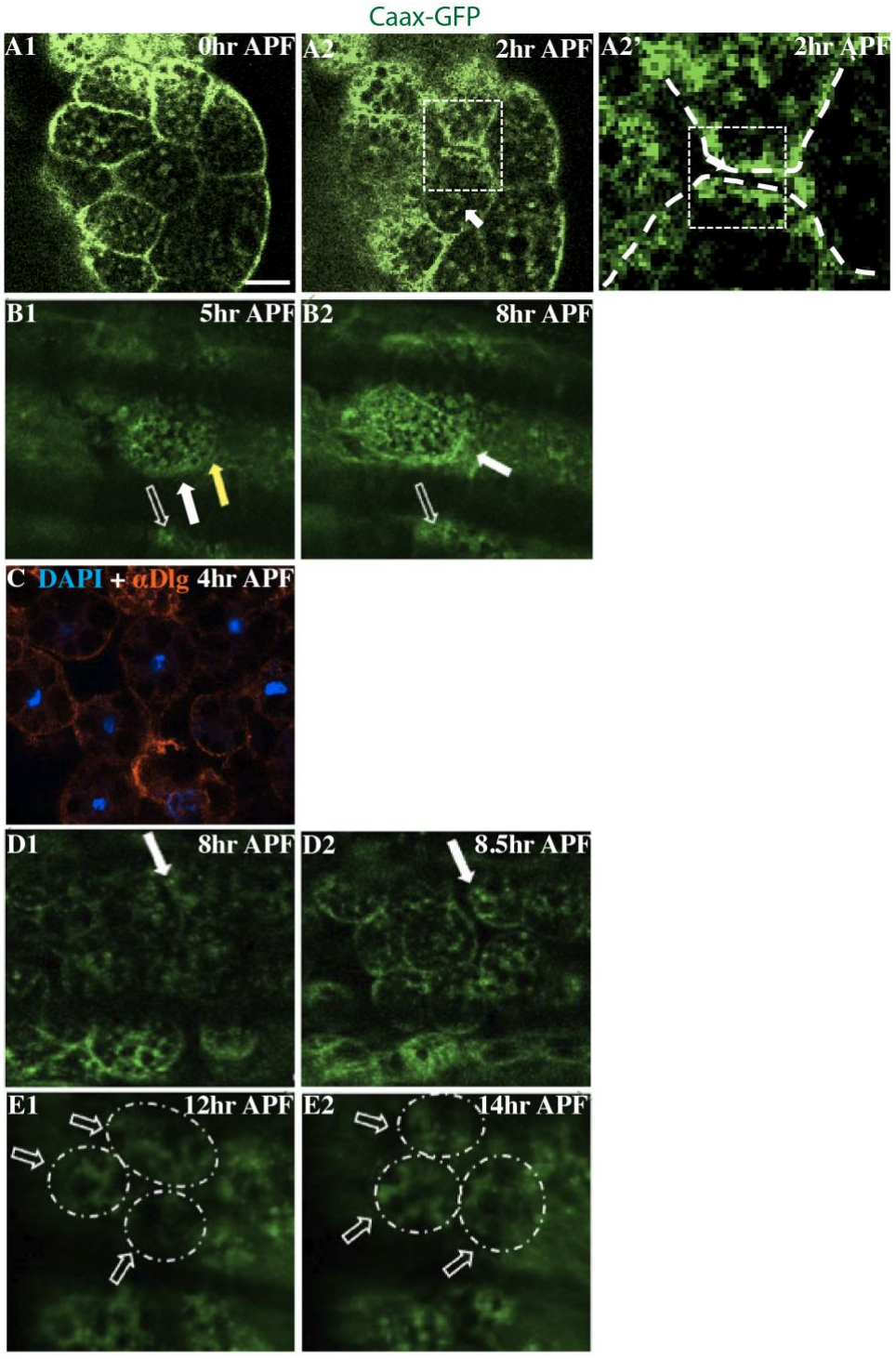

F

	Polygonal Shape	Cell Rounding	Detachment	Motility
Bond et al., 2011	0-4hr APF	6-8hr APF	9-12hr APF	?
My data	0-1hr APF	2-5hr APF	2-8hr APF	10hr APF

Figure 3.8: *In vivo* live imaging of the process of FBR through the pupal case.

(A-E) Confocal images from time-lapse movies of fat body from pupae expressing Ubi-Caax-GFP to label the plasma membrane (A, B, D, E) or expressing Ubi-Caax-GFP and stained using a Dlg antibody and DAPI (C).

(A1) At 0hr APF, FBCs are polygonal in shape and remain closely attached to each other.

(A2-A2') Shows FBC dissociation from 0hr-2hr APF. (A2') shows a zoomed image of cell-cell separation in A2.

(B1-B2) Shows FBC dissociation "filled arrows" with thread like structures in the gap formed between two FBCs during dissociation in (B2), as well as, FBCs oscillating along the X-Z axis "empty arrows" in B1-B2.

(C-D) Shows an immunostaining of FBCs dissected from 4hr APF pupae, and stained with the polarity protein Dlg in red and DAPI in blue. Not all FBCs dissociate at the same time, some dissociate earlier in the process of FBR while others dissociate later such as 8.5hr APF as shown in (D2, "filled allows").

(E1-E2) Shows spherical shaped FBCs floating freely in the hemolymph "empty arrows".

(F) Shows a summary table comparing results of *in vivo* live imaging to previous results that have been published.

Imaged using Zeiss-MP 40x oil immersion lens. Scale bars = 20μm.

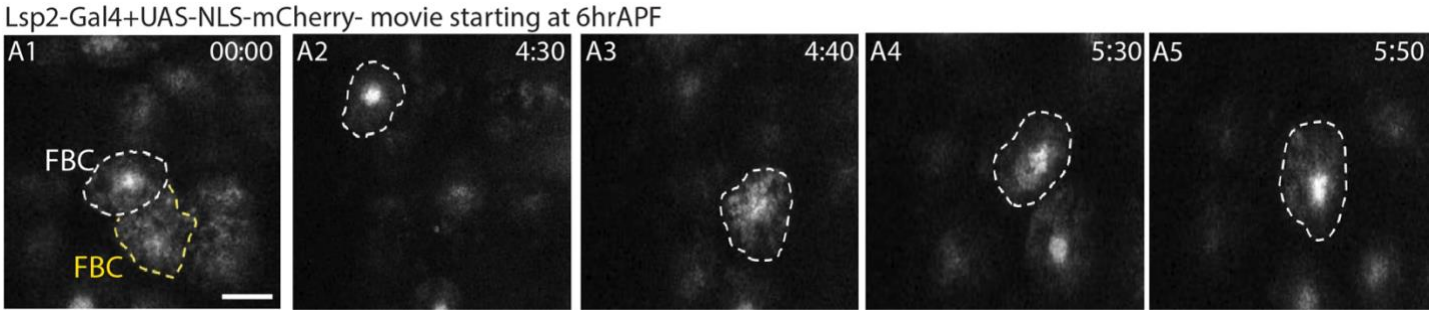

Figure 3.9: Still images of *in vivo* live imaging displaying the initiation of migration during the process of FBR. Pupa expressing a nuclear marker (UAS-NLS-mCherry) using a late fat body driver (Lsp2).

(A1-5) Still images from movie of FBCs (marked in white) migrating in the hemolymph. (A1) FBCs remain closely attached to each other at 6hr APF. Initiation of migration happens at ~10hr APF (A2) and continues up to ~12hr APF (A5)

Imaged using Zeiss-MP 40x oil immersion lens. Scale bars = 20μm. Time in min:sec

3.4 Discussion

This chapter explored various methods to study FBR by live imaging in greater detail, each with its own advantages and limitations. The initial approach aimed to delay FBR by approximately 10 hours when there are no muscle twitches and when it is possible to dissect the pupa out of the opaque pupal case, thus allowing *in vivo* high-resolution live imaging. While this method had the potential to provide detailed visualization and characterization of morphological changes during FBR, it was not very successful since the delay was often only partial. In other words, this approach would only allow imaging later stages of FBR but not the early stages. Additionally, this method was suboptimal since it involved artificially blocking Ecdysone signaling in that fat body, thereby delaying the changes that it would normally induce in the fat body which might have negative side effects. Ecdysone signaling is known to play a critical role in multiple tissues during early developmental stages. Therefore, to avoid any potentially more subtle negative effects, I adjusted the protocol to only block Ecdysone signaling during late 3rd instar larval stages instead. However, my results again showed that FBR was successfully delayed only in very few pupae. Most of the pupae had undergone a partial delay, meaning that FBR has been delayed by only a couple of hours and by the time dissecting the pupa out of the pupal case was possible the pupa might have already been half way through the remodeling process. Yet, imaging the second half of the remodeling process would have been possible but details on morphological changes and dissociation that happen early on in the remodeling process would not be possible to observe.

Two alternative *ex vivo* approaches were tested in parallel. The first approach, adapted from the Fernandes lab, involves dissecting and embedding the fat body tissue in low-gelling agarose with insect media added on top. While this approach has been effective for imaging the

brain, it was not suitable for the fat body tissue, due to the fact that the fat body tissue is not as dense as the brain, thus it could not be held in place within the agarose and ended up floating in media. Though troubleshooting was done by using higher percentages of pure agarose to hold the fat body tissue within the agarose and forceps were also used to hold the fat body tissue in the agarose until it solidifies, none of the trials were successful. Pure agarose temporarily stabilized the tissue within the gel, but once confocal imaging commenced, the fat body tissue would instantly float in the media. This could be due to the fact that during imaging, laser beams caused the temperature in the dish to increase which caused the agarose to melt while it scans, even with the use of a low laser power settings. The second *ex vivo* approach, adapted from the Mao lab, involved placing the dissected fat body tissue in a well with a permeable membrane covering the well to prevent tissue movement. Similar to first *ex vivo* approach used, floating was again an issue using the second *ex vivo* approach. Troubleshooting was done to prevent the sample from floating in the well and going out of focus during live imaging by applying a thick layer of low gelling agarose on top of the well instead of the permeable membrane. This method worked, though sometimes the layer of agarose would float during imaging. Additionally, I have attempted to try adjusting the amount of media pipetted into the well and orienting the fat body tissue flat to the bottom of the fluorodish before applying the permeable membrane while additionally keeping the brain floating in the media on top of the permeable membrane. The brain was kept floating in media because it is known that Ecdysone hormone is derived from prothoracic glands in the brain (Herboso et al., 2015). This adjustment indeed allowed me to take a 10hr movie overnight, thus allowing close observations of the process of FBR. Interestingly, not only cell morphological changes and detachment were observed, but also blebbing was observed after the cells have rounded up and detached. Since blebbing is a hallmark of

apoptosis, it was initially thought that fat body cells are undergoing apoptosis. However, the experiment was repeated the same way but without the addition of Ecdysone and Insulin hormone and cell death have been observed and indicated by cell shrinkage but no blebbing. While both *ex vivo* approaches showed potential for capturing detailed changes during FBR, they required further optimization, particularly in adjusting Ecdysone levels to enable long-term imaging. Moreover, since *ex vivo* imaging involves creating an artificial environment, any observed results would need to be validated *in vivo*.

Ultimately, in my opinion, the *in vivo* live imaging approach through the pupal case proved to be the most suitable, since it allowed observation of FBR under natural physiological conditions, without disrupting Ecdysone signaling. Using live *in vivo* imaging, I found that cell rounding beings from 2-5 hours APF and cell detachment is observed from 2-8 hours APF. Although other studies managed to study FBR by dissecting the fat body tissue at several timepoints, my results of *in vivo* live imaging did not match their results which revealed cell rounding to happen 6-8 hours APF and cell detachment from 9-12 hours APF. Moreover, my data also revealed that initiation of migration happens at 10hr APF, which was previously not studied. Although this method enabled the observation of changes that occur during FBR, its effectiveness was limited by muscle twitching, reducing image clarity and making it hard to track cells over time. Inhibitors such as, shi-ts which blocks endocytosis, could be expressed in the muscle to stop muscle twitching, however this could interfere with organ functions and other developmental processes crucial for metamorphosis. Furthermore, while the resolution of the images was not optimal, testing alternative markers, particularly those that only label the fat body cell membranes (Lpp-gal4+UAS-Myr-td-Tomato), could improve image quality by avoiding labeling membranes of surrounding tissues and organs.

Overall, these live imaging techniques could offer deeper insights into the FBR process by uncovering the underlying mechanisms and identifying key genes involved in regulating FBR.

Chapter IV. The fat body tissue of a 3rd instar larva exhibits apicobasal polarity

A major aim of my PhD was to assess whether the fat body tissue in wandering L3-stage larvae has an apicobasal polarity when the tissue is still a connected sheet and before cell dissociation happens during FBR. This is because apicobasal polarity had never been reported for the fat body. Thus, I decided to perform antibody staining's for a range of classic polarity proteins known to localize to the apical (aPKC, Par-6, Crumbs), basolateral domain (Lgl and Dlg) or to the adherens junction at the apicolateral domain (Par-3=Baz and E-Cad) of classic epithelia. I wanted to see whether these proteins are also present in the fat body tissue and if there is an asymmetric localization on the two surfaces of the fat body. However, it is usually not possible to image fat body cells from top to bottom due to their large size and light scattering issues deeper in the tissue because of lipid droplets. Hence, I came up with a way to overcome this issue by mounting the fixed and stained fat body tissue from wandering L3-stage larvae between two coverslips. This allowed me to image the fat body tissue from both sides, which I will be referring to as side (a) and side (b). Caax-GFP was used as a tool to check if the fat body tissue was equally close to the cover slip on both sides as well as to visualize membranes to find the cell surface and lateral domains. I then encountered the problem that after dissecting the fat body tissue from the larva, there didn't seem to be a way of identifying the two sides of the fat

body (corresponding to a potentially ‘apical’ and ‘basal’ side) through some visual markers to be able to pool the data from sides (a) and sides (b) from several fat body tissues. Hence, I initially mounted the dissected fat body tissue randomly and couldn’t know which side was mounted up or down, in other words, which side is the one facing inside the animal and which is facing outside. I decided to test for a potential asymmetry in the localization of certain polarity proteins by imaging the fat body from one single animal in 10 different regions first on one side then turning the sample around (in other words, flipping the coverslip around) to the opposite side and imaged the same 10 regions in a paired manner from the opposite side. This was repeated for 10 different fat body tissues dissected from 10 different wandering L3-stage larvae, for each polarity protein immunostaining separately. Since the samples were mounted at a random orientation, this means that side a (first side imaged) and side b (second side imaged) can differ between the fat body tissues dissected from different animals. An ROI (shown in Figure 4.1 A) was then used to measure the mean fluorescent intensities of Caax-GFP as well as of polarity proteins and this was done on side a versus side b for 10 regions per larvae to obtain the overall mean and to calculate the percentage difference between the two sides.

Although this method of randomly mounting the fat body tissue was not ideal, I was still able to answer the question of whether the fat body tissue of an L3-stage larvae is polarized. My results showed that Caax-GFP was symmetrical and randomly distributed with a small percentage difference in intensities between the two sides (Figure 4.1 A-E). In other words, the graphs showed short bars from 10 different regions pointing randomly either left or right. Moreover, Caax-GFP displayed a percentage difference between the two sides in the range of 0.04-4%. The percentage differences are shown in red in Figure 4.1 A-E. In contrast, Par-3, (average percentage difference 17-43%, Figure 4.1 A) and aPKC (average percentage

difference 21-56%, Figure 4.1 B), Par-6 (average percentage difference 9-50%, Figure 4.1 C), Dlg (average percentage difference 6-87%, Figure 4.1 D) and Lgl (average percentage difference 13-71%, Figure 4.1 E) showed a strong asymmetrical localization in the fat body tissue of an L3-stage larvae (bars from 10 regions mostly pointing either left or right). A negative percentage difference value would just mean that the fluorescence intensities are higher on side a (the side imaged first) when compared to side b.

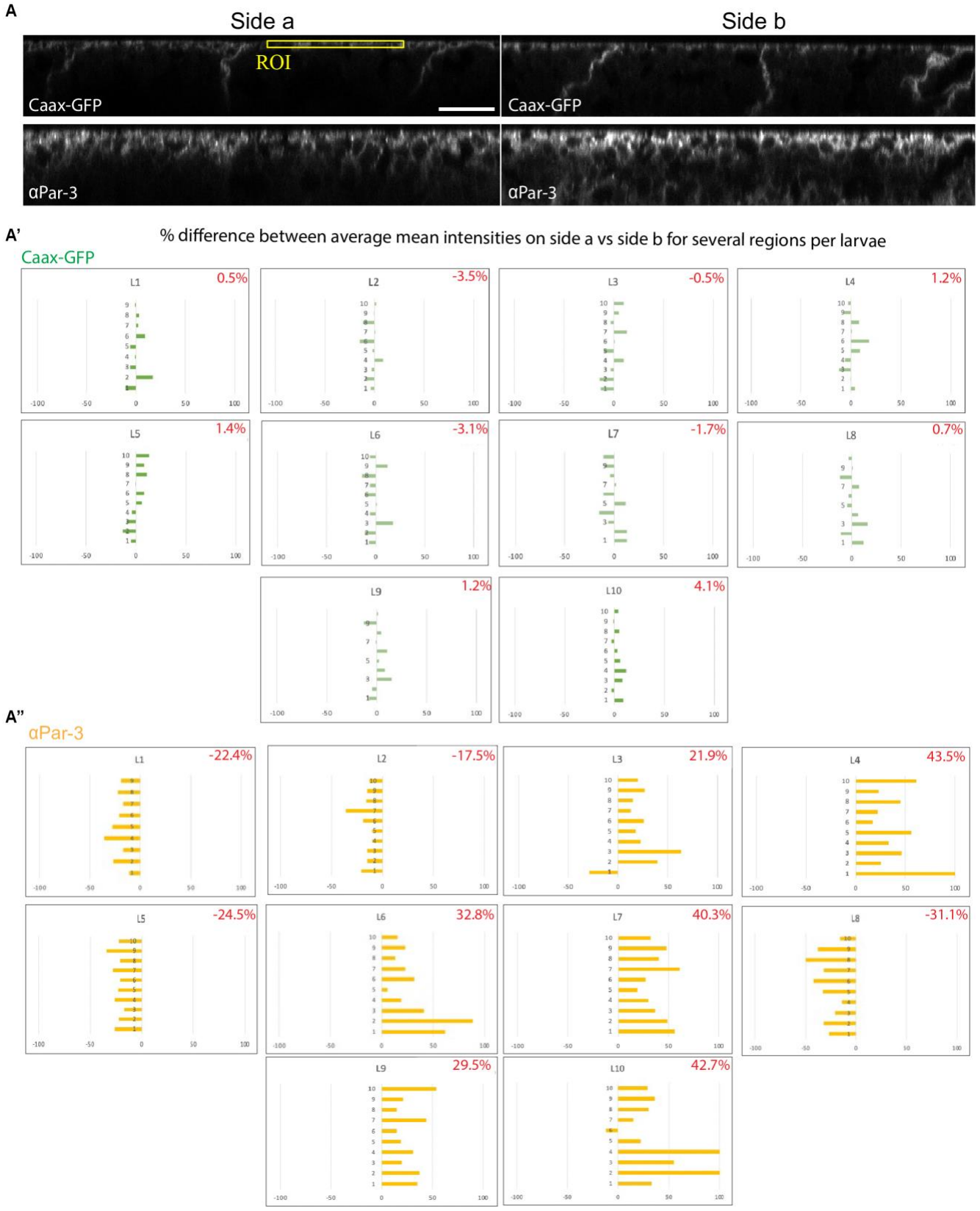
A
Side a
Side b
ROI
Caax-GFP
Caax-GFP
αPar-3
αPar-3
A'
% difference between average mean intensities on side a vs side b for several regions per larvae
Caax-GFP
L1 0.5%
L2 -3.5%
L3 -0.5%
L4 1.2%
L5 1.4%
L6 -3.1%
L7 -1.7%
L8 0.7%
L9 1.2%
L10 4.1%
A"
αPar-3
L1 -22.4%
L2 -17.5%
L3 21.9%
L4 43.5%
L5 -24.5%
L6 32.8%
L7 40.3%
L8 -31.1%
L9 29.5%
L10 42.7%

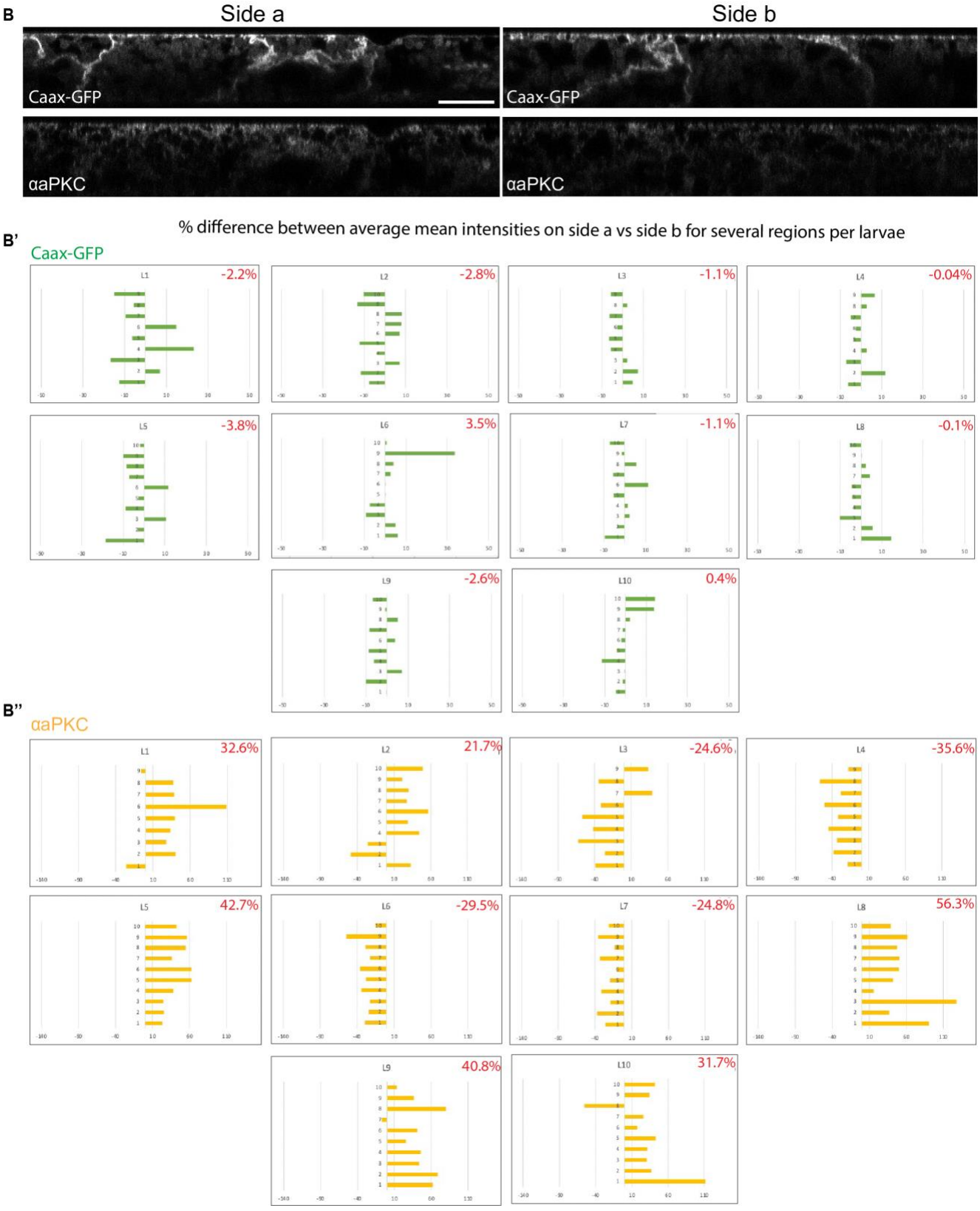
B
Side a
Side b
Caax-GFP
Caax-GFP
αaPKC
αaPKC
B'
% difference between average mean intensities on side a vs side b for several regions per larvae
Caax-GFP
L1 -2.2%
L2 -2.8%
L3 -1.1%
L4 -0.04%
L5 -3.8%
L6 3.5%
L7 -1.1%
L8 -0.1%
L9 -2.6%
L10 0.4%
B''
αaPKC
L1 32.6%
L2 21.7%
L3 -24.6%
L4 -35.6%
L5 42.7%
L6 -29.5%
L7 -24.8%
L8 56.3%
L9 40.8%
L10 31.7%

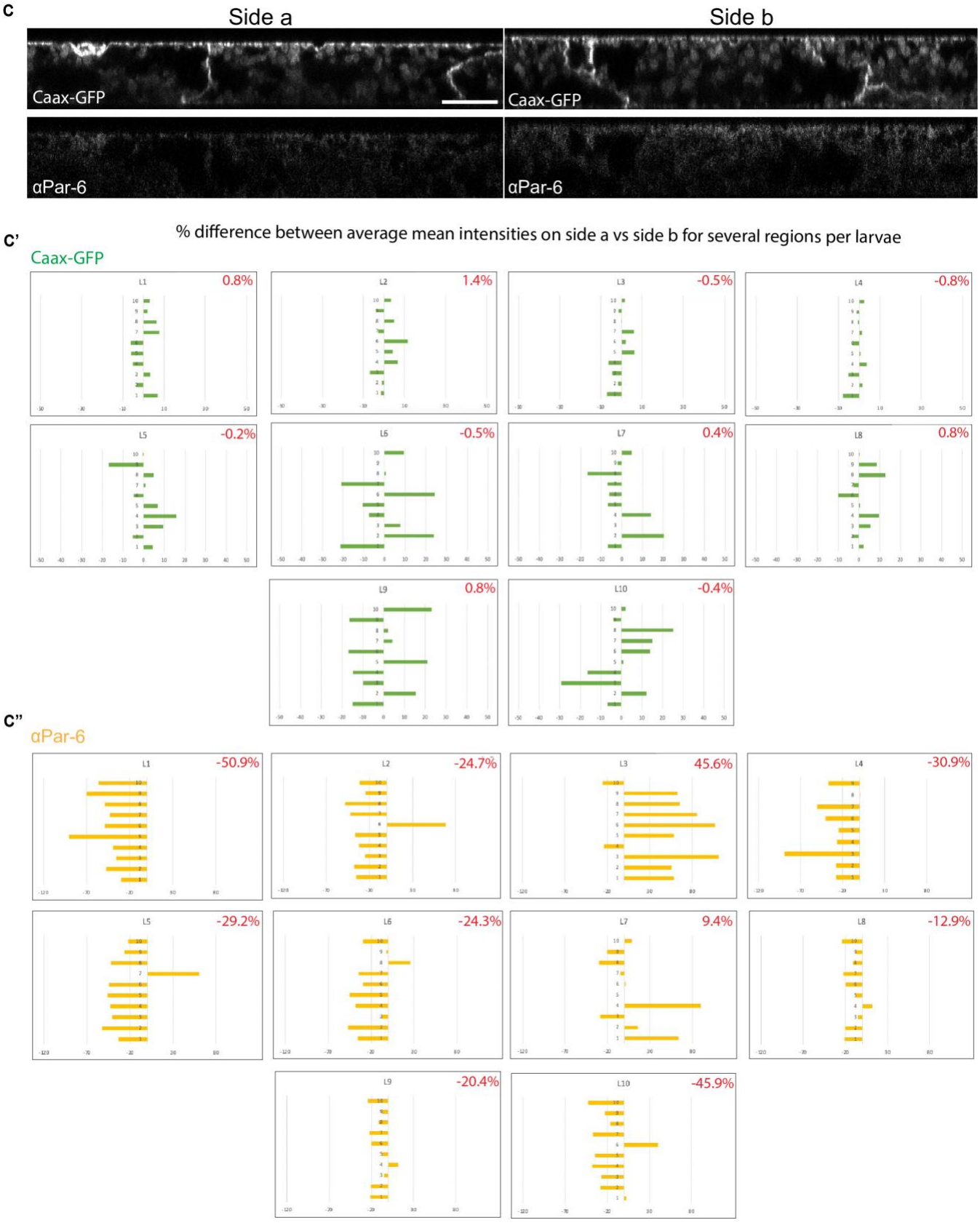
c
Side a
Side b
Caax-GFP
Caax-GFP
αPar-6
αPar-6
c'
% difference between average mean intensities on side a vs side b for several regions per larvae
Caax-GFP
L1 0.8%
L2 1.4%
L3 -0.5%
L4 -0.8%
L5 -0.2%
L6 -0.5%
L7 0.4%
L8 0.8%
L9 0.8%
L10 -0.4%
c''
αPar-6
L1 -50.9%
L2 -24.7%
L3 45.6%
L4 -30.9%
L5 -29.2%
L6 -24.3%
L7 9.4%
L8 -12.9%
L9 -20.4%
L10 -45.9%


D
Side a
Side b
Caax-GFP
Caax-GFP
αDlg
αDlg
D'
% difference between average mean intensities on side a vs side b for several regions per larvae
Caax-GFP
L1 -0.8%
L2 -1.8%
L3 -1.1%
L4 -1.1%
L5 1.5%
L6 0.4%
L7 -0.6%
L8 2.3%
L9 -0.8%
L10 1.3%
D"
αDlg
L1 -25.8%
L2 -6.6%
L3 23.6%
L4 18.3%
L5 -21.5%
L6 87.3%
L7 28.3%
L8 -15.5%
L9 26.6%
L10 -27.9%

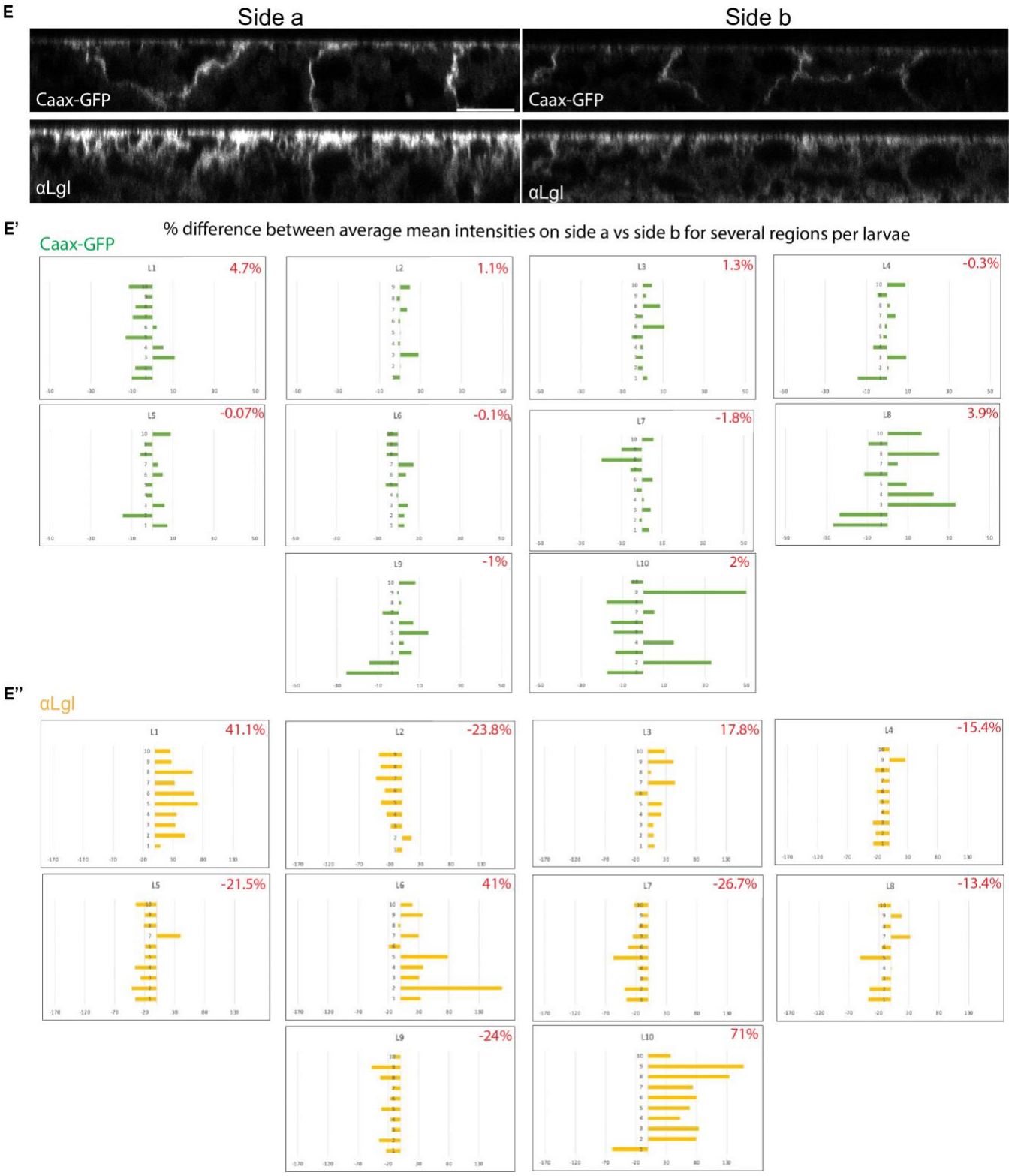
E
Side a
Side b
Caax-GFP
Caax-GFP
αLgl
αLgl
E'
% difference between average mean intensities on side a vs side b for several regions per larvae
Caax-GFP
L1 4.7%
L2 1.1%
L3 1.3%
L4 -0.3%
L5 -0.07%
L6 -0.1%
L7 -1.8%
L8 3.9%
L9 -1%
L10 2%
E''
αLgl
L1 41.1%
L2 -23.8%
L3 17.8%
L4 -15.4%
L5 -21.5%
L6 41%
L7 -26.7%
L8 -13.4%
L9 -24%
L10 71%

Figure 4.1: Percentage difference between average mean intensities of polarity proteins on side a and b for several regions per larvae. All fat body tissues expressing Caax-GFP.

(A-E) Shows images of fluorescent intensities of Caax-GFP and the staining for polarity proteins using αPar-3 (A), αaPKC (B), αPar-6 (C), αDlg (D) and αLgl (E) on each side (side a and side b) of the fat body tissue of wandering L3-stage larvae.

(A'-E') Shows that Caax-GFP is symmetrically localized and is randomly distributed with a small average percentage difference (shown in red) between the two sides (side a and side b). (N≥10 fat body tissues, 10 regions imaged on each side).

(A''-E'') αPar-3 (A''), αaPKC (B''), αPar-6 (C''), αDlg (D'') and αLgl (E'') are asymmetrically localized in the fat body tissue of an L3-stage larvae. The average percentage differences are shown on each graph in red. (N≥10 fat body tissues, 10 regions imaged on each side).

Imaged using Zeiss-vis 63x oil immersion lens. Scale bars = 20μm

Altogether, these results showed that polarity proteins (Dlg, Lgl, aPKC, Par-3 and Par-6) are present in the fat body tissue of wandering L3-satge larva and are also asymmetrically localized suggesting that the fat body tissue is likely polarized. Next, to assess this more thoroughly, I thought that it would be key to overcome the problem of mounting the fat body tissue randomly. In other words, I had to figure out a way to distinguish the two sides of the fat body to be able to tell which actual side faces up or down to be able to pool results from different animals and perform statistical analysis.

Finally, I came up with a solution to overcome this problem, to be able to pool results from different animals for further analysis. We noticed a morphological asymmetry in the structure of an L3-stage larval fat body tissue. From a dorsal view of an L3-stage larva, anterior to posterior (left to right in schematic on left in Figure 4.2 A), the two sheet of the fat body tissue (the top and bottom ones in the schematic) have several gaps present along in the tissue (anterior to posterior). For the right half of the fat body (the top one in the schematic), the fat body region located to one side of the gaps, pointing left in the animal towards the left fat body sheet but pointing down in Figure 4.2 A seems to be thicker and is around 4-7 fat body cells wide, while the other side is thinner and is only 1-2 fat body cells wide (Figure 4.2 A). The left sheet of the fat body has a mirror image morphology.

I then tried this new approach making use of this apparent innate asymmetry in the tissue. This ensured mounting the fat body tissue with that the same actual cell side up from all animals by always dissecting the right sheet of the fat body from the animals and mounting the fat body tissue in a way where the anterior end of the fat body was at the top, the posterior at the bottom, and the thick side of the fat body tissue always mounted on the left side. With this setup the side being imaged was the side facing in the animal outwards (being referred to from now on as side

(a)) and after flipping over the cover glass, the opposite side being imaged was the side facing in the animal inwards (referred to as side (b)). I then repeated the immunostaining experiments and quantified the mean intensities in the surface boxes (shown in yellow in Figure 4.2 A on right), as well as in lateral boxes near the surface (shown in orange; connected dots in graphs representing the average mean intensity of 10 different regions imaged on each side of the fat body tissue from a particular animal). This resulted in aPKC, Par-6 and Crumbs having higher average mean intensities on side (a) (Figure 4.2 B-D) with no difference in the lateral domain boxes, and Dlg and Lgl being higher on the opposite side (side (b)) as well as higher in the lateral domain near side (b), shown in Figure 4.2 E-F. In addition, my results again showed a symmetrical distribution of Caax-GFP, indicating that the fat body tissues were mounted equally far from the cover slip on both sides (Figure 4.2 B-F). I then wanted to further validate my results by using a protein trap line. The Lgl-GFP protein trap line also showed a similar result with a higher average intensity on side b on the surface as well as the lateral box (Figure 4.2 G).

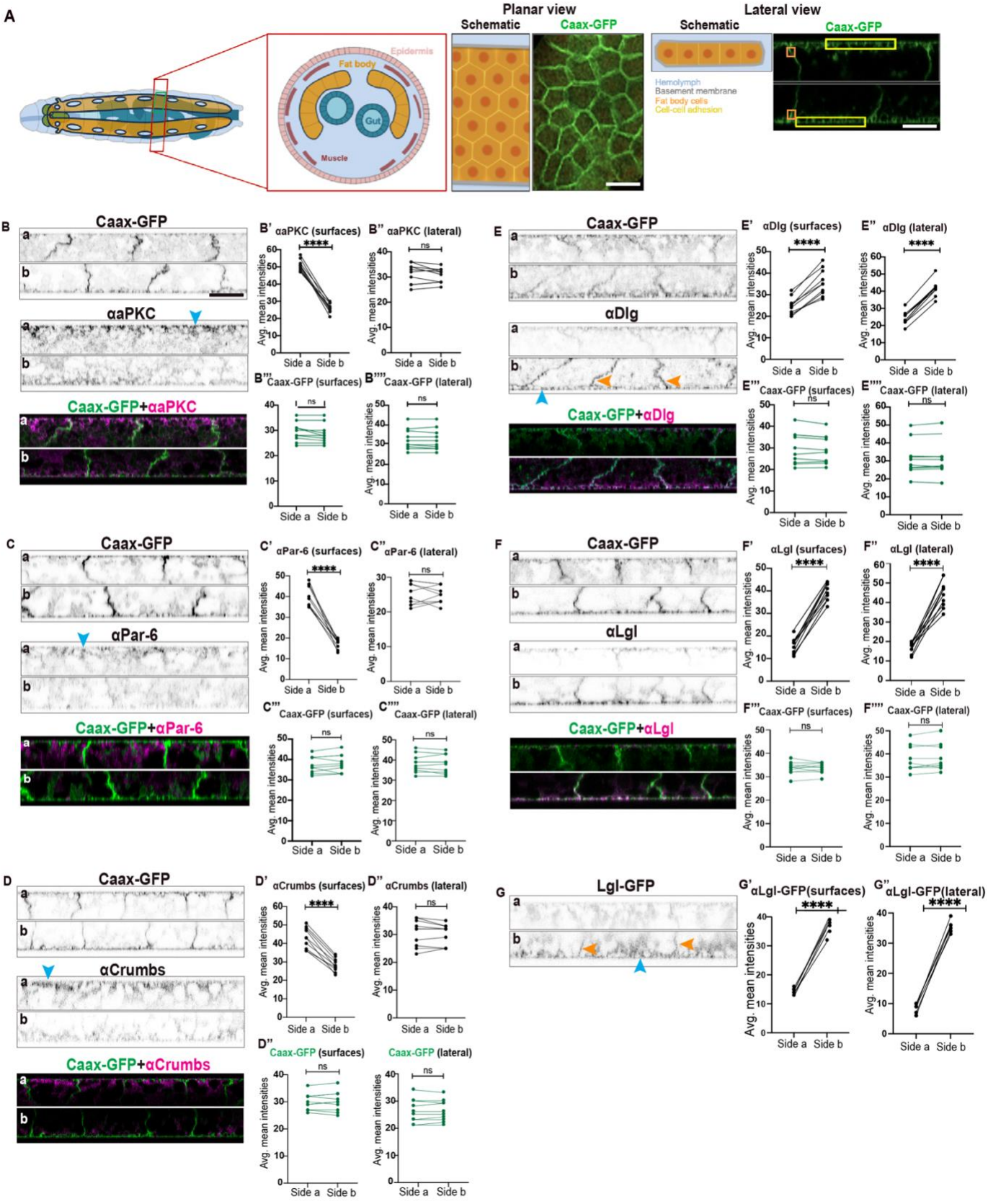
A
Planar view
Schematic
Caax-GFP
Lateral view
Schematic
Caax-GFP
Epidermis
Fat body
Gut
Muscle
Hemolymph
Basement membrane
Fat body cells
Cell-cell adhesion
B
Caax-GFP
αaPKC
Caax-GFP+αaPKC
B' αaPKC (surfaces)
B'' αaPKC (lateral)
B''' Caax-GFP (surfaces)
B'''' Caax-GFP (lateral)
C
Caax-GFP
αPar-6
Caax-GFP+αPar-6
C' αPar-6 (surfaces)
C'' αPar-6 (lateral)
C''' Caax-GFP (surfaces)
C'''' Caax-GFP (lateral)
D
Caax-GFP
αCrumbs
Caax-GFP+αCrumbs
D' αCrumbs (surfaces)
D'' αCrumbs (lateral)
D'' Caax-GFP (surfaces)
Caax-GFP (lateral)
E
Caax-GFP
αDlg
Caax-GFP+αDlg
E' αDlg (surfaces)
E'' αDlg (lateral)
E''' Caax-GFP (surfaces)
E'''' Caax-GFP (lateral)
F
Caax-GFP
αLgl
Caax-GFP+αLgl
F' αLgl (surfaces)
F'' αLgl (lateral)
F''' Caax-GFP (surfaces)
F'''' Caax-GFP (lateral)
G
Lgl-GFP
G' αLgl-GFP(surfaces)
G'' αLgl-GFP(lateral)
Avg. mean intensities
Side a
Side b
****
ns

Figure 4.2: The fat body tissue of wandering 3rd instar larvae exhibits apicobasal polarity. All fat body tissues expressing Caax-GFP.

(A) Schematic of the fat body tissue in wandering L3-stage larvae. Yellow and orange boxes indicate where ROIs were placed for intensity measurements.
(B-F) Fat body from third instar larvae expressing Caax-GFP fixed and stained using antibodies for various polarity proteins. Caax-GFP is symmetrically localized on the surface and lateral domains between the two sides of the fat body tissue (side a and side b). αaPKC (B), αPar-6 (C), and αCrumbs (D) are localized on the apical surface (side a) (blue arrows) (B'-D') and not on the lateral domains (B''-D''). αDlg (E) and αLgl (F) are localized on the basal surface (blue arrow) (side b) (E'-F') and on the basolateral domain (orange arrows) (E''-F''). (N≥10 fat body tissues, 10 regions imaged on each side, Paired T-test, ****P<0.0001, ns P>0.9999).
(G) Polarity protein trap line Lgl-GFP is localized on the basal surface (G') and basolateral domain (G''). (N≥6 fat body tissues, 2 regions imaged on each side, Paired T-test, ****P<0.0001). Imaged using Zeiss-vis 63x oil immersion lens. Scale bars = 20μm.

4.1 Discussion

It has long been presumed that the *Drosophila* fat body tissue of wandering L3-stage larvae is non-polarized due to it's mesodermal origin and the presence of a basement membrane on both its surfaces. However, this theory has never been experimentally validated. In this chapter I tested several epithelial polarity proteins, by dissecting fat body tissues expressing Caax-GFP and staining for polarity proteins including Par-3, Par-6, aPKC, Lgl, and Dlg. A major technical challenge was the inability to acquire a Z-stack spanning the entire thickness of the fat body. To address this issue, fat body tissues were mounted between two coverslips and imaging was conducted on both sides of the coverslip. Given that the two sides were indistinguishable, I've referred to the side imaged first as side a and the corresponding side as side b. If the fluorescence of one polarity protein is asymmetrical, then it would be consistently higher on one side versus the other within the fat body dissected from the same animal. However, among different animals the side with higher fluorescence may vary between one side and the other. Caax-GFP was not only used as a control but also to give me an indication of whether the fat body tissue is mounted equally close to the cover slip from both sides, avoiding differences in polarity protein mean fluoresce intensities that could arise due to different proximities to the cover glass. My initial findings, not only revealed that polarity proteins Par-3, Par-6, aPKC, Lgl, and Dlg are present in the fat body but also that they display asymmetric localization. This suggests that the fat body tissue of L3-stage larvae exhibits polarity. However, using this random method, I couldn't tell which polarity proteins are localized on the same side and which ones are on the opposite side. In order to draw definitive conclusions and perform statistical analyses, it was essential to address the issue of random tissue mounting, to be able to tell which actual cell

side faces up or down and hence always resulting in a polarity protein being higher on the same side (either side a or b) relative to the other side of the tissue.

Upon closer examination, I found that the fat body tissue on wandering L3-stage larva seems to have a structural symmetry. From a dorsal view, anterior to posterior (top to bottom), the right sheet of the fat body tissue seems to exhibit a certain structure. The fat body region located to one side of the gap, pointing left in the animal but pointing up in Figure 3.4 seems to be thicker and is around 4-7 fat body cells wide, while the other side (pointing down in Figure 4.3) is thinner and is only 1-2 fat body cells wide (Figure 4.3) (Marchetti et al., 2003). Using this new mounting method, I always dissected the right sheet of the fat body tissue and ensured that all tissues are mounted on the same cell side up, in other words, I ensured that tissues were mounted in a way where the thick side was always on the left side of the coverslip while the thin side was on the right. This way all dissected fat body tissues were mounted in the same orientation. Using the new mounting method, my results showed that aPKC, Par-6, and Crumbs are localized to side a, corresponding to the apical domain facing outwards towards the body wall, while Dlg and Lgl were restricted to the basal domain, facing the gut. Lgl and Dlg were also enriched in the basolateral domain. Testing additional polarity proteins such as Scribble and Stardust would provide further insights into the apicobasal cell polarity of the fat body. Moreover, colocalization antibody staining of polarity proteins localized on opposite sides of the fat body tissue could be done to further validate my results on the exact localization of polarity proteins within the fat body.

A striking aspect of this finding is the presence of Crumbs, a classic apical

polarity determinant, on the apical domain which is typically restricted to primary epithelia, derived from the blastoderm (Tepass et al., 2001). This is also because in a secondary epithelium which form later during development via MET, do not rely on Crumbs to establish polarity (Tepass et al., 1990). Given that the fat body is neither a primary nor a secondary epithelium and is rather a mesoderm-derived tissue; the presence and asymmetric distribution of Crumbs was not expected. This result suggests that the fat body could follow an epithelial-like polarity program, despite the differences in morphology and origin. These results also raise the possibility that polarity proteins like Crumbs is not exclusive to epithelia but could indicate underlying functional demands such as directed secretion.

Moreover, that fact that the fat body tissue is polarized points towards the presence of polarized functional activity. Although, secretion occurs apically in classic epithelia, such as in *Drosophila* embryonic tracheal tubes (Tal Rousso et al., 2013), secretion has been seen to sometime occur basally such as in *Drosophila* follicular epithelium, where secretion is regulated by Kinesin motor proteins (Zajac & Horne-Badovinac, 2022). A future direction would be to investigate whether a similar basal secretion mechanism is present in the fat body tissue. This could be done by labeling Kinesin-1 with UAS-KHC-GFP, in addition to a basal polarity marker, in order to assess whether they co-localize basally. This would offer functional evidence of directional secretion in the fat body tissue despite having a basement membrane on both sides and further validating that the fat body tissue is not only structurally polarized but is also functionally polarized.

What makes this finding significant is it's implication for adipose tissues across species. In vertebrate, the adipose tissue, which originates from mesenchymal stem cells has a poorly understood polarity status, and it remains unclear whether it exhibits classic epithelial polarity. However, studied have reported forms of functional polarization, such as insulin-stimulated translocation of GLUT4 vesicles to specific regions of the plasma membrane (Karylowski et al., 2004). The presence of directional trafficking suggests some form of physiological polarity.

Altogether, these results suggest that polarity in adipose tissues, either in *Drosophila* of vertebrates, may not only be defined by developmental origin of epithelial identity, but instead by functional requirements, such as directed secretion or trafficking. Therefore, this discovery of polarity in *Drosophila* raises the possibility that polarity in adipose tissue may be evolutional conserved, potentially supporting their common roles when compared to vertebrates, such as metabolic regulation.

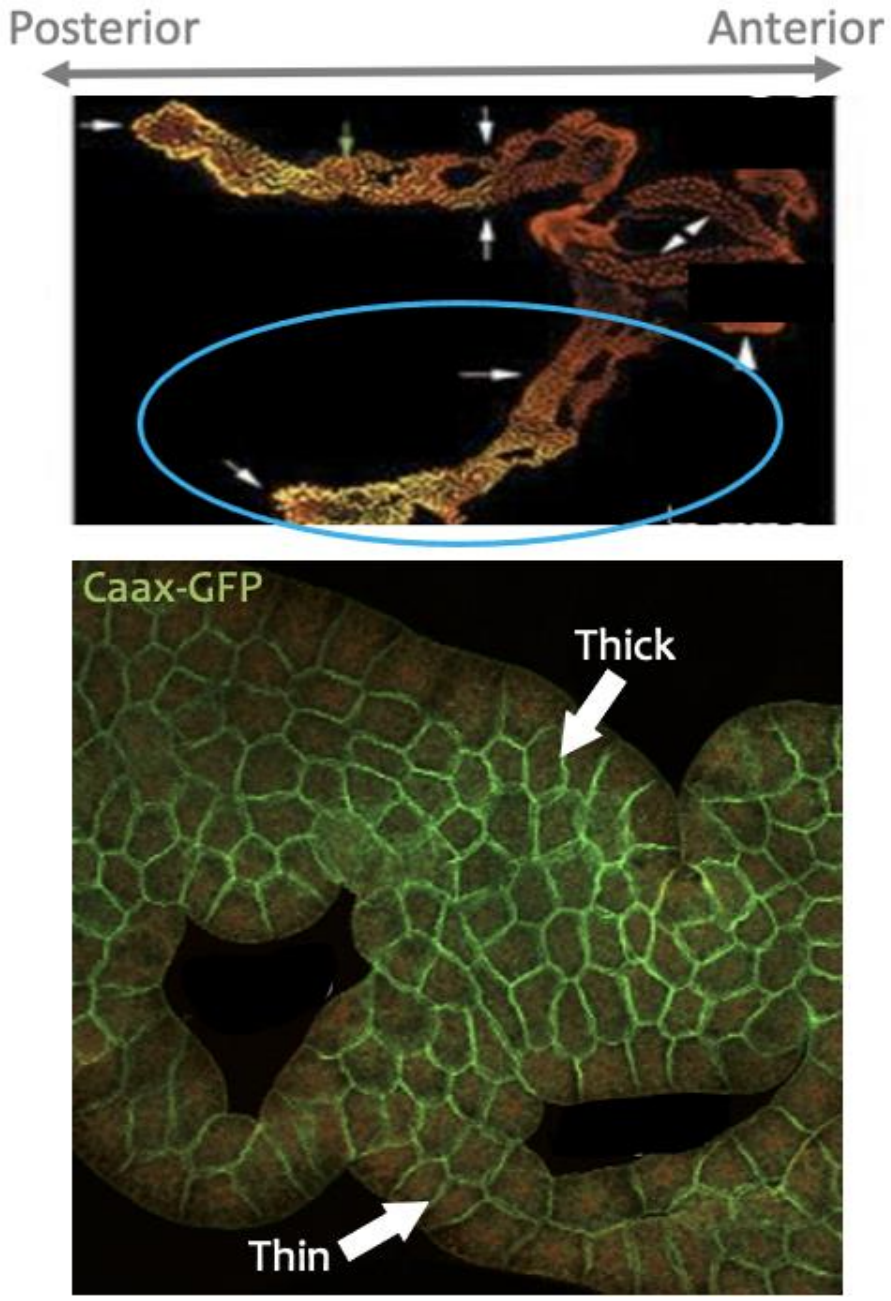

Figure 4.3: Structure of the right sheet of the fat body tissue.

Adapted from Marchetti et al., 2003.

Chapter V. Cell-cell adhesion in larval fat body is mediated by collagen-dependent cell-cell adhesion and does not require E-Cad

One of the key functions of apicobasal polarity proteins in classic epithelia is to regulate cell-cell adhesion via Par-3 and E-Cad-based adherens junctions. Before cellularization, the egg chamber is divided into two distinct regions, the supranuclear and internuclear region (Mavrakis et al., 2009). The intranuclear domains are enriched in Par-3 and E-Cadherin. During cellularization, Par-3 gets recruited in the upper third of the lateral membrane and forms spot adherens junction on the apicolateral membrane (Harris & Peifer, 2004). Each Par-3 molecule consists of seven E-Cadherin and seven Armadillo molecules at spot adherens junctions (McGill et al., 2009). Now that I found that the fat body tissue of an L3-stage larva has an apicobasal polarity somewhat similar to epithelia, I asked myself whether this polarity is involved in the regulation of cell-cell adhesion in the fat body. Two mechanisms have been suggested to be involved in cell-cell adhesion in the fat body: one via E-Cadherin-based adherens junctions (Jia et al., 2014) and one via Collagen IV Intercellular Adhesion concentrations (Dai et al., 2017). In agreement with a role of E-Cad in fat body cell-cell adhesion, Jia et al. (2014), reported that the larval fat body has E-Cadherin at its lateral junctions which gets removed during FBR as cells dissociate (Jia et al., 2014). Hence, I decided to investigate further, if E-Cad indeed regulates cell-cell adhesion. First, I tested, if E-Cadherin and Par-3 which are known to be localized on adherens junctions in standard epithelial tissues might also be similarly localized on the apicolateral domain in the fat body. To test this, I performed the same method previously used to

test whether polarity proteins are asymmetrically localized in the fat body tissue of an L3-stage larva. The fat body tissues were dissected out of wandering 3rd-instar larvae, and immunostained for Par-3 and E-Cad in two different sets of experiments. The same ROI previously used to measure the surface and lateral sides of polarity proteins was also used to measure the mean intensities on the surface and lateral sides of Par-3 and E-Cad. Each dot in Figure 5.1 represents the average mean intensity of 10 different regions imaged on each side of the fat body tissue. This was done on 10 fat body tissues dissected from different animals. Caax-GFP was again used to identify cells. My results revealed that both Par-3 and E-Cad were localized more strongly on the apical surface and apicolateral domain (Figure 5.1 A-B), showing asymmetrical localization with average mean intensities higher on side a as shown in the graph in (Figure 5.1 A'-A'', B'-B''). However, the E-Cad staining was overall rather weak and diffuse and differed clearly from the predominant belt-like localization of E-Cadherin at the apicolateral domain described for many classic *Drosophila* epithelia. Moreover, I only saw a very week staining with the E-Cadherin protein trap line (E-Cad-GFP expression driven under endogenous promoter, data not shown) or Ubi-GFP-Ecad (E-Cad-GFP expression driven under ubiquitous promoter, data not shown).

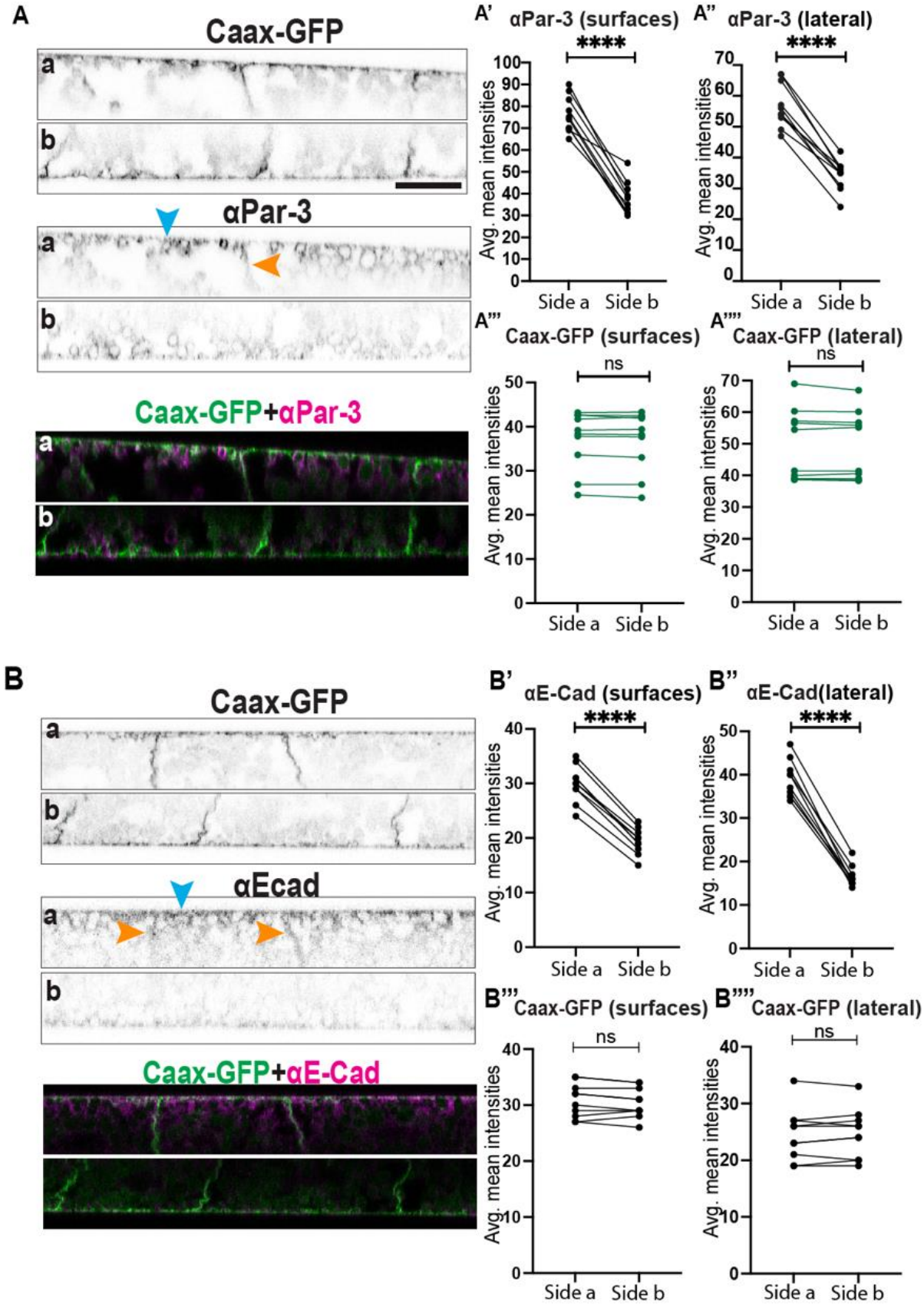
A
Caax-GFP
a
b
αPar-3
a
b
Caax-GFP+αPar-3
a
b
A'
αPar-3 (surfaces)
****
Avg. mean intensities
Side a
Side b
A''
αPar-3 (lateral)
****
Avg. mean intensities
Side a
Side b
A'''
Caax-GFP (surfaces)
ns
Avg. mean intensities
Side a
Side b
A''''
Caax-GFP (lateral)
ns
Avg. mean intensities
Side a
Side b
B
Caax-GFP
a
b
αEcad
a
b
Caax-GFP+αE-Cad
B'
αE-Cad (surfaces)
****
Avg. mean intensities
Side a
Side b
B''
αE-Cad(lateral)
****
Avg. mean intensities
Side a
Side b
B'''
Caax-GFP (surfaces)
ns
Avg. mean intensities
Side a
Side b
B''''
Caax-GFP (lateral)
ns
Avg. mean intensities
Side a
Side b

Figure 5.1: Polarity protein αPar-3 and E-Cadherin are localized on the apical surface and apicolateral domain in the fat body of wandering 3rd instar larvae.

(A-B) Fat body from third instar larvae expressing Caax-GFP fixed and stained using antibodies for Par-3 (A) and E-Cad (B). Caax-GFP on the surface and lateral domains is not significantly different when compared between the two sides (side a and side b). (A) αPar-3 is asymmetrically localized and exhibits a higher average mean intensity on apical surface (side a) (blue arrow) (A') and on the apicolateral domain (orange arrow) (A''). (B) αE-Cad is asymmetrically localized and have a higher average mean intensity on the apical surface (side a) (blue arrow) (B'), as well as, the apicolateral domain (orange arrow) (B''). (N≥10 fat body tissues, Paired T-test, ****P<0.0001, ns P>0.9999).

Imaged using Zeiss-vis 63x oil immersion lens. Scale bars = 20μm.

To investigate further whether E-Cadherin regulates cell-cell adhesion in the larval fat body, I performed RNAi knockdown of E-Cad using three different independent RNAi constructs expressed under a fat body driver Lpp-Gal4. UAS-Myr-td-Tom, was not only used as a membrane marker, but also, to ensure that the fat body is mounted equally close to the cover slips on each side. Immunostaining of E-Cad was used to confirm the effectiveness of the RNAi knockdowns. Each dot in graphs of Figure 5.2 represents the average mean intensities measured in 3 different surface regions on each side of 3 different fat body tissues dissected from different animals. Quantifications of the average mean fluoresce intensities of E-Cad further validated the high knockdown efficiency of E-Cad in the three different E-Cad RNAi knockdowns (UAS-E-Cad-RNAi^{103962}, UAS-E-Cad-RNAi^{32904}, UAS-E-Cad-RNAi^{27082}, Figure 5.2 C'-D', respectively, and E) when compared to the control (Figure 5.2 A) where again an asymmetrical distribution of E-Cad was observed that was significantly higher on the apicolateral side of the fat body tissue despite having a dim stain. In addition, UAS-Myr-td-Tomato (Figure 5.2 A''-D'') seemed to be symmetrically localized suggesting no discrete difference between side a and side b of the fat body tissue. Importantly, using three different E-Cad RNAi lines, I did not find any evidence of cell-cell adhesion defects. These findings, suggest that E-Cad knockdown is not sufficient to induce cell-cell dissociation in the larval fat body.

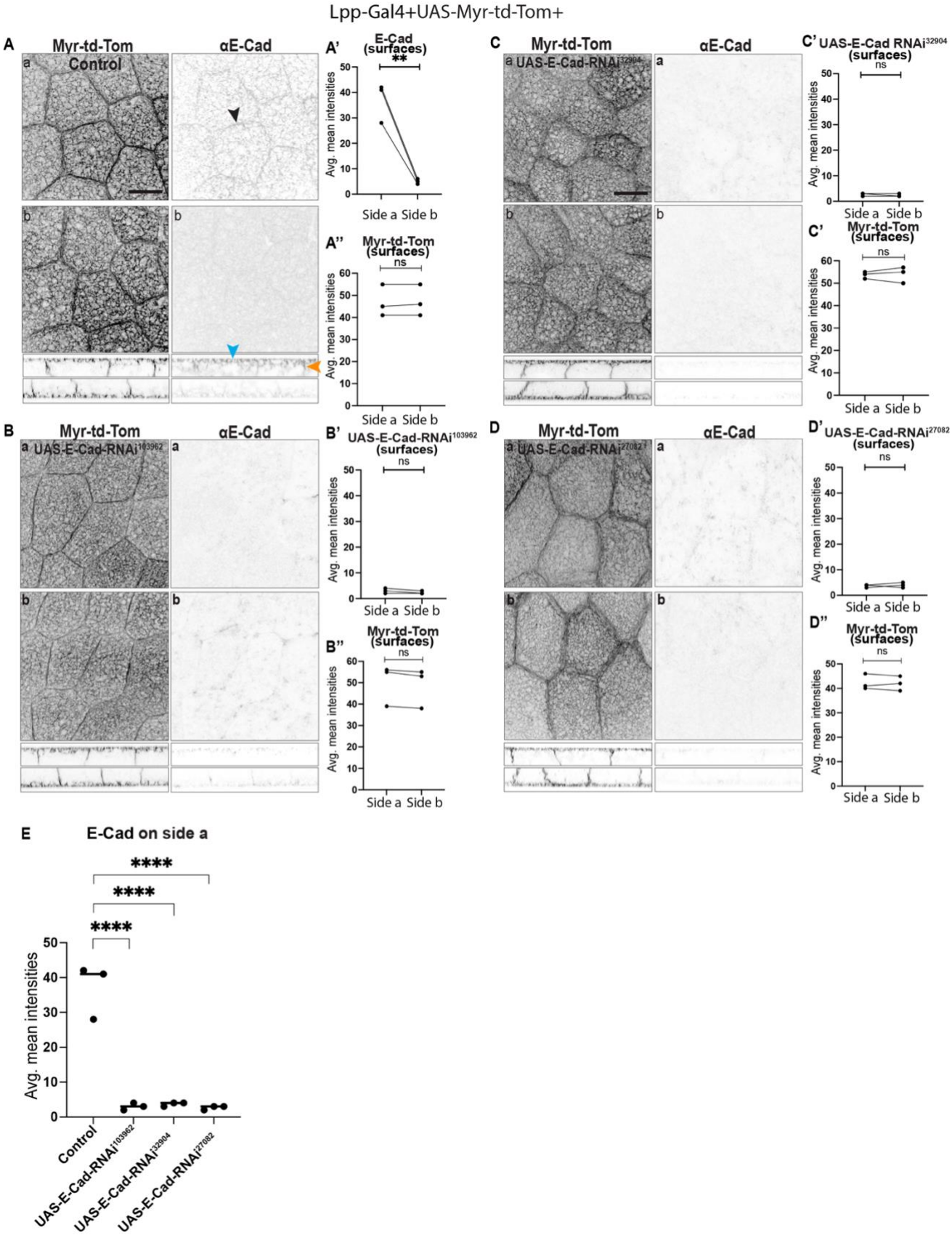
Lpp-Gal4+UAS-Myr-td-Tom+
A
Myr-td-Tom
αE-Cad
Control
a
b
A'
E-Cad (surfaces)
**
Avg. mean intensities
Side a Side b
A''
Myr-td-Tom (surfaces)
ns
B
UAS-E-Cad-RNAi103962
B'
UAS-E-Cad-RNAi103962 (surfaces)
B''
C
UAS-E-Cad-RNAi32904
C'
UAS-E-Cad RNAi32904 (surfaces)
D
UAS-E-Cad-RNAi27082
D'
UAS-E-Cad-RNAi27082 (surfaces)
D''
E
E-Cad on side a
****
Control
UAS-E-Cad-RNAi103962
UAS-E-Cad-RNAi32904
UAS-E-Cad-RNAi27082

Figure 5.2: Cell-cell adhesion in the fat body tissue of wandering L3-stage larvae is not mediated by E-Cadherin. Fat body tissues expressing Lpp-Gal4+UAS-Myr-td-Tomato.

(A-D) Shows images of UAS-Myr-td-Tom and E-Cad staining in control (A) and E-Cad knockdown's using three different RNAi lines (UAS-E-Cad-RNAi^{103962} (B), UAS-E-Cad-RNAi^{32904} (C), UAS-E-Cad-RNAi^{27082} (D))

(A'-D') Shows no significant difference in E-Cad staining between sides a and b in fat body tissues expressing E-Cad knockdowns (B'-D') when compared to the control (A').

(A''-D'') Shows that UAS-Myr-td-Tom is symmetrically distributed on the two opposite sides of the fat body tissues.

(E) Graph comparing E-Cad staining on the higher side of E-Cad (side a) to the control.

(N≥3 fat body tissues, 3 regions imaged on each side, Multiple comparison Ordinary one-way Anova, ****P<0.0001).

Imaged using Zeiss-vis 63x oil immersion lens. Scale bars = 20μm.

My findings showing a rather weak and diffuse concentration of E-Cadherin and Par-3 at both the apical and apicolateral domain of FBCs in combination with the lack of a dissociation phenotype upon E-Cad RNAi suggested that cell-cell adhesion in the fat body is likely mostly mediated via the Collagen IV Intercellular Adhesion Concentrations (CIVICs) described before (Dai et al., 2017). Indeed, Dai et al. (2017) reported moderate cell-cell-dissociation of FBCs caused by Col IVα1 (=Cg25C) RNAi, Col IVα2 (=Viking) RNAi or Integrin beta (=Mys) RNAi (Dai et al., 2017). Hence, I decided to study the localization of CIVICs in the fat body tissue in a wandering 3rd instar larva by looking at Viking-GFP. I hypothesized that CIVICs might be asymmetrically localized along the lateral domain. To do this, Viking-GFP (protein trap line that drives expression under endogenous promotor, marks CIVICs and basement membrane marker) and UAS-Myr-td-Tom (membrane marker) were expressed under the fat body driver, Lpp-Gal4. The fat body tissue was then dissected from 10 different animals and imaged. I then quantified the number of CIVICs in the projection of the first 10 layers of the z-stacks (corresponding to the top 2.5 micrometer of the tissue), using a unified threshold for all samples. My results showed that CIVICs were, as expected, seen as punctae of various sizes along the lateral junctions of FBCs (Figure 5.3 A). Please note that the broader distribution of CIVICs seen along junctions is due to junctions not being perfectly straight in the Z axis. Interestingly, this also showed, that the number of CIVICs was significantly higher on side b compared to side a (Figure 5.3 C), which can also be visually seen in the images in Figure 5.3 A “black arrows”. Moreover, the sum area of these CIVICs was similarly higher on side b, as shown in the graph in Figure 5.3 D. This suggests, that while CIVICs are found along the lateral junctions, as shown before (Dai et al., 2017), there is an asymmetric distribution of CIVICs along the lateral junctions, with fewer being present near the apical surface.

This experiment also allowed me to assess the basement membranes on both surfaces of the fat body, which have been reported to be the same on both sides (Jia et al., 2014). This would be an unusual feature for a tissue with apicobasal polarity since epithelia usually only have a basement membrane on their basal side. Hence, we decided to also compare the Viking-GFP mean intensities in the basement membrane on both surfaces to see if there was any difference using the same surface ROI that was previously used in Figure 4.1. My quantifications indicated that there is no significant difference between the two sides (Figure 5.3 B). However, since the laser settings were set to be optimal for the much brighter CIVICs, the signal in the basement membranes was rather low, which is suboptimal for this quantification. Moreover, our electron microscopy images of dissected fat body also suggested no obvious difference between the two sides of the basement membranes (Figure 5.3 E' "arrowhead"). Together, this suggests that the basement membrane is likely uniform on both sides of the fat body tissue of wandering L3-stage larva. However, despite having a uniform basement membrane on both surfaces, I found that Integrins, which are major adhesion proteins that facilitate linkage between basement membrane components and the cytoskeleton, were asymmetrically localized in the fat body tissue and were significantly higher on side b (basal side) compared to side a (Figure 5.3 F).

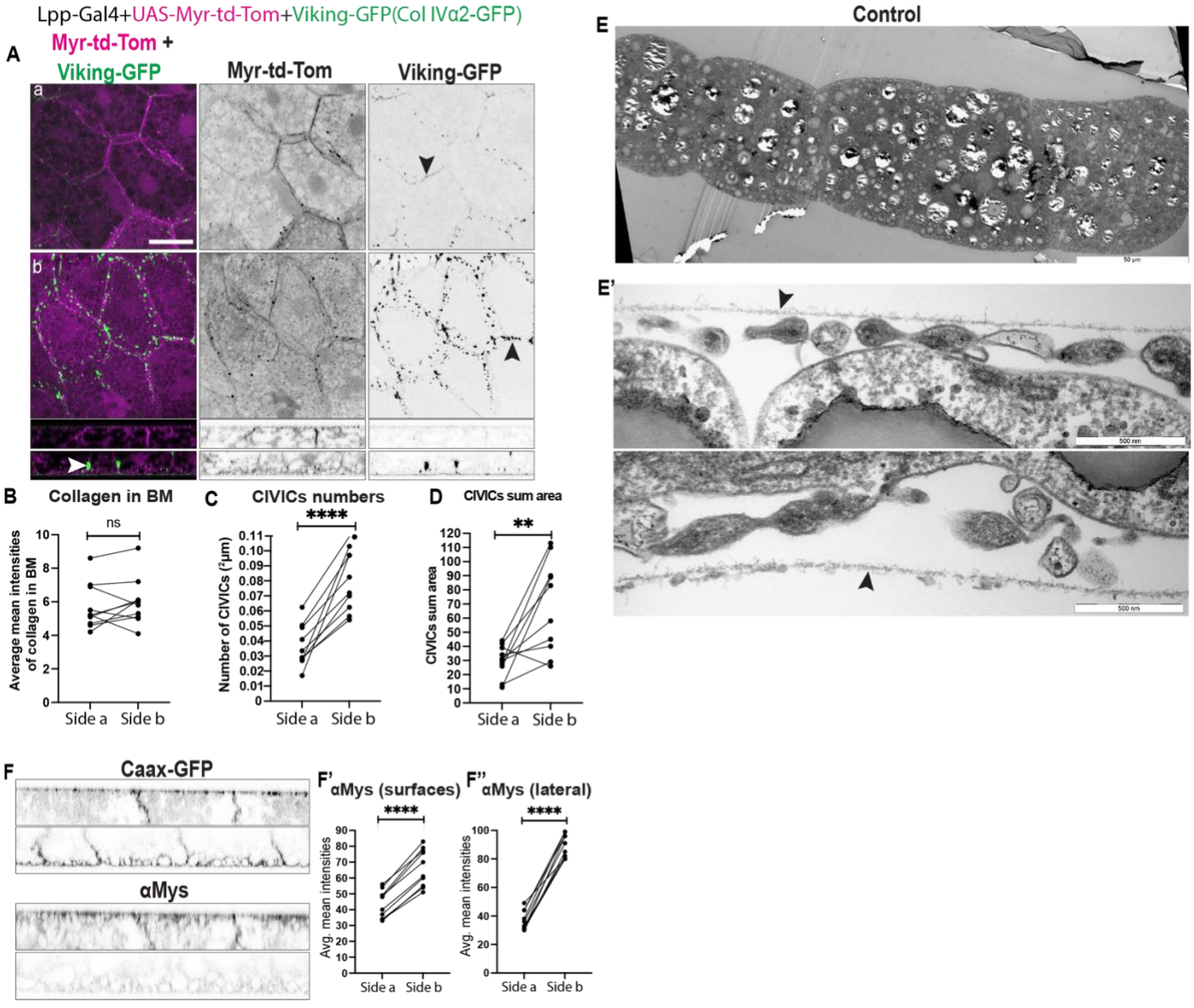
Lpp-Gal4+UAS-Myr-td-Tom+Viking-GFP(Col IVα2-GFP)
A
Myr-td-Tom +
Viking-GFP
Myr-td-Tom
Viking-GFP
a
b
B
Collagen in BM
ns
Average mean intensities of collagen in BM
Side a
Side b
C
CIVICs numbers
****
Number of CIVICs (²µm)
D
CIVICs sum area
**
CIVICs sum area
E
Control
E'
F
Caax-GFP
αMys
F'
αMys (surfaces)
Avg. mean intensities
F''
αMys (lateral)

Figure 5.3: CIVICs is asymmetrically localized in the fat body tissue of wandering L3-stage larvae. Fat body tissues expressing Lpp-Gal4+UAS-Myr-td-Tomato+Viking-GFP.

(A) Max-projection images from top ten layers of UAS-Myr-td-Tomato “magenta” (membrane marker) merged with CIVICs “green”.
(B) There no significant difference in the basement membrane average mean intensities when comparing the two sides of the fat body tissue.
(C-D) The number of CIVICs is significantly higher on side b and is also slightly bigger in size (D). Each dot represents the average mean intensities of 3 regions measured on each side of each fat body tissue. (N≥10 fat body tissues, 3 regions imaged on each side, Paired T-test, ****P<0.0001, ** P>0.01, ns P>0.9999).
(E-E’) Transmission electron microscopy used to visualize the basement membrane “arrowhead” on both sides of the fat body tissue in wandering L3-stage larva. A zoomed in image is shown in (E’).
(F) Shows integrin asymmetry with integrin being higher on side b compared.
Imaged using Zeiss-vis 63x oil immersion lens. Scale bars = 20μm.

5.1 Discussion

In a classic epithelium, apicobasal polarity proteins are known to regulate cell-cell adhesion via Par-3 and E-Cadherin adherens junction. Therefore, in this chapter I aimed to investigate the localization of Par-3 and E-Cadherin in the fat body tissue on wandering L3-stage larva. Using a similar method used to quantify polarity proteins in 3rd instar larvae in Chapter IV; in this chapter I showed that E-Cadherin and Par-3 show a weak and diffuse yet increased localization at the apical and apicolateral domain of the fat body, unlike in an epithelium where E-Cadherin is present either in an apicobasal belt or in spot adherens junctions. Moreover, although a previous study showed that cell-cell adhesion in *Drosophila* fat body relies on Collagen IV Intercellular Adhesion Concentrations (CIVICs) (Dai et al., 2017), the localization and distribution of CIVICs in the fat body remained unclear. This is due to the fact that imaging the two sides of the fat body was previously not thought to be possible. Thus, I aimed to investigate CIVICs localization and distribution in the fat body tissue of wandering L3-stage larva by dissecting fat body tissue expressing Vkg-GFP along with a membrane marker and quantifying the number of CIVICs on both sides of the basement membrane. I showed that CIVICs are present in lower levels in the apicolateral domain but otherwise found along the remaining lateral domain. Given the weak staining for E-Cadherin using both antibody staining and protein trap lines (data not shown), I aimed to determine whether E-Cadherin indeed plays a role in cell-cell dissociation in the fat body. I tested the effects of knocking down E-Cadherin using three different RNAi isoforms and validated the efficiency of my staining for E-Cadherin protein. My results revealed that E-Cad RNAi is not sufficient to induce cell-cell dissociation in the fat body tissue of wandering 3rd instar larva, in contrast to Col IV RNAi and Integrin RNAi as shown by Dai et al. (2017). Together this suggests that cell-cell adhesion in the fat body tissue of

an L3-stage larva is likely mainly mediated by CIVICs (Dai et al., 2017) rather than E-Cadherin. However, we cannot rule out that E-Cad might contribute to cell-cell adhesion, since a double knockdown of E-Cad together with Col IV or Integrin could potentially lead to a stronger dissociation. This type of adhesion does not only highlight the unique nature of the fat body tissue, but also the diversity of adhesion mechanisms that are present in different types of tissues. Moreover, unlike human and mammalian epithelia, where tight junctions are apically localized and adherens junctions extend along the lateral domain, *Drosophila* epithelia exhibits a reversed epithelium, where adherens junctions are positioned apically and tight junctions lie just beneath them (Coopman & Djiane, 2016). To gain a better understanding on the structural organization of the fat body tissue, it is vital to determine the precise localizations of adherens junctions and tight junctions in the fat body tissue of wandering 3rd instar larva in future experiments.

In this chapter, I also showed that Collagen IV on the surface of the basement membrane is not asymmetrically localized and validated my result with electron microscopy images that showed no difference between the two opposite sides of the basement membrane in the fat body tissue of wandering L3-stage larva. This aligns with a previous study reporting that the basement membrane is the same on both sides of the tissue (Jia et al., 2014). However, to ensure the accuracy of my quantifications, Collagen IV measurements must be repeated using the optimal laser settings. Interestingly, despite the uniformity of the basement membrane on both sides of the fat body tissue, the fact that the basolateral domain (side b) contained higher number of CIVICs which were slightly larger in size compared to the opposite side (side a), potentially suggests that the two sides of the basement membrane of the fat body are different. In addition to CIVICs asymmetry, my findings also indicate that Integrin asymmetry, with higher levels on

side b, serves as a key factor to distinguish the two sides of the fat body tissue. Since the function of CIVICs depends on cell attachment through Integrin and Syndecan (Dai et al., 2017), it would be key to test whether Syndecan is also localized on the basal side (side b) of the fat body tissue, similar to Integrin. This raises an important question on whether the composition of the basement membrane is truly identical on both surfaces of the fat body tissue. While I showed that Collagen IV appears to be evenly distributed, other basement membrane components like Laminin, Nidogen and Perlecan may be asymmetrically localized, potentially creating distinct structural and functional properties on the two opposite sides of the fat body tissue.

Chapter VI. Apicobasal polarity regulates collagen-dependent cell-cell adhesion in the larval fat body

The fact that the fat body tissue of wandering L3-stage larva had not been known to exhibit apicobasal polarity opened intriguing questions about the functional importance of this polarity. In classic epithelia apicobasal polarity proteins are known to regulate cell-cell adhesion via E-Cadherin, tissue integrity and cellular behavior (Nistico et al., 2012). To explore the role of apicobasal polarity proteins in the fat body, I next investigated the effects of knocking down several polarity proteins, such as aPKC, Scribble, Crumbs, and Lgl in the fat body. To do this, I imaged fat body from wandering third instar larvae expressing UAS-aPKC-RNAi^{34332}, UAS-Scribble-RNAi^{105412}, and UAS-Crumbs-RNAi^{39177} and a membrane marker (UAS-Myr-td-Tom) under the control of an early fat body driver Lpp-Gal4 that is expressed from the first instar larval stage that was mounted in DAPI (a nuclear stain) containing vectashield. My results showed that

unlike the control where fat body cells remain closely attached to each other (Figure 6.1 A); knocking down apKC (UAS-aPKC-RNAI^{34332}, Figure 6.1 B), Crumbs (UAS-Crumbs-RNAi^{39177}, Figure 6.1C), and Scribble (UAS-Scribble-RNAi^{105412}, Figure 6.1D) individually resulted in some aberrant dissociation of fat body cells (shown in asterisks). UAS-Myr-td-Tom was used to clearly observe the membranes of fat body cells and to be able to visualize the gaps between fat body cells in the fat body tissue. Moreover, DAPI was used to confirm that the cellular gaps represent true dissociation rather than another overlapping cell or any other phenomenon like multilayering.

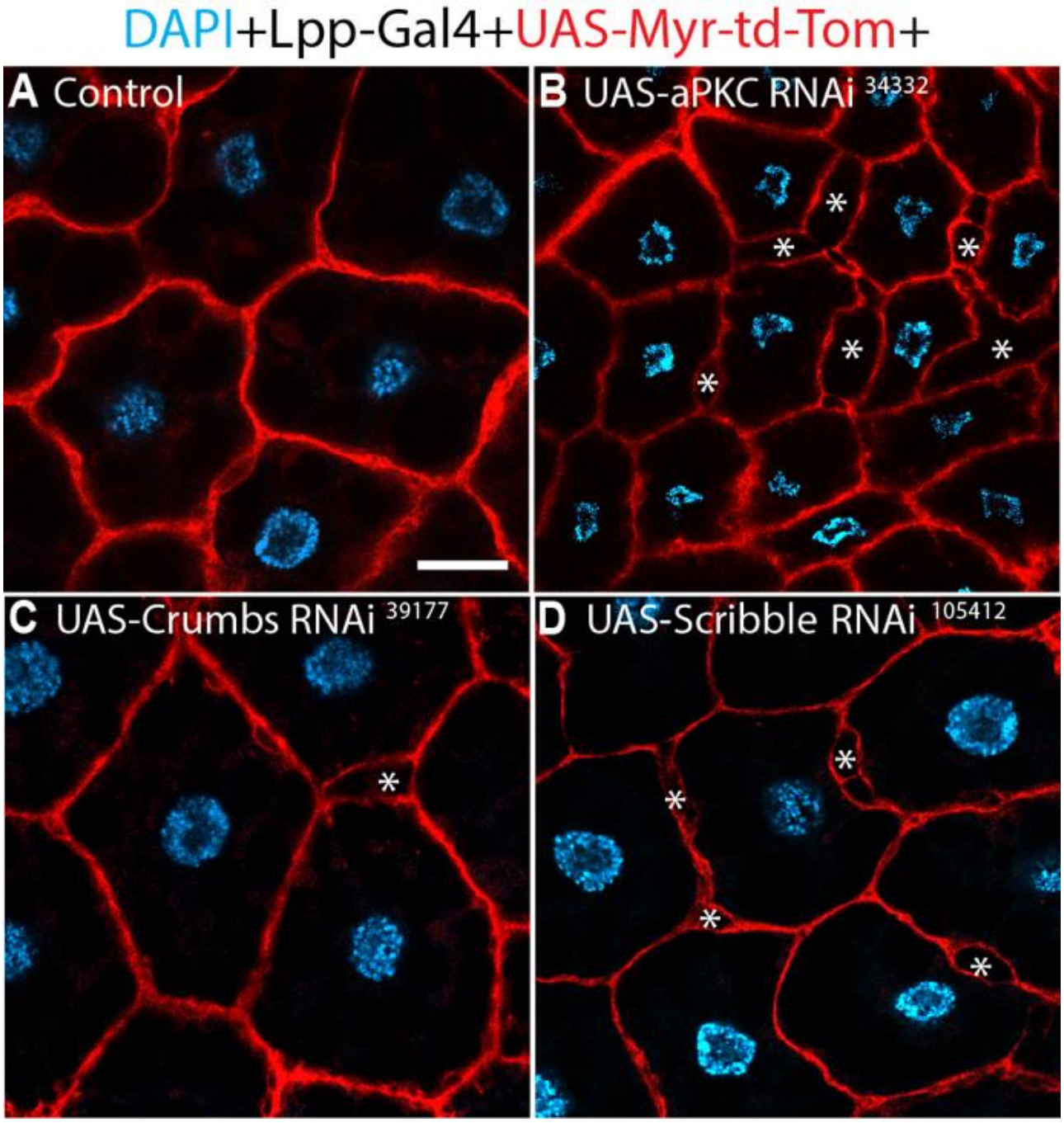
DAPI+Lpp-Gal4+UAS-Myr-td-Tom+
A Control
B UAS-aPKC RNAi 34332
C UAS-Crumbs RNAi 39177
D UAS-Scribble RNAi 105412

Figure 6.1: Knocking down polarity proteins (aPKC, Crumbs and Scribble) results in premature cell-cell dissociation. Fat body tissues expressing Lpp-Gal4+UAS-Myr-td-Tomato.

(A-D) In the control, fat body cells are closely attached to each other (A). Knocking down polarity proteins apKC (UAS-aPKC-RNAI^{34332}) (B), crumbs (UAS-Crumbs-RNAi^{39177}) (C), and Scribble (UAS-Scribble-RNAi^{105412}) (D), individually results in fat body cell dissociation at tricellular and bicellular gaps shown in asterisks. Nuclear maker DAPI (blue). Plasma membranes marked with Myr-td-Tomato (red). (N≥5 fat body tissues).
Imaged using Zeiss-vis 63x oil immersion lens. Scale bars = 20μm.

To validate my findings, I tested additional isoforms of the polarity protein knockdowns. UAS-Myr-td-Tom was again used as a membrane maker to provide clear visualization of cell membranes without using DAPI. My results showed that knocking down aPKC using an alternate RNAi line (UAS-aPKC-RNAi^{105624}, Figure 6.2 B “asterisks”) led to a similar result of premature dissociation of fat body cells in wandering 3rd instar larvae. Additionally, knocking down Crumbs using two additional lines (UAS-Crumbs-RNAi^{34999} and UAS-Crumbs-RNAi^{330135}, Figure 6.2 C and D “asterisks”), and another line for Scribble (UAS-Scribble-RNAi^{35748}, Figure 6.2 E “asterisks”) and Lgl (UAS-Lgl-RNAi^{109604}, Figure 6.2 F “asterisks”) also resulted in early dissociation of fat body cells. These results suggest that polarity proteins aPKC, Lgl, Scribble and Crumbs are important in maintaining cell-cell adhesion and tissue integrity in the fat body tissue of wandering L3-stage larvae in *Drosophila.*

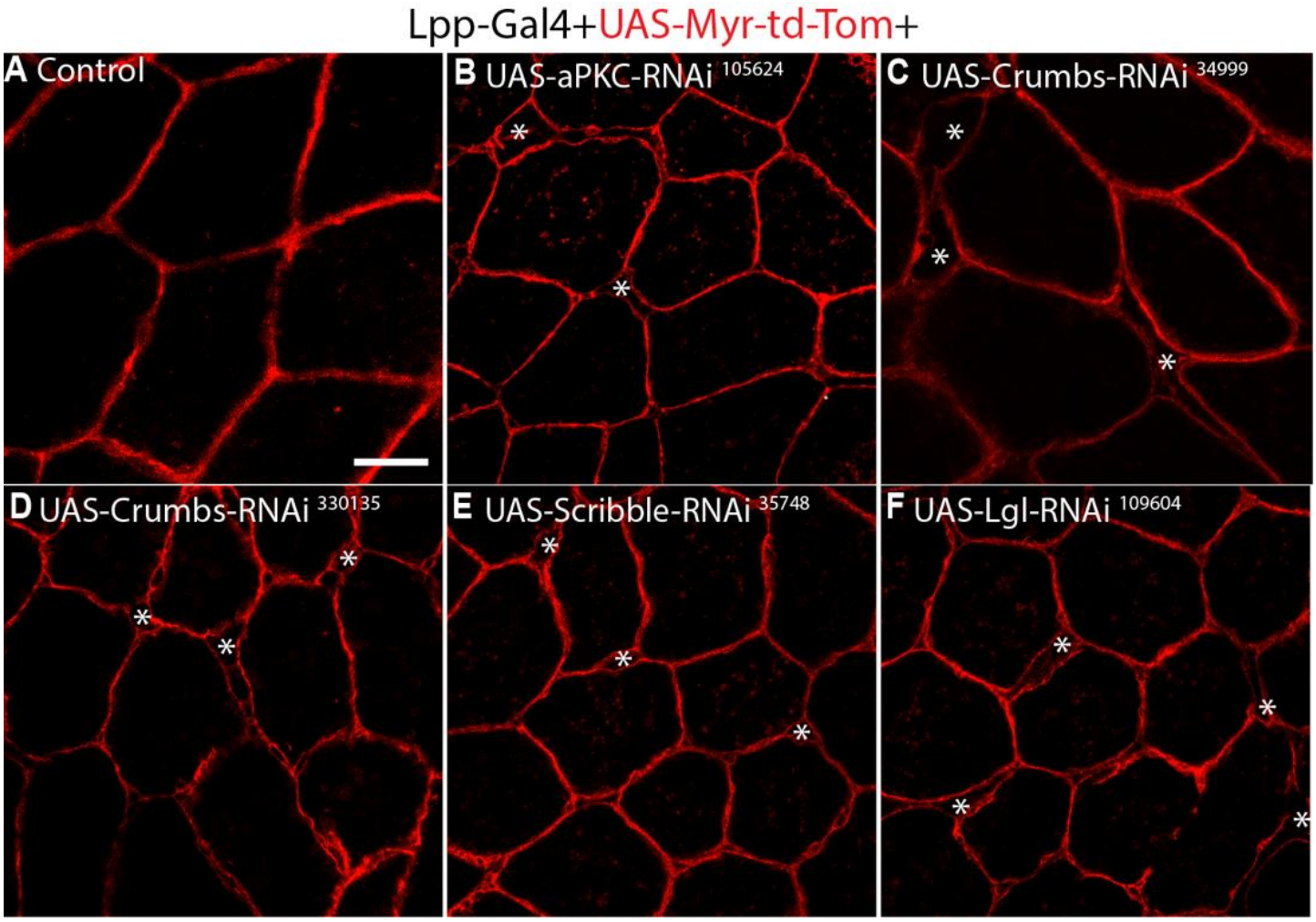
Lpp-Gal4+UAS-Myr-td-Tom+
A Control
B UAS-aPKC-RNAi 105624
C UAS-Crumbs-RNAi 34999
D UAS-Crumbs-RNAi 330135
E UAS-Scribble-RNAi 35748
F UAS-Lgl-RNAi 109604

Figure 6.2: Knocking down polarity proteins (aPKC, Crumbs, Scribble and Lgl) results in premature cell-cell dissociation. Fat body tissues expressing Lpp-Gal4+UAS-Myr-td-Tomato.

(A-F) In the control fat body cells remain closely attached to each other (A). Knocking down polarity proteins apKC (UAS-aPKC-RNAI^{105624}) (B), Crumbs (UAS-Crumbs-RNAi^{34999} and UAS-Crumbs-RNAi^{330135}) (C and D respectively), Scribble (UAS-Scribble-RNAi^{35748}) (D), and Lgl (UAS-Lgl-RNAi^{109604}) individually results in early fat body cell dissociation at tricellular and bicellular gaps shown in asterisks. Plasma membranes marked with Myr-td-Tomato (red). (N≥5 fat body tissues).

Imaged using Zeiss-vis 63x oil immersion lens. Scale bars = 20μm.

While these initial experiments were informative, the low N number for these experiments needed for further replication. Thus, I repeated this experiment but this time with a different marker. Polarity protein knockdowns (UAS-aPKC-RNAi^{34332}, UAS-Crumbs-RNAi^{39177}, and UAS-Scribble-RNAi^{105412} were expressed with the Lpp-Gal4 driver alongside with UAS-Myr-td-Tom for membrane labelling and Viking-GFP in order to visualize and quantify the mean intensities of the basement membrane and CIVICs. This then allowed me to quantify dissociation defects as well as numbers of CIVICs, the adhesion complexes responsible for cell-cell adhesion (Dai et al., 2017). I initially started by quantifying the number of tricellular and bicellular gaps. In order to quantify the extent of fat body cell dissociation, I set a threshold where I counted tricellular and bicellular gaps only including the ones present in deeper areas of the tissue (from 10 layers deep from where the cell starts all the way to where the z-stack ends). Statistical comparison was conducted using a paired t-test to evaluate the difference in the number of gaps of the polarity protein knockdowns compared to the control. As shown in the graph (Figure 6.3 A and B), the control samples showed almost no gaps at tricellular or bicellular junctions, while aPKC (UAS-aPKC-RNAi^{34332}) resulted in a significant increase in the number of both tricellular (Figure 6.3 A) and bicellular gaps (Figure 6.3 B). Although, Crumbs-RNAi^{39177} showed a slight significant increase in the number of tricellular gaps (Figure 6.3 A), it was less pronounced than that observed in the aPKC knockdown. Moreover, Crumbs knockdown (UAS-Crumbs-RNAi^{39177}) revealed no significant increase in the number of bicellular gaps when compared to the control. Quantifications of tricellular and bicellular gaps of Scribble knockdown (UAS-Scribble-RNAi^{105412}) showed a significant increase in the number of tricellular gaps compared to the control (Figure 6.3 A) but not bicellular gaps (Figure 6.3 B).

A

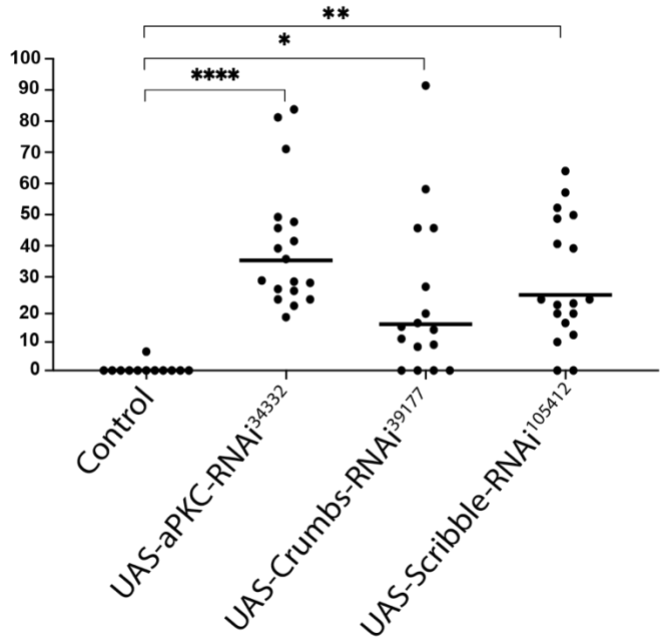
Tricellular gaps (%)
**
*
****
100
90
80
70
60
50
40
30
20
10
0
Control
UAS-aPKC-RNAi34332
UAS-Crumbs-RNAi39177
UAS-Scribble-RNAi105412

B

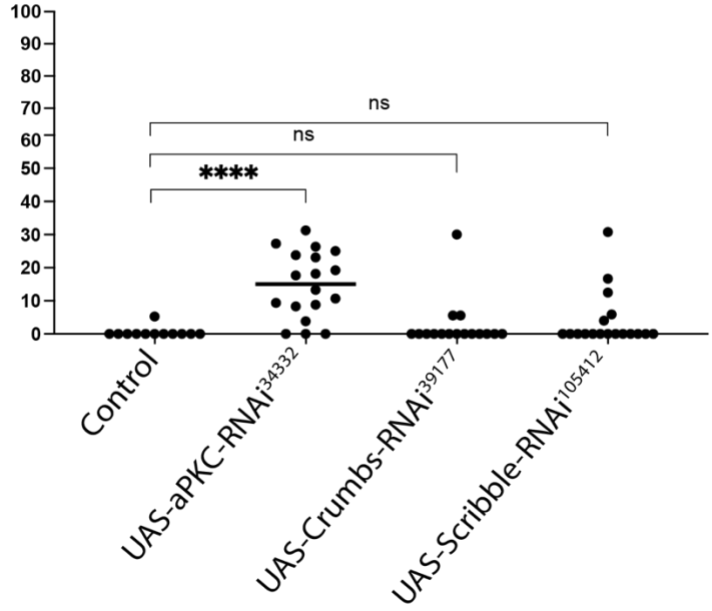
Bicellular gaps (%)
ns
ns
****
100
90
80
70
60
50
40
30
20
10
0
Control
UAS-aPKC-RNAi34332
UAS-Crumbs-RNAi39177
UAS-Scribble-RNAi105412

Figure 6.3: Knocking down polarity protein aPKC results in premature fat body cell dissociation, with a significant increase in both tricellular and bicellular gaps. Fat body tissues expressing Lpp-Gal4+UAS-Myr-td-Tomato+Viking-GFP.

(A-B) Shows percentage of tricellular (A) and bicellular gaps (B). Premature knockdown of polarity proteins aPKc (UAS-aPKC-RNAI^{105624}) results in a significant increase in the number of both tricellular (A) and bicellular gaps (B). However, premature knockdowns of Crumbs (UAS-Crumbs-RNAi^{34999}), and Scribble (UAS-Scribble-RNAi^{35748}) individually, results in a significant increase in the number of tricellular gaps (A) but not bicellular gaps (B). (N≥12 control, N≥18 aPKC-RNAi^{105624}, N≥16 Crumbs-RNAi^{34999}, N≥18 Scribble-RNAi^{35748}, Multiple comparison Ordinary one-way Anova, ****P<0.0001, ** P>0.01, * P=0.037, ns P>0.9999).
Imaged using Zeiss-vis 63x oil immersion lens.

Due to the fact that polarity protein knockdowns led to early dissociation of fat body cells, next I wanted to assess if these dissociation defects would be due to impacted CIVICs, which is known to be the critical mediator of cell-cell adhesion in the fat body tissue (Dai et al., 2017). Viking-GFP-positive CIVICs were assessed as before in Chapter V on each side of the fat body (side a and b). Control samples exhibited asymmetric localization of CIVICs, with higher numbers on side b (Figure 6.4 A, A'), as seen before (Figure 5.3). However, this asymmetry was disrupted in all polarity protein knockdowns (UAS-aPKC-RNAi^{34332}, UAS-Crumbs-RNAi^{39177}, and UAS-Scribble-RNAi^{105412}, please note that only a single layer is shown in Figure 6.4 A-D while the projection of the first 10 layers was shown in Figure 5.3, hence the difference in CIVICs numbers seen in the pictures from the two figures). Precisely, aPKC knockdown (UAS-aPKC-RNAi^{34332}) resulted in a complete loss of CIVICs on both sides, a and b (Figure 6.4 B and B'). Interestingly, when Crumbs was knocked down (UAS-Crumbs-RNAi^{39177}) in the fat body, there was still a high number of CIVICs present but with a reversed distribution along the junctions, with higher numbers of CIVICs on side a rather than side b (Figure 6.4 C and C'). Moreover, Scribble knockdown (UAS-Scribble-RNAi^{105412}) led to an overall strongly reduced number of CIVICs as well as a loss in CIVICs asymmetry (Figure 6.4 D and D'). The graph in Figure 6.4 E emphasizes the significant differences in the number of CIVICs on side b of the polarity protein knockdowns compared to the control. These findings highlight the intricate role of polarity proteins in regulating CIVIC numbers and distribution as well as adhesion in the fat body tissue.

In addition to understanding whether polarity protein knockdowns would impact CIVICs localization, I wanted to test whether it also affected the basement membranes. Due to the fact that the laser intensity was optimized for CIVICs imaging to avoid oversaturation, the basement membrane measurements were less robust. However, despite that, the data still provided

valuable insights. The same ROI was used as before (Figure 5.3 B) to measure the basement membrane on the two surfaces of the fat body. Each dot represents the mean intensity of one region in each fat body tissue. Replicating my previous result, there seems to be no difference between the two sides of the basement membrane in the control (Figure 6.4 A''). However, premature knockdown of the polarity protein aPKC (UAS-aPKC-RNAi^{34332}) (Figure 6.4 B and B'') and Scribble (UAS-Scribble-RNAi^{105412}) (Figure 6.4 D and D'') revealed almost no/less basement membrane present on either of the two surfaces (Figure 6.4 F). In contrast, Crumbs knockdown (UAS-Crumbs-RNAi^{39177}) did not appear to reduce but rather increase Collagen IV levels in the basement membranes (Figure 6.4 C and C'', F).

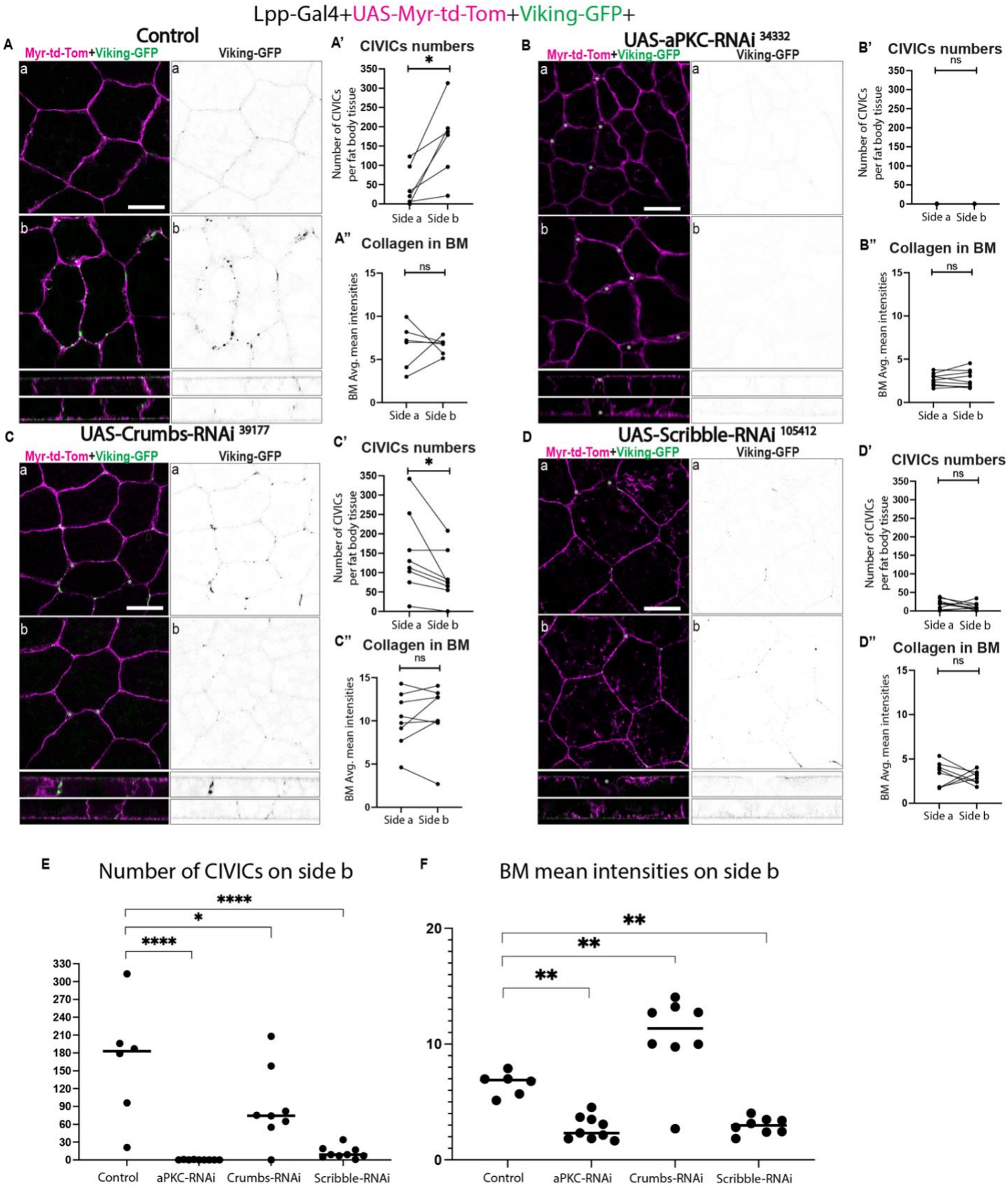
Lpp-Gal4+UAS-Myr-td-Tom+Viking-GFP+
A
Control
Myr-td-Tom+Viking-GFP
Viking-GFP
A'
CIVICs numbers
Number of CIVICs per fat body tissue
Side a Side b
A"
Collagen in BM
BM Avg. mean intensities
ns
B
UAS-aPKC-RNAi 34332
B'
B"
C
UAS-Crumbs-RNAi 39177
C'
C"
D
UAS-Scribble-RNAi 105412
D'
D"
E
Number of CIVICs on side b
Control
aPKC-RNAi
Crumbs-RNAi
Scribble-RNAi
F
BM mean intensities on side b

Figure 6.4: Apicobasal polarity is needed for collagen dependent cell-cell adhesion. Fat body tissues expressing Lpp-Gal4+UAS-Myr-td-Tomato + Viking-GFP.

(A-D) Knocking down polarity proteins disrupts adhesion I the fat body tissue, leading to cell-cell dissociation shown in “asterisk”.
(A’-D’) Knocking down polarity proteins aPKC (UAS-aPKC-RNAi^{34332}) (B’) and Scribble (UAS-Scribble-RNAi^{105412}) (D’) disrupts CIVICs numbers. Premature knockdown of polarity protein crumbs ((UAS-Crumbs-RNAi^{39177}) leads to a reversed distribution of CIVICs.
(A’’-D’’) Premature knockdown of polarity protein aPKC (UAS-aPKC-RNAi^{34332}) (B’’) and Scribble (UAS-Scribble-RNAi^{105412}) (D’’) resulted in no/less basement membrane present on both surfaces of the fat body tissue, while Crumbs knockdown (UAS-Crumbs-RNAi^{39177}) (C’’) led to an increased levels of Collagen IV in the basement membrane. (N≥6 control, N≥9 aPKC-RNAi^{34332}, N≥8 Crumbs-RNAi^{39177}, N≥9 Scribble-RNAi^{105412}, 1 region imaged on each side, Paired T-test, * P=0.037, ns P>0.9999).
(E-F) Graphs comparing the number of CIVICs (E) and the levels of Collagen IV on the higher side (side b) in the polarity knockdowns versus the control. Statistical test used was Multiple comparison Ordinary one-way Anova.
Imaged using Zeiss-vis 63x oil immersion lens. Scale bars = 20μm

6.1 Discussion

Up to this point, my previous results revealed that the fat body tissue of wandering L3-stage larvae exhibits apicobasal polarity, raising questions about the role of polarity proteins in regulating tissue integrity. In this chapter I showed that knocking down polarity proteins aPKC (two RNAi isoforms), Scribble (two RNAi isoforms), Crumbs (three RNAi isoforms), and Lgl (one RNAi isoform) led to premature cell dissociation, where tricellular gaps increased in all knockdowns, while bicellular gaps were significant only in aPKC knockdown. This suggests that polarity proteins may have distinct roles in maintaining cell junctions. The fact that Crumbs and Scribble knockdown only resulted in tricellular gaps could be due to the greater complexity of tricellular junctions that may rely on the coordination between polarity and junctional proteins like Gliotactin, which is concentrated at tricellular junctions (Sharifkhodaei et al., 2016). Bicellular adhesion, on the other hand, is maintained by other adhesion systems, like integrin (Brown, 2000), that may possibly compensate at bicellular junctions if polarity is disrupted. To validate the fact that Crumbs and Scribble may work in coordination with junctional proteins, knocking down Crumbs and Scribble and staining for tricellular markers like Gliotactin will be informative.

To confirm that these gaps represent true dissociation and not overlapping cells or multilayering, DAPI staining was used for some of the knockdowns (one RNAi isoform of aPKC, Crumbs, Scribble and Lgl). Although Lgl knockdown led to aberrant fat body cell dissociation, testing a second RNAi isoform would be critical to validate my results. Furthermore, staining for each polarity protein and quantifying their levels on the surface of each side of the fat body tissue, similar to the method used to measure polarity proteins in wandering 3rd instar larva

(Chapter IV) or western blotting to assess protein levels, can be employed to assess the effectiveness of the RNAi knockdowns.

Overall, premature cell dissociation upon polarity protein knockdowns indicates the importance of these polarity proteins in maintaining cell-cell adhesion and raised a major question on whether the number of CIVICs might be reduced, since CIVICs was previously shown to play a role in fat body cell-cell adhesion (Dai et al., 2017). To investigate this, Viking-GFP was expressed along with a membrane marker UAS-Myr-td-Tomato. My findings revealed that disruption of polarity proteins aPKC, Scribble, and Crumbs (one RNAi isoform tested for each) impairs CIVICs numbers. Knocking down aPKC and Scribble resulted in complete loss or reduced number of CIVICs, respectively, which could potentially mean that both polarity proteins (aPKC and Scribble) may play a role in pathways involved in the formation of CIVICs with aPKC playing a major role and Scribble playing a minor role. On the other hand, Crumbs knockdown, surprisingly, reversed CIVICs localization. This unexpected result suggest that Crumbs may be involved in trafficking CIVICs to the lateral domain and its absence leads to mislocalized secretion. It is likely that Crumbs acts upstream of trafficking regulators like Kinesin-1. To test this, a double RNAi knockdown (Crumbs-RNAi + Kinesin-1-RNAi) could be perfumed to determine whether CIVICs mislocalization is enhanced or suppressed.

Furthermore, my results show that aPKC and Scribble knockdowns reduced Collagen IV levels in basement membranes, whereas Crumbs knockdown increased them. In *Drosophila* follicle cells Collagen IV is secreted first into the pericellular space before being incorporated into the basement membrane. This secretion is directed via Rab10, a trafficking protein (Isabella & Horne-Badovinac, 2016). It may be that cell adhesion mediated by CIVICs is unique to tissues

that secrete collagen just like the fat body. Interestingly, the fat body (Dai et al., 2017) and follicle cells (Isabella & Horne-Badovinac, 2016) produce two populations of Collagen IV, one secreted to form the BM at the surface and the other secreted laterally to form Collagen IV concentrations in the pericellular space. One explanation behind having reduced Collagen IV in the BM could be that both aPKC and Scribble play a role in the secretion of CIVICs, specifically the population that gets secreted to the BM. In contrast, Crumbs knockdown led to increased Collagen IV intensity in the basement membrane despite resulting in gaps at tricellular junctions. This might suggest that Crumbs knockdown affects a yet unidentified adhesion mechanism or regulates collagen distribution without disrupting the other forms of adhesion, if there is another form of adhesion in the *Drosophila* fat body tissue, which still needs to be studied further. Examples from myotendinous junctions show that Integrin-ECM interactions can mediate adhesion between cells via an intermediate ECM scaffold. Thus, it could be that that fat body involves two forms of adhesion mechanisms one via integrin and the other via CIVICs and Crumbs might play a role in pathways involved integrin mediated cell-cell adhesion rather than CIVICs which is why partial dissociating is seem upon Crumbs knockdown despite having high numbers of CIVICs present between cells and in the BM. In fact, Dia et al. (2017) showed that knocking down integrin results in adhesion defects in *Drosophila* fat body tissue. These findings hint at complex and possibly compensatory mechanisms that regulate adhesion in *Drosophila* fat body. To further validate these results, repeating Collagen IV quantifications In the BM using the optimal laser setting is critical to draw the conclusion of Collagen IV being symmetrically localized upon polarity protein knockdowns, since the settings currently used were adjusted to CIVICs.

In general, disrupting polarity alters the formation of polarity complexes, which can in turn affect the localization of other polarity proteins within the cell. Therefore, knocking down specific

polarity proteins and analyzing the distribution of other polarity proteins could offer deeper insights into the mechanisms regulating polarity in the *Drosophila* larval fat body. For instance, previous studies on *Drosophila* ovariole demonstrated that inhibiting Dlg or Scribble led to mislocalization of aPKC throughout the cell, rather than being restricted to the apical domain (Schmidt & Peifer, 2020). In addition, since the effects of polarity proteins were only assessed for a few proteins (aPKC, Crumbs and Scribble), investigating additional polarity proteins, such as Dlg, could provide insights into the functional roles of individual polarity proteins, particularly in cell-cell adhesion.

So far, my findings indicate that polarity in the fat body is essential for maintaining cell-cell adhesion via CIVICs and tissue integrity. This raises questions on the broader functional roles of polarity proteins in the *Drosophila* larval fat body. Given that *Drosophila* adipocytes play a role in lipid storage and release (Liu & Huang, 2013), further investigation of these proteins in maintaining proper lipid organization could provide valuable insights into their contributions to fat body function. This can be achieved by knocking down polarity proteins and staining lipid droplets with BODIPY, followed by quantitative analysis to determine whether polarity knockdown affects lipid droplet distribution or size.

Overall, this work revealed the importance of polarity proteins in *Drosophila* fat body in maintaining tissue integrity and cell-cell adhesion, particularly via CIVICs. Unlike primary epithelia such as the embryonic epithelium, where polarity is essential in organizing apical junctions, like E-Cadherin, and epithelial morphology; the fat body does not reply on classic epithelium adhesion mechanisms the but instead it relies on ECM-based adhesion structures, possibly as a consequence of its mesodermal origin and role in systemic physiology. This highlights how polarity pathways uniquely adapt to meet tissue specific structural needs.

Altogether, this underscores the adaptability of polarity proteins in organizing tissue architecture and physiological role across different *Drosophila* tissues.

Chapter VII. Ecdysone signaling and Serpent regulate cell-cell-dissociation during fat body remodeling through the loss of apicobasal polarity and the loss of CIVICs

7.1 Apicobasal polarity is lost during fat body remodeling by 3hr APF

A major aim of my PhD was to investigate fat body remodeling, a process we hypothesized to be similar to an epithelial-to-mesenchymal/amoeboid transition (EMT/EAT) which many tissues undergo in development and disease including cancer metastasis. Epithelial to mesenchymal transition is characterized by loss of cell-cell adhesion initiated through the loss of apicobasal cell polarity resulting in E-Cadherin downregulation and loss of adherens junctions (Yang et al., 2020). My findings from the previous chapters revealed that the fat body in the larva before undergoing FBR displays an apicobasal polarity which regulates cell-cell adhesion mostly by CIVICs rather than E-Cadherin. This suggests that the fat body tissue likely undergoes a unique mechanism of cell-cell dissociation during fat body remodeling. To study how loss of cell-cell adhesion is regulated during FBR, I first investigated whether apicobasal polarity is lost during FBR, similar to classic EMT. Fat body tissues were dissected from 3hr after puparium formation (3hr APF), early during the process of fat body remodeling. This timepoint was chosen because, at later stages, when fat body cells undergo partial/complete dissociation, I was unable to dissect the fat body and could not use it for immunostaining and imaging. Using a similar

approach to the L3-stage experiments, the fat body tissues were dissected from several pupae (3hr APF), immunostained for polarity proteins (aPKC, Par-6, Crumbs, Par-3, Dlg and Lgl) and mounted between two coverslips. Ubi-Caax-GFP was again used to ensure that the fat body tissues were mounted equally close to the coverslip on both sides and to visualize the cells. The same quantification method that was used to quantify polarity proteins in the fat body tissue of 3rd instar larvae, using the same set of ROIs to quantify the mean intensities on the surface of the cells and on the lateral sides close to the surface was used here. My results showed that the asymmetric localization of polarity proteins previously shown for fat body from third instar larvae (Figure 4.2) was lost early during remodeling at 3hr APF well before complete tissue dissociation (aPKC (Figure 7.1 B), Par-6 (Figure 7.1 C), Crumbs (Figure 7.1 D), Par-3 (Figure 7.1 E), Dlg (Figure 7.1 F) and Lgl (Figure 7.1 G).

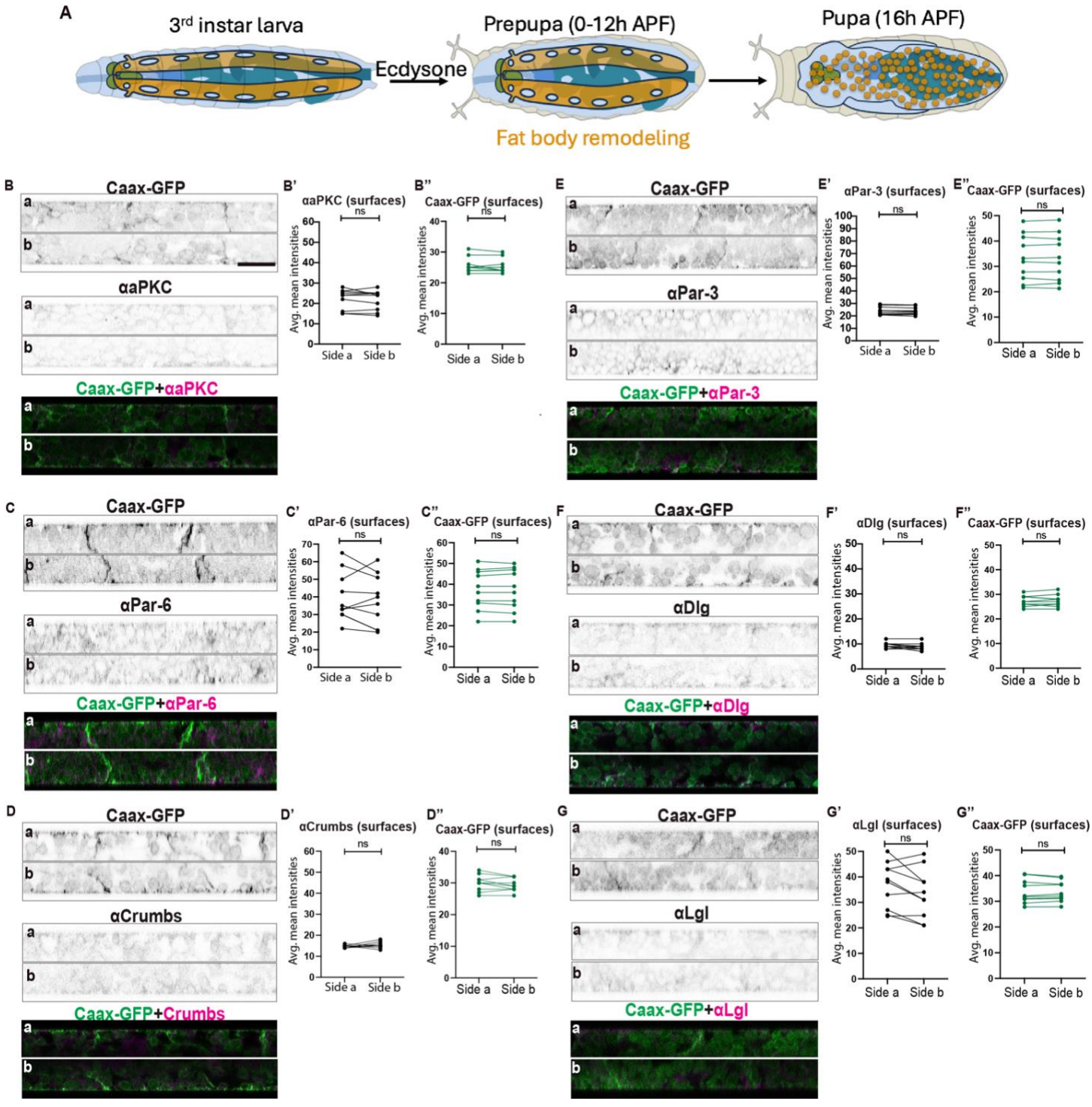
A
3rd instar larva
Ecdysone
Prepupa (0-12h APF)
Pupa (16h APF)
Fat body remodeling
B
Caax-GFP
αaPKC
Caax-GFP+αaPKC
B'
αaPKC (surfaces)
B''
Caax-GFP (surfaces)
E
Caax-GFP
αPar-3
Caax-GFP+αPar-3
E'
αPar-3 (surfaces)
E''
Caax-GFP (surfaces)
C
Caax-GFP
αPar-6
Caax-GFP+αPar-6
C'
αPar-6 (surfaces)
C''
Caax-GFP (surfaces)
F
Caax-GFP
αDlg
Caax-GFP+αDlg
F'
αDlg (surfaces)
F''
Caax-GFP (surfaces)
D
Caax-GFP
αCrumbs
Caax-GFP+Crumbs
D'
αCrumbs (surfaces)
D''
Caax-GFP (surfaces)
G
Caax-GFP
αLgl
Caax-GFP+αLgl
G'
αLgl (surfaces)
G''
Caax-GFP (surfaces)
Avg. mean intensities
Side a
Side b
ns

Figure 7.1: Apicobasal polarity is lost early during fat body remodeling. All fat body tissues expressing Caax-GFP.

(A) Schematic of the fat body tissue in wandering L3-stage larvae undergoing fat body remodeling (0-12h APF), resulting in fat body cells free floating in the hemolymph.
(B-G) Caax-GFP symmetrically localized on the surface and lateral domains between the two sides of the fat body tissue (side a and side b) (B''-G''). Asymmetry of polarity proteins αaPKC (B-B'), αPar-6 (C-C'), and αCrumbs (D-D'), αPar-3 (E-E'), αDlg (F-F'), and αLgl (G-G') is lost by 3hr APF, before fat body remodeling is complete. Each dot in the graphs shows in Figure 7.1 represents the average mean intensity of 10 different regions imaged on each side of each fat body tissue. (N≥10 fat body tissues, 10 regions imaged on each side, Paired T-test, ns $P<0.9999$).
Imaged using Zeiss-vis 63x oil immersion lens. Scale bars = 20μm.

7.2 Screen to identify new regulators of fat body remodeling reveals Serpent as a new key regulator of fat body remodeling

Having found that apicobasal polarity is lost early during fat body remodeling, I next wanted to uncover the molecular mechanism driving this loss of polarity as well as other steps during FBR. So far, only few regulators including Ecdysone receptor (Bond et al., 2011) have been known to regulate FBR, thus I wanted to screen for candidate genes that are known to regulate tissue remodeling and EMT in other model systems. First, I had to establish an assay that could be used to test whether these candidates regulate FBR. I initially optimized this assay using expression of Ecdysone receptor dominant negative (EcD-R-DN) as a positive control, since Ecdysone signaling is previously known to play a role in FBR. I expressed RNAi constructs against these candidates together with this I crossed Lpp-Gal4+UAS-NLS-mCherry to w67 (control) and UAS-EcD-R-DN^{6869}. I dissected the Lpp-Gal4+UAS-NLS-mCherry+UAS-EcD-R-DN or Lpp-Gal4+UAS-NLS-mCherry (control) expressing pupae out of the pupal case at 16hr APF, when fat body remodeling is complete. Generally, by the end of the process of FBR, FBCs move in to the head of the pupa just after head eversion happens at 12hAPF, as shown in the control pupae at 16hAPF in Figure 7.2 A and B. Moreover, since EcD-DN was used as a positive control to block FBR, here FBCs did not dissociate, thus remaining as a sheet and failed to enter the head of the pupa (Figure 7.2 C). Quantification of the number of FBCs in the front half of the head of pupa showed that FBCs expressing UAS-EcD-R-DN^{6869} have significantly lower numbers of FBCs compared to the control (Figure 7.2 D). In fact, no FBCs were observed in the head of the EcD-R-DN^{6869} expressing pupae at 16hr APF. To validate that FBCs indeed failed to undergo dissociation in pupa expressing EcR-DN at 16hr APF, I live imaged pupae expressing

UAS-EcD-R-DN^{6869} as well as a membrane marker (Lpp-Gal4+UAS-Myr-td-Tomato+UAS-EcD-R-DN). Confocal images in the dorsal abdomen, thorax and head of these pupae in Figure 7.2 E shows that unlike the control where fat body cells had undergone complete dissociation at 16 APF hours after FBR is complete, FBCs in pupa expressing UAS-EcD-R-DN^{6869} remained closely attached in the dorsal abdomen and thorax of the pupa at 16 APF (Figure 7.2 E), thus no fat body cells migrated to the head. Based on my results, this shows that this is a suitable assay to identify new genes involved in FBR.

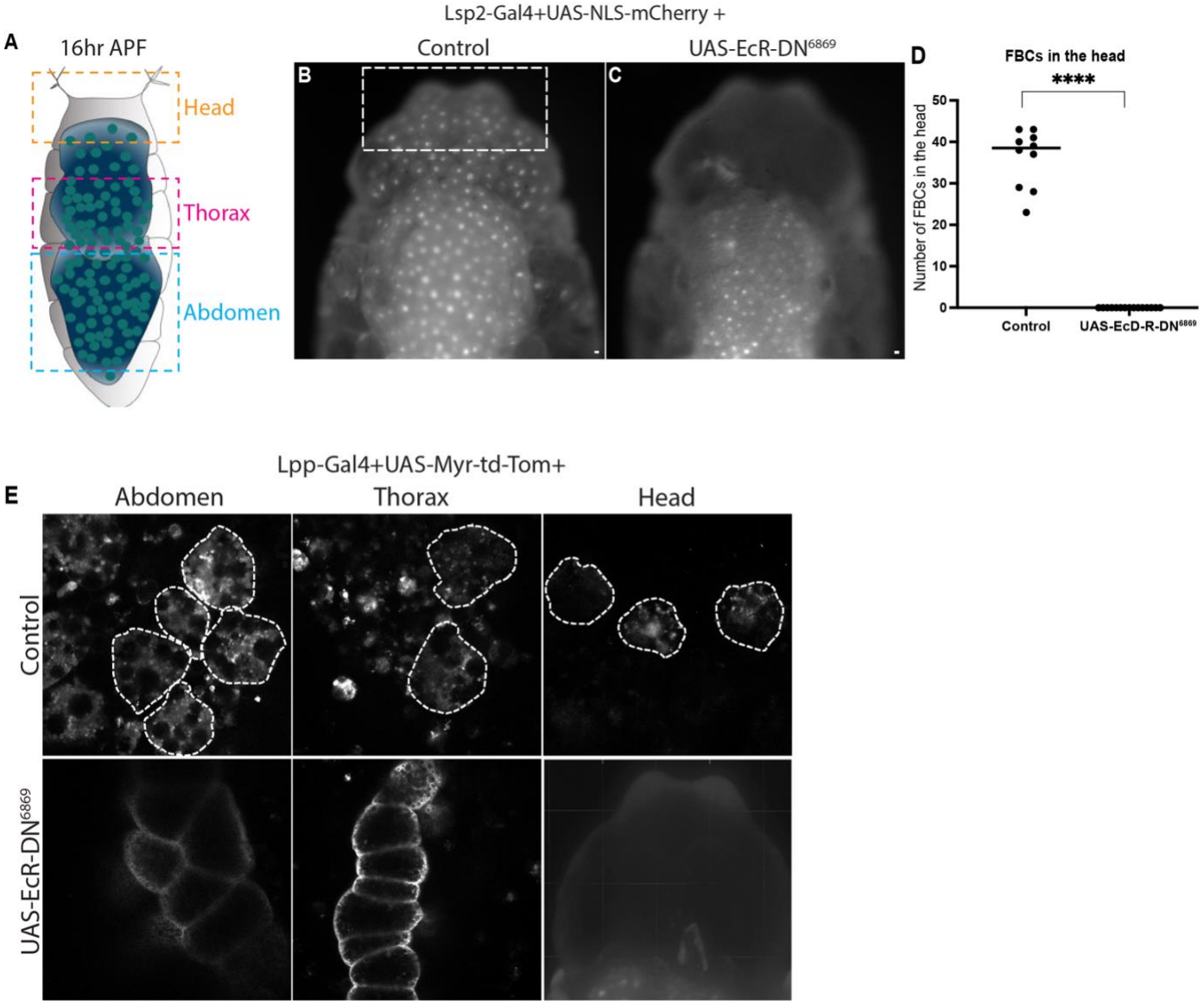
A
16hr APF
Head
Thorax
Abdomen
Lsp2-Gal4+UAS-NLS-mCherry +
Control
UAS-EcR-DN6869
B
C
D
FBCs in the head
****
Number of FBCs in the head
50
40
30
20
10
0
Control
UAS-EcD-R-DN6869
Lpp-Gal4+UAS-Myr-td-Tom+
E
Abdomen
Thorax
Head
Control
UAS-EcR-DN6869

Figure 7.2: Ecdysone signaling is required for fat body remodeling.

(A) Schematic of pupa at 16hr APF, when fat body cells have undergone complete dissociation and are free floating in the hemolymph.

(B-D) At 16hr APF fat body cells are present in the head of the control pupa (A). However, fat body remodeling is blocked in pupa expressing UAS-EcD-DN^{6869}, therefore no fat body cells are seen in the head of the pupa at 16hr APF (B). Quantification of the number of fat body cells in the head of the pupa reveals a significant decrease in pupa expressing EcD-DN to that of the control. (N≥10 control, N≥10 15 UAS- EcD-DN^{6869}).

(D) Confocal images of fat body cells in the abdomen, thorax and head pupa at 16hr APF in the control and in pupa expressing UAS-EcD-DN^{6869}. In the control, FBCs have undergone complete dissociation in the dorsal abdomen and thorax and moved to the head. Pupa expressing UAS-EcD-DN^{6869}, blocked the process of fat body remodeling, thus, fat body cells did not undergo dissociation and remained closely attached to each other in the dorsal abdomen and thorax at 16hr APF and no fat body cells are shown in the head of pupa at 16hr APF. Plasma membranes are marked with Myr-td-Tomato. (N≥10 pupa, Mann-Whitney test, ****P<0.0001)

Imaged using Zeiss-vis 63x oil immersion lens and fluorescent dissecting microscope. Scale bars = 20μm.

The same assay of counting FBCs in the head of the pupa at 16hr APF, when FBR is complete, was used to test several other genes that are involved in EMT-like models, cell-detachment, and migration in other tissues of *Drosophila melanogaster* as well as, genes involved in the Ecdysone signaling cascade. The ModENCODE tissue expression data on flybase was used to give a slight indication on whether a certain gene might be involved in the process of FBR, since it reveals gene expression data in the fat body of L3 wandering larvae (before FBR begins), white pre-pupa (when FBR begins), and pupae P8 (when FBR is complete). In other words, if a gene is either weakly (or even highly) expressed in L3-wandering larvae and then highly expressed in white pre-pupa, then it gives a slight indication that this gene might play a role in the process of FBR. The ModENCODE tissue expression data revealed that all the genes tested in this study were expressed in white pre-pupa. I then tested the requirement of the candidate genes in FBR through gene knockdown experiments and assessed whether it leads to a reduction in the number of FBCs having been translocated to the head of the pupa at 16hr APF, when FBR is usually complete. A reduction in the number of FBCs in the head of the pupa at 16hr APF would indicate a defect in fat body cell dissociation, thus indicating the importance of that certain gene in the process of FBR. The genes that were tested (twist, serpent, pebble, snail and broad complex) along with a short description are shown in Table 7.1. My results show that in addition to blocking Ecdysone signaling which is already known to be vital for the process of FBR, knocking down Serpent (UAS-Serpent-RNAi^{109521}) results in much lower numbers of FBCs in the head at 16hr APF (Figure 7.3 B). This was also validated using a second isoform of serpent RNAi (UAS-Serpent-RNAi^{35578}, Figure 7.3 C, J). Additionally, confocal imaging of pupae expressing UAS-Serpent-RNAi^{109521} together with the membrane marker UAS-Myr-td-Tom using Lsp2-Gal4 further validated the disruption of FBR, since FBCs failed to

undergo complete dissociation (Figure 7.3 A). In contrast, the control samples show complete detachment of FBCs at 16hr APF (Figure 7.4 A). In addition, expectedly, broad complex (UAS-BrC-RNAi^{104648}) which is involved in the Ecdysone signaling cascade also seems to have blocked FBR resulting in no FBCs in the head of the pupa at 16hr APF (Figure 7.3 D, J). Moreover, the graph in Figure 7.3 J also shows that EMT-regulators in other tissues, such as Snail (UAS-Snail-RNAi^{50004} and UAS-Snail-RNAi^{50003} , Figure 7.3 E and F)), Twist, (UAS-TWIST-RNAI^{37092}, Figure 7.3 G), and Pebble (UAS-Pebble-RNAi^{109305} and UAS-Pebble-RNAi^{35350} , Figure 7.3 H and I)), all seem to not be involved in the process of FBR, since knocking down these genes resulted in FBCs being present in the head of the pupa at 16hr APF (Figure 7.3 E-I, respectively), similar to the control.

Gene name	Description
Twist	TF required for mesoderm induction in *Drosophila*. Ectopic expression of Twist induced EMT in kidney and mammary epithelial cells resulting in loss of E-cadherin cell-cell adhesion, activation of mesenchymal markers and gain of cell motility (Yang et al., 2006).
Serpent	TF needed for proper development of mesoderm derivatives (fat body, hemocytes, etc.). Expression In imaginal wing disc induces loss of epithelial polarity and tissue organization and increased the size of wing disc (Campbell et al., 2018).
Pebble (PB1)	Involved in cell migration and detachment in EMT during mesoderm development in *Drosophila*. Mesodermal cells in PB1/PB3 mutant flies failed to disaggregate and migrate towards the dorsal area while in WT it succeeded (Smallhorn et al., 2004).
Snail	EMT inducing TF involved *Drosophila* imaginal wing disc where its expression induced loss of epithelial polarity (Campbell et al., 2018).
Broad Complex (BrC)	Acts in the ecdysone pathway and is required for metamorphosis in *Drosophila melanogaster* (Spokony & Restifo, 2007).

Table 7.1: List of genes involved in EMT-like models in *Drosophila melanogaster.*

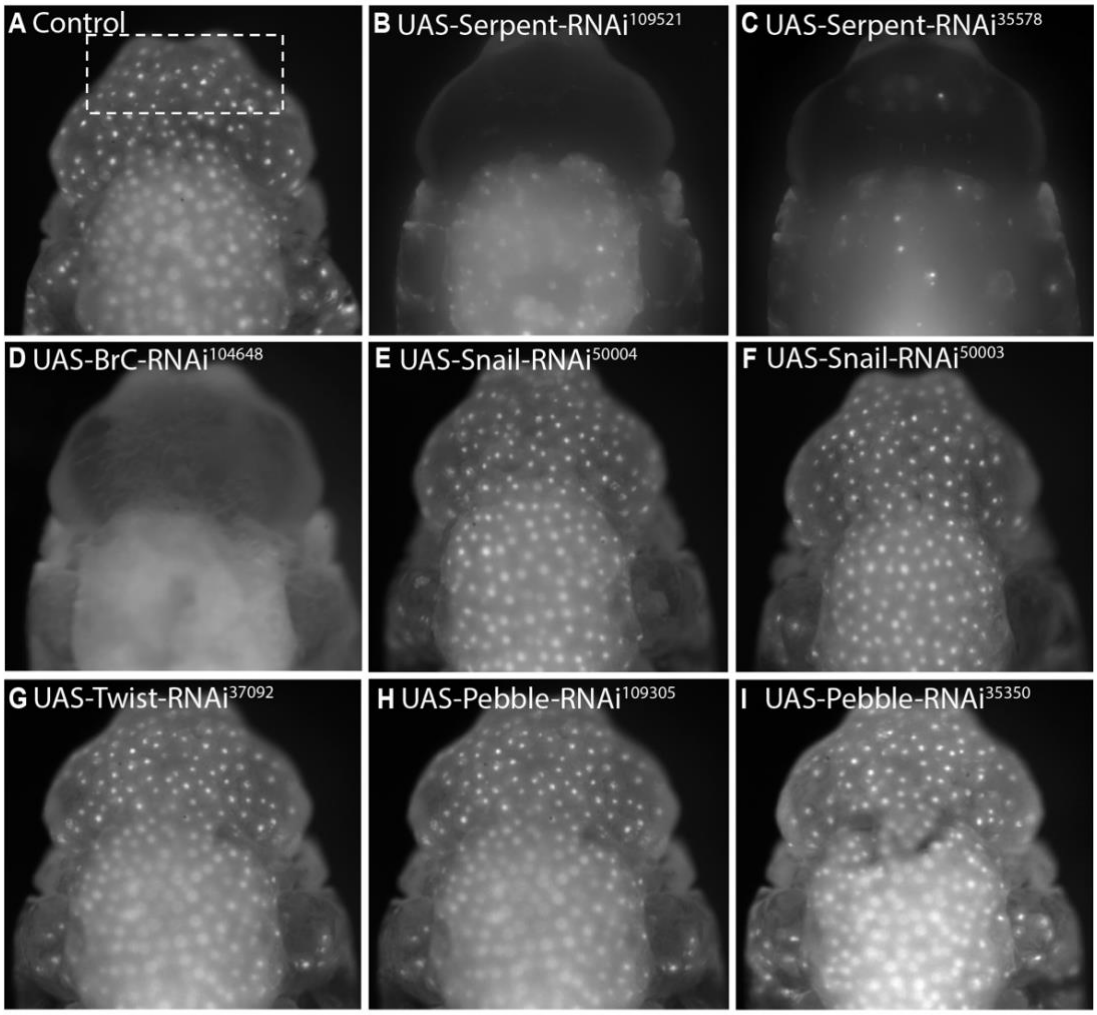
A Control
B UAS-Serpent-RNAi109521
C UAS-Serpent-RNAi35578
D UAS-BrC-RNAi104648
E UAS-Snail-RNAi50004
F UAS-Snail-RNAi50003
G UAS-Twist-RNAi37092
H UAS-Pebble-RNAi109305
I UAS-Pebble-RNAi35350

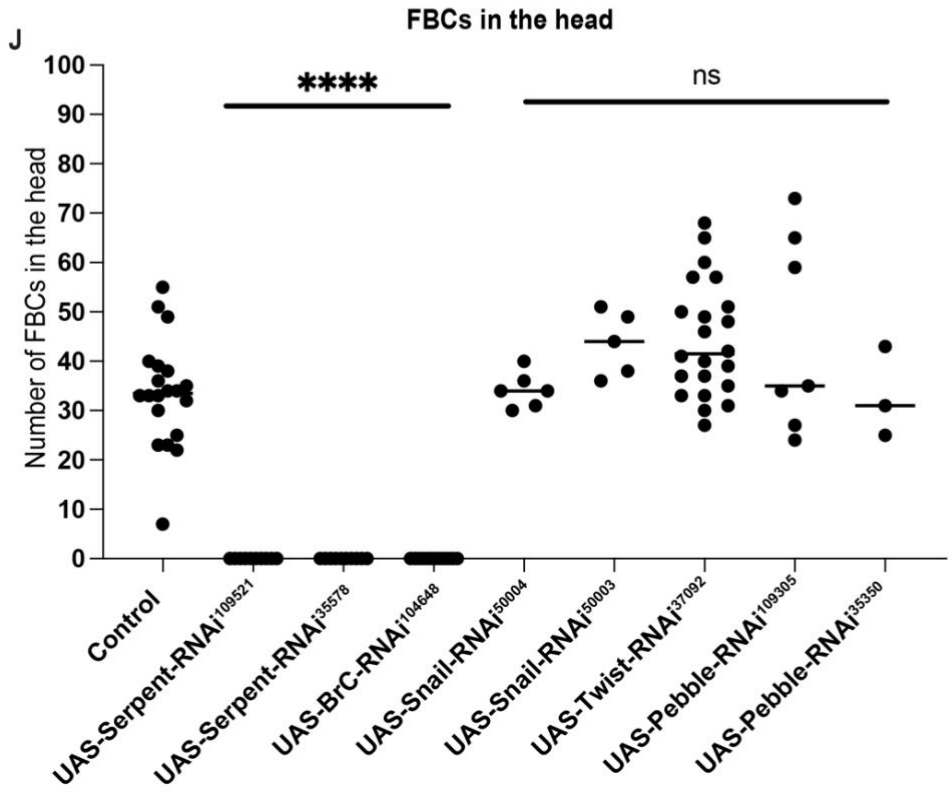
J
FBCs in the head
Number of FBCs in the head
****
ns
100
90
80
70
60
50
40
30
20
10
0
Control
UAS-Serpent-RNAi109521
UAS-Serpent-RNAi35578
UAS-BrC-RNAi104648
UAS-Snail-RNAi50004
UAS-Snail-RNAi50003
UAS-Twist-RNAi37092
UAS-Pebble-RNAi109305
UAS-Pebble-RNAi35350

Figure 7.3: Serpent is needed for cell-cell dissociation during fat body remodeling. All pupa expressing Lsp2-Gal4+UAS-NLS-mCherry.

(A-I) Fat body cells are present in the head of the pupa at 16hr APF in the control, indicating the fat body cells have undergone complete dissociation (A). Serpent (B-C) and broad-complex (D) is shown to be needed for cell-cell dissociation, since no fat body cells are seen in the head at 16hr APF. On the other hand, knocking down Snail (UAS-Snail-RNAi^{50004} (E) and UAS-Snail-RNAi^{50003} (F)), Twist, (UAS-TWIST-RNAI^{37092} (G)), and Pebble (UAS-Pebble-RNAi^{109305} (H)) and UAS-Pebble-RNAi^{35350} (I)) are not needed for cell-cell dissociation during fat body remodeling. (J) Quantifications of the number of fat body cells in the head of the pupa reveals a significant decrease in serpent knockdowns (UAS-Serpent-RNAi^{109521} and UAS-Serpent-RNAi^{35578}) and broad-complex (UAS-BrC-RNAi^{104648}), while no significant difference is shown when Snail (UAS-Snail-RNAi^{50004} and UAS-Snail-RNAi^{50003}), Twist, (UAS-TWIST-RNAI^{37092}), and Pebble (UAS-Pebble-RNAi^{109305} and UAS-Pebble-RNAi^{35350}). (N=20 control, N=10 UAS-Serpent-RNAi^{109521} and UAS-Serpent-RNAi^{35578} , N=5 UAS-Snail-RNAi^{50004}, N=6 UAS-Snail-RNAi^{50003}, N=12 UAS-BrC-RNAi^{104648}, N=22 UAS-TWIST-RNAI^{37092}, N=7 UAS-Pebble-RNAi^{109305}, N=3 UAS-Pebble-RNAi^{35350}, Kruskal-Wallis test, ****P<0.0001, ns P<0.9999)
Imaged using fluorescent dissecting microscope. Scale bars = 20μm.

A After fat body remodeling: 16h APF

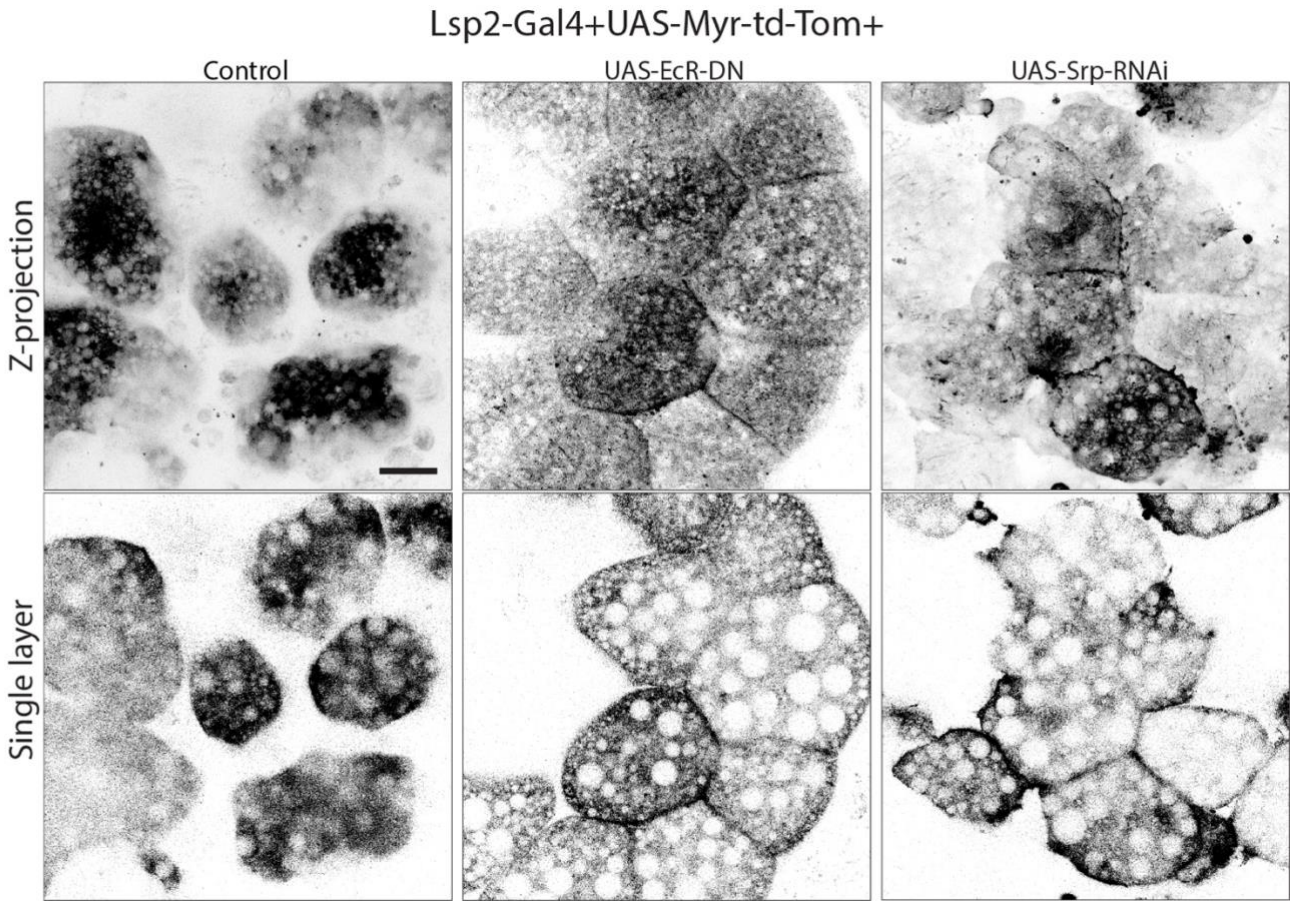

Figure 7.4: Pupa expressing Serpent-RNAi^{109521} failed to undergo fat body remodeling. All pupa expressing Lpp-Gal4+UAS-Myr-td-Tomato.

(A) Unlike the control where animals undergo FBR, leading to complete cell-cell dissociation of FBCs,

Pupa expressing Serpent-RNAi^{109521} failed to undergo FBR, thus FBCs failed to dissociate, mimicking the phonotype of pupa expressing EcR-DN^{6869}. (N≥20)

Imaged using fluorescent dissecting microscope. Scale bars = 20μm.

7.3 Ecdysone signaling and Serpent regulate loss of cell polarity and loss of CIVICs during fat body remodeling

Since Ecdysone and Serpent are both needed for cell-cell dissociation during fat body remodeling, I wanted to dissect the molecular mechanism behind the importance of Ecdysone signaling and Serpent in the process of FBR. To do this, I first tested whether blocking Ecdysone signaling or knocking down Serpent would affect the loss of polarity in the fat body tissue which I saw in WT at 3hr APF. Thus, I dissected the fat body tissue from 3hr APF (early during fat body remodeling) and immunostained for polarity proteins (αDlg, αPar-3 and αCrumbs), then mounted the fat body tissue between two coverslips as previously stated in chapter IV. The same surface ROI used to measure fluorescence mean intensities of polarity proteins in wandering 3rd instar larvae in chapter IV was used. Figure 7.5 A-C shows that animals expressing UAS-EcR-DN and UAS-Serpent-RNAi^{109521}, failed to lose polarity at 3hr APF when polarity is usually lost as shown in the control. Quantifications of the average mean intensities on both sides also showed that polarity proteins Dlg (Figure 7.5 A''-A'''), Par-3 (Figure 7.5 B''-B''') and Crumbs (Figure 7.5 C''-C''') remained asymmetrically localized when blocking Ecdysone and Serpent, with Dlg being concentrated in side b and Par-3 and Crumbs on side a, in contrast to the control fat body at 3hr APF which had lost its polarity (Figure 7.5 A-F) but similar to WT fat body in third instar larvae before FBR happens (Figure 4.2 and 5.1).

Finally, having found that Ecdysone signaling and Serpent regulate the loss of polarity of FBCs early during FBR at 3hr APF, as well as regulating cell-cell dissociation, I next wanted to investigate how cell-cell dissociation is regulated during FBR. It had previously been reported

that cell-cell dissociation gets regulated by Ecdysone-induced, MMP1-dependent cleavage of E-Cadherin (Jia et al., 2014). Yet, my new findings from chapter V, as well as the findings from Dai et al. (2017) have indicated that cell-cell-adhesion in third instar larval fat body is regulated by CIVICs and likely not or less so by E-Cad. However, it was unknown, whether CIVICs get dissolved during FBR. Hence, I wanted to see next, if CIVICs get removed from the cell-cell junctions during FBR and if so, whether this depends on Ecdysone signaling and Serpent. To test this, I imaged fat body from 3h APF pupae expressing Lpp-Gal4+UAS-Myr-td-Tomato+Viking-GFP (control) as well as UAS-EcR-DN or UAS-Serpent-RNAi^{109521}. I found that CIVICs numbers were very low in the control fat body (Figure 7.6 A, A'), much lower than the numbers seen in the WT fat body of third instar larvae (Figure 5.3; please note that only a single layer is shown in Figure 7.6 A-C while the projection of the first 10 layers was shown in Figure 5.3, hence the difference in CIVICs numbers seen in the pictures from the two figures). In contrast, animals expressing UAS-EcR-DN^{6869} and UAS-Serpent-RNAi^{109521}, failed to lose CIVICs (Figure 7.6 B'-C') and had much larger number of CIVICs than the control (Figure 7.6 D). This suggests that CIVICs get removed from the cell-cell junctions early during FBR and this depends on Ecdysone signaling and Serpent.

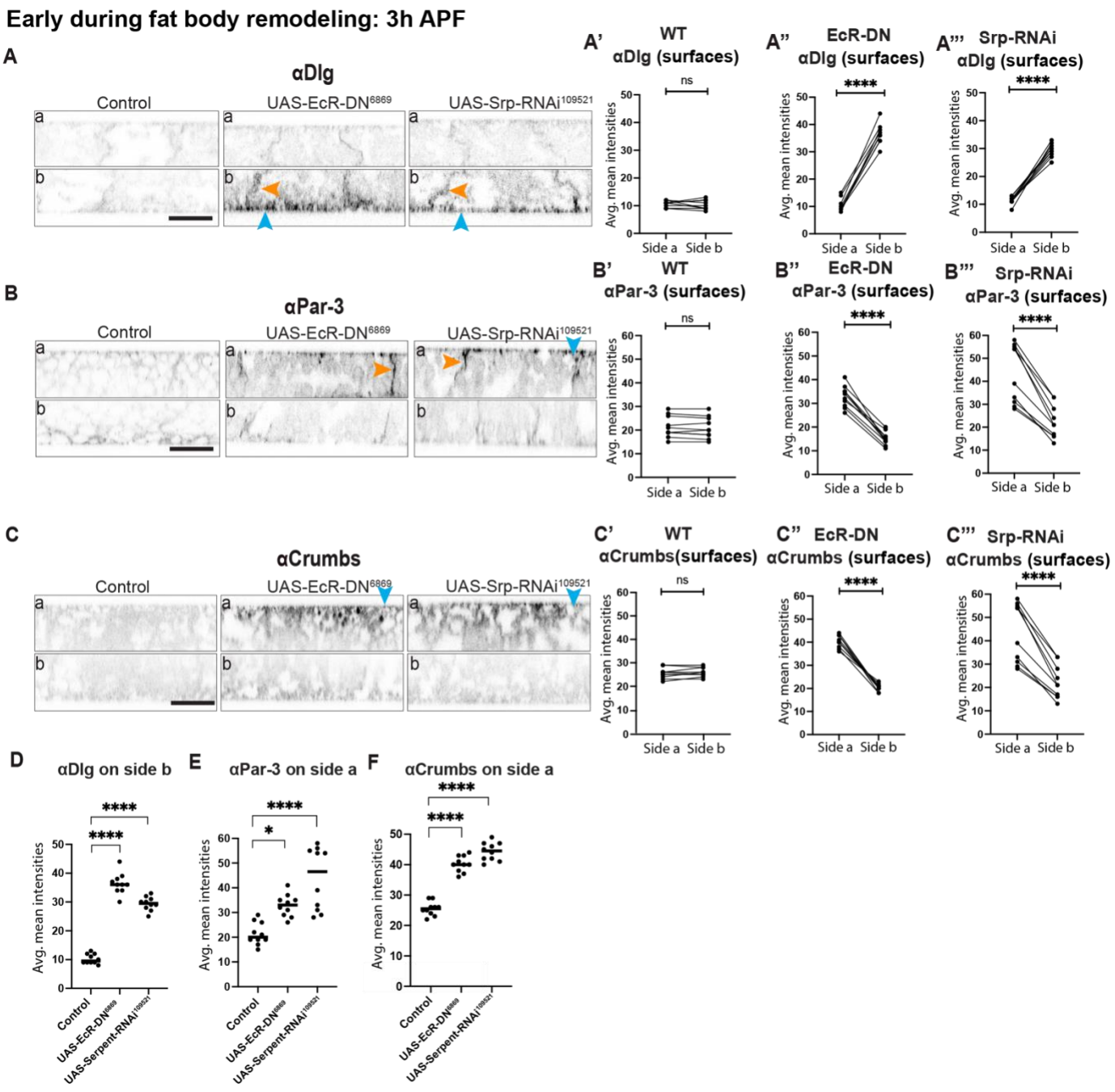
Early during fat body remodeling: 3h APF
A
αDlg
Control
UAS-EcR-DN6869
UAS-Srp-RNAi109521
a
b
A'
WT
αDlg (surfaces)
A''
EcR-DN
αDlg (surfaces)
A'''
Srp-RNAi
αDlg (surfaces)
ns
****
Avg. mean intensities
Side a
Side b
B
αPar-3
B'
WT
αPar-3 (surfaces)
B''
EcR-DN
αPar-3 (surfaces)
B'''
Srp-RNAi
αPar-3 (surfaces)
C
αCrumbs
C'
WT
αCrumbs(surfaces)
C''
EcR-DN
αCrumbs (surfaces)
C'''
Srp-RNAi
αCrumbs (surfaces)
D
αDlg on side b
E
αPar-3 on side a
F
αCrumbs on side a
*
UAS-Serpent-RNAi109521

Figure 7.5: Ecdysone and Serpent regulate loss of apicobasal polarity during fat body remodeling. All fat body tissues expressing Lsp2-Gal4+UAS-NLS-mCherry.

(A-C) Knocking down ecdysone signaling or serpent impairs loss of polarity proteins αDlg (A''-A'''), αPar-3 (B''-B'''), and αCrumbs (C''-C''') at 3hr APF (during FBR), unlike the control where polarity proteins asymmetry is usually lost by 3hr APF (A'-C'). Each dot in Figure 7.5 A-G represents the average mean intensity of 10 regions imaged on each side of the fat body tissue in several different animals. (N≥10 fat body tissues, Paired T-test, ****P<0.0001, ns P<0.9999). (D-F) Shows the average mean intensities of polarity proteins αDlg on side b (D), αPar-3 on side a (E), and αCrumbs on side a (F) being significantly different to that of the control when ecdysone and serpent are knocked down individually (N≥10 fat body tissues, Multiple comparison Ordinary one-way Anova, ****P<0.0001, * P=0.037).
Imaged using Zeiss-vis 63x oil immersion lens. Scale bars = 20μm.

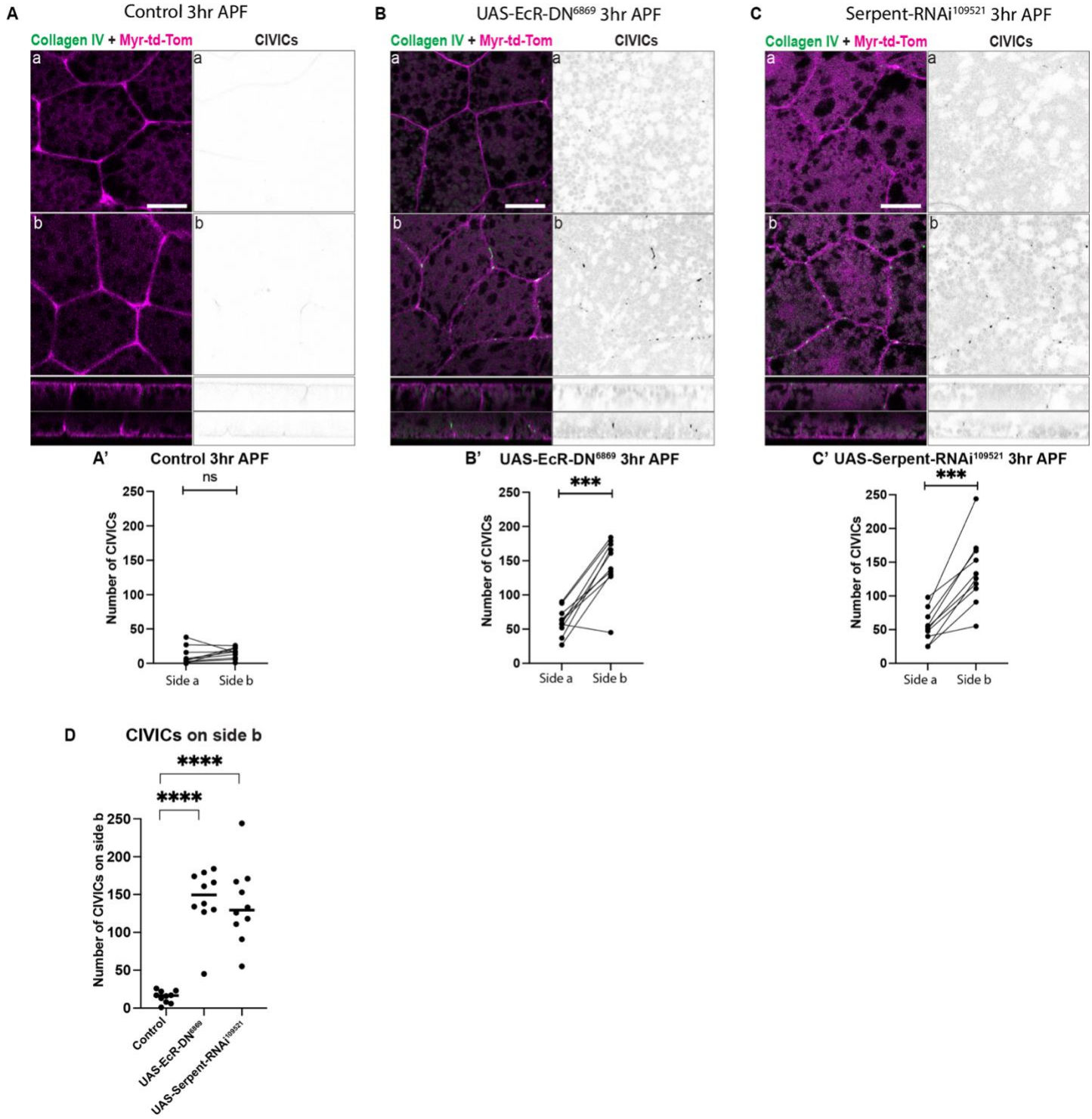
A
Control 3hr APF
Collagen IV + Myr-td-Tom
CIVICs
a
b
B
UAS-EcR-DN6869 3hr APF
C
Serpent-RNAi109521 3hr APF
A'
Control 3hr APF
ns
Number of CIVICs
Side a
Side b
B'
UAS-EcR-DN6869 3hr APF
***
C' UAS-Serpent-RNAi109521 3hr APF
D
CIVICs on side b
****
Number of CIVICs on side b
Control
UAS-EcR-DN6869
UAS-Serpent-RNAi109521

Figure 7.6: Ecdysone signaling and serpent are needed for loss of CIVICs during fat body remodeling. All fat body tissues expressing Lsp2-Gal4+UAS-Myr-td-Tomato.

(A-C) In control animals, CIVICs is lost by 3hr APF (A), early during fat body remodeling. However, blocking Ecdysone signaling (B) or Serpent (C-) impairs loss of CIVICs by 3hr APF as shown in the images in (B-C). Quantifying the number of CIVICs further validates the presence of CIVICs being asymmetrically localized in animals expressing UAS-EcD-DN^{6869} (B') and UAS-Serpent-RNAi^{109521} (C'), unlike the control where CIVICs asymmetry is lost by 3hr APF. (N≥10 fat body tissues, 3 regions imaged on each side, Paired T-test, *** P<0.001, ns P<0.9999).
(D) Shows multiple comparison of the number of CIVICs on side b. (Multiple comparison Ordinary one-way Anova, ****P<0.0001).
Imaged using Zeiss-vis 63x oil immersion lens. Scale bars = 20μm.

7.4 Discussion

One of the key hallmarks of EMT is the loss of apicobasal polarity. The fat body was previously believed to lack polarity since it is not classified as a classic epithelium due to presence of a basement membrane on both sides of the fat body tissue. However, since my findings in Chapter IV showed that that fat body tissue in fact exhibits apicobasal polarity, I aimed to investigate whether, similar to EMT, fat body cells lose cell polarity during the process of FBR.

Fat body tissues were dissected from 3hr APF pupae, as this timepoint was the latest timepoint at which dissection was feasible. Beyond this timepoint, dissecting and immunostaining fat body cells became increasingly difficult due to complete cell-cell dissociation, resulting in individual fat body cells in the hemolymph. Additionally, this timepoint was the latest stage where I could successfully dissect the right side of the fat body tissue from the pupa and still be able to orient and mount fat body cells with the same cell side up. In other words, I was able to tell which side corresponded to side a and which to side b as discussed in Chapter IV as the new mounting method. Consequently, in this chapter I showed that the polarized localization of several polarity proteins (aPKC, Par-6, Crumbs, Par-3, Dlg, and Lgl) are lost by 3hr APF, early during FBR. Since apicobasal polarity is present in the fat body tissue of wandering 3rd instar larva and is lost early during the process of FBR, similar to EMT. I aimed to dissect the molecular mechanism driving the process of FBR. Using a screening assay, I tested several genes including EMT transcription factors and identified that in addition to Ecdysone signaling, a previously known regulator of FBR, Serpent is another candidate gene required for FBR, since its knockdown impaired cell-cell dissociation during the process FBR. Because confocal imaging was done

using only one Serpent RNAi line, it would be essential to image the second RNAi line to validate my results that suggest the importance of Serpent in the process of FBR.

The requirement of Serpent and Ecdysone signaling for fat body cell dissociation and polarity loss during the process of FBR, indicates the importance of both Serpent and Ecdysone signaling in initiating FBR. This possibly suggest that Serpent an Ecdysone might act within a common regulatory pathway, with Serpent acing downstream of Ecdysone signaling, since UAS-Serpent RNAi led to partial dissection while UAS-Ecdysone RNAi prevents fat body dissociation. However, the precise connection specifically in the fat body remains unclear. Given the importance of Ecdysone signaling during metamorphosis, where Ecdysone triggers early response genes, which induce the transcription of late response genes, such as BFTZ-F1 (Bond et al., 2011), it is possible that Serpent may act as part of the gene regulatory program of Ecdysone signaling, regulating the expression of downstream genes involved in cell dissociation and polarity loss. It has been shown that BFTZ-F1 regulates MMP2 expression, which acts as a key effector in the process of FBR. In fact, premature expression of BFTZ-F1 induces early Mmp2 expression, thus resulting in premature remodeling; while blocking either BFTZ-F1 or Ecdysone signaling prevent Mmp2 induction and thus prevents FBR from taking place (Bond et al., 2011). Overall, this would propose a model where Ecdysone signaling acts upstream to regulate downstream targets such as Serpent and BFTZ-F1, which in turn controls Mmp2 expression and other downstream effectors required for fat body cell dissociation, loss of polarity and ECM remodeling during metamorphosis.

In addition to Serpent, knocking down Broad Complex also resulted in a head phenotype similar to that observed in Serpent RNAi, where fat body cells were absent in the head of the

pupa at 16hr APF, when cells would normally be present in the head as in the control. However, assessing the presence of fat body cells in the head alone is insufficient to determine whether a certain gene is essential for FBR. Therefore, confocal imaging of the dorsal abdomen and thorax is necessary to validate and confirm that Broad Complex knockdown disrupts FBR. Confocal imaging would help determine whether fat body cells fail to undergo cell-cell dissociation and remain tightly attached to one another, ultimately preventing fat body cell migration to the head of the pupa. It is surprising and somewhat unexpected that knockdown of snail did not affect FBR, since Snail is known to act as a central regulator of EMT, especially in *Drosophila* mesoderm formation, that gives rise to the fat body, where is plays a role in loss of cell polarity and initiating EMT (Tepass & Hartenstein, 1994). However, despite the importance of Snail in driving EMT during mesoderm development, EMT during *Drosophila* endoderm formation is also independent of Snail (Reuter & Leptin, 1994; Tepass & Hartenstein, 1994). This example serves as a relevant model to FBR, which is possibly a unique EMT-like process that occurs independent of Snail.

To conclude that some genes are indeed not required for FBR, confocal imaging in the dorsal thorax is necessary. It may be that knocking down these genes causes only a partial delay in FBR, leading to clusters of fat body cells, attached to one another, persisting in the thorax or abdomen, while others successfully undergo dissociation and migrate to the head as seen in the control. This suggests that some cells may undergo dissociation at normal timings, similar to the control, while others experience a delay. Since only one RNAi isoform was tested for Broad Complex and Pebble, additional isoforms should be examined to validate these findings. Furthermore, assessing the efficiency of the RNAi knockdowns through western blot

analysis or quantitative polymerase chain reaction (qPCR) is crucial to confirm the effectiveness of the knockdowns.

As both Serpent and Ecdysone signaling are essential for fat body cell dissociation during the process of FBR, and given my findings that apicobasal polarity is lost during this process, I aimed to investigate their specific roles in FBR. To do this, I dissected fat body tissues from 3hr APF pupa expressing a membrane marker UAS-Myr-td-Tomato along with UAS-EcR-DN and Serpent RNAi and stained for polarity proteins (Dlg, Par-3, and Crumbs). I then quantified polarity protein distributions using the same method applied to quantify polarity proteins in 3rd instar larval fat body tissues in Chapter IV. My results revealed that while polarity was lost in the control; Dlg, Par-3, and Crumbs remained asymmetrically localized when Ecdysone and Serpent were disrupted. This highlights the crucial role of both Ecdysone signaling and Serpent in the loss of apicobasal polarity during FBR. To further validate these findings, it is necessary to test the second isoform of Serpent RNAi to determine whether knocking down Serpent using an alternative RNAi line similarly disrupts polarity loss early during FBR. Additionally, testing additional polarity proteins such as Lgl, aPKC, and Par-6 would provide further insights on which polarity proteins are specifically regulated by Ecdysone signaling and Serpent.

The fact that it is now clear that cell-cell adhesion and loss of apicobasal polarity is regulated by Ecdysone signaling and Serpent raises questions on whether Ecdysone signaling and Serpent regulate cell-cell adhesion via CIVICs. To test this, I dissected 3hr APF pupa expressing a membrane marker UAS-Myr-td-tomato as well as UAS-Vkg-GFP under the fat body driver Lsp2-Gal4 and quantified whether disrupting Ecdysone signaling or Serpent impairs loss of CIVICs early during FBR. My findings revealed that loss of CIVICs is indeed dependent on

Ecdysone signaling and Serpent. Although, my findings in chapter V suggest that cell-cell adhesion is mainly mediated by CIVICs and less likely by E-Cadherin; Jia et al. (2014) reported loss of E-Cadherin during FBR. This raises the question on whether loss of E-Cadherin observed in Jia et al. (2014) is also regulated by Ecdysone signaling and Serpent. In conclusion, fat body remodeling is an unusual, novel version of an EMT-like process that implicates the loss of polarity in order to induce loss of CIVICs leading to cell-cell dissociation.

Chapter VIII. Discussion and future directions

8.1 Apicobasal Polarity in the fat body tissue

Cell polarity is fundamental to epithelia cell function and plays a role in regulating the function of most organs (Paniagua et al., 2021; Pasquier et al., 2024). In animals, the architecture of epithelial tissues is defined by both the apicobasal polarity of individual cells and the formation of adhesions between cells (Vasquez et al., 2021). In addition, cell polarity acts as a barrier that separates distinct cellular domains. Loss of apicobasal polarity is a hallmark of epithelial to mesenchymal transition as illustrated in Figure 8.1 Classic epithelial tissues exhibit three major protein complexes: the Par complex (comprising Par-3, Par-6, and aPKC), the Crumbs complex (Crumbs, Stardust, and PatJ), and the Scribble complex (Scribble, Dlg, and Lgl) (Ellenbroek et al., 2012).

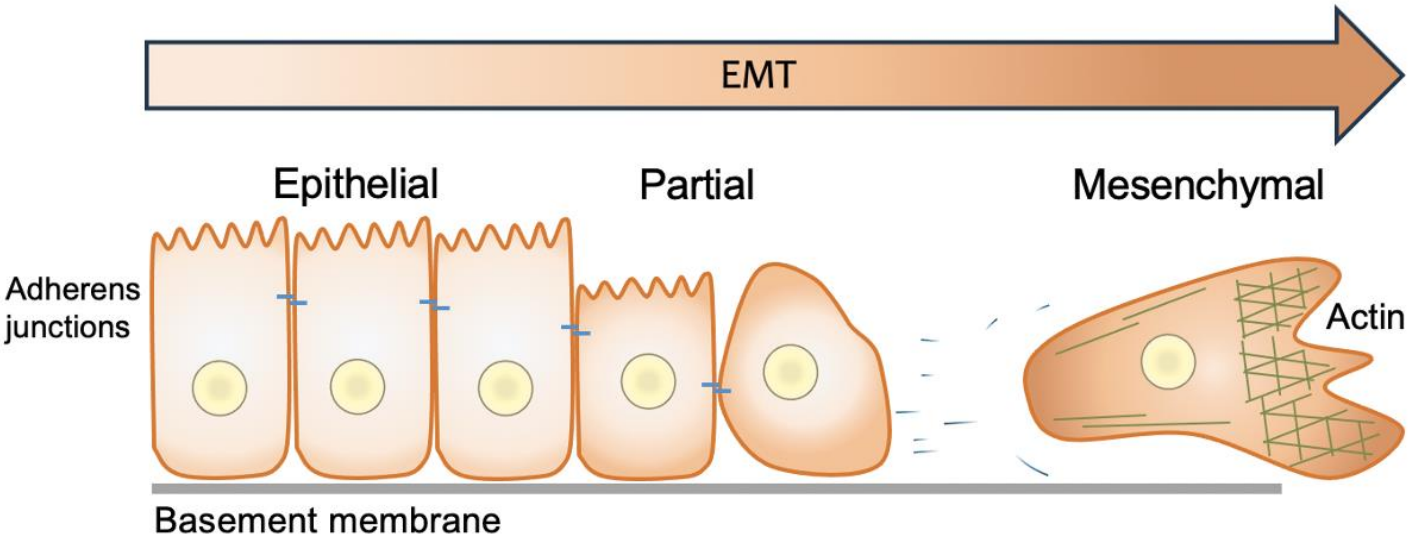

Epithelial state:

- Apicobasal polarity
- Cell-cell adhesion (E-Cad)
- Cell-basement membrane adhesion
- Not migratory

Loss of apicobasal polarity ?
Cell shape changes ✓
Loss of cell-cell adhesion ✓
Loss of cell-BM adhesion ✓
MMP expression ✓

Mesenchymal state:

- Ability to migrate

Figure 8.1: Characteristics of Epithelial to mesenchymal transition (EMT) in comparison to FBR. Similar to EMT, during FBR, fat body cells undergo loss of cell-cell adhesion, cell-BM adhesion through MMP expression leading to cell shape changes. However, it is still unknown whether FBR exhibits apicobasal polarity and whether polarity is lost during FBR.

Unlike epithelial tissues, that possess distinct apical and basal domains, the *Drosophila* fat body tissue is an unusual, noncontinuous structure that surrounds several organs, including the gut, in an apron-like fashion and used to be thought to lack a defined apical and basal domain. This was in part, because a basement membrane surrounds the entire tissue (Jia et al., 2014). To date, apicobasal polarity has not been reported in the fat body, though this assumption has never been experimentally validated. However, the presence of a basement membrane on both sides of the tissue does not rule out the potential presence of apicobasal polarity.

In this study, I first wanted to investigate whether polarity proteins are present in the fat body tissue of wandering 3rd instar larvae, and whether they are asymmetrically localized. My results revealed that aPKC, Par-6, and Crumbs are localized to the apical domain, facing the cuticle, while Dlg and Lgl are localized to the basal domain, facing the gut, and are also concentrated on the basolateral domain, similar to a classic epithelium. Although, secretion in an epithelium normally happens through the apical domain, such as the apical secretion of epithelial tubes in *Drosophila* embryo (Tal Rousso et al., 2013), secretion has been shown to sometimes occur basally, such as in *Drosophila* follicular epithelium (Zajac & Horne-Badovinac, 2022). In *Drosophila* follicular epithelium, secretion of basement membrane proteins is controlled by Kinesin motor proteins (Kinesin-1 and Kinesin-3) that help move basement membrane proteins along microtubules, thus ensuring proper cell migration and maintaining tissue integrity. Similar to all epithelia, follicle cells have polarized microtubules along the apical-basal axes. Disruption of Kinesins impairs basement membrane protein secretion, leading to the formation of abnormal basement membrane network between cells, impeding migration and altering tissue integrity, suggesting the importance of basement membrane proteins to be secreted basally (Zajac &

Horne-Badovinac, 2022). Overall, my findings provide strong evidence of the existence of polarity in fat body tissue despite its unusual organization. Testing additional polarity proteins like Scribble and Stardust, could offer deeper insights on whether they are needed for polarity in *Drosophila* fat body. This is because not all epithelial polarity proteins are essential for polarity in all tissues. For instance, Crumbs is absent in *Drosophila* adult midgut epithelium, consistent with prior observations in the embryo (Tepass et al., 1990). Moreover, Par-3 null mutant enterocytes successfully integrate into the epithelium and establish normal apicobasal polarity (Tepass et al., 1990),unlike other *Drosophila* epithelia, where Par-3 is essential given its role in forming spot adherens junction in the apicolateral domain (Harris & Peifer, 2004). The adult midgut maintains homeostasis through the division of basal intestinal stem cells that divide and generate new cells that replace dying enterocytes in the epithelium (Tepass et al., 1990). Further research is needed to understand the functional implications of this polarity in fat body tissue development and homeostasis.

One of the primary functions of apicobasal polarity proteins in classical epithelia is the regulation of cell-cell adhesion through Par-3 and E-Cadherin-based adherens junctions (Gibson & Perrimon, 2003). Having found that the fat body tissue of L3- stage larva in *Drosophila* exhibits apicobasal polarity similar to an epithelium, I next investigated whether this polarity contributes to cell-cell adhesion in the fat body. Two mechanisms of cell-cell adhesion in *Drosophila* have been previously proposed, which are via E-Cadherin-based adherens junctions (Jia et al., 2014) and through (CIVICs) (Dai et al., 2017). CIVICs are inter-adipocyte adhesion in *Drosophila* fat body that are thicker in structure, unlike the basement membrane which are usually thin and continuous (Dai et al., 2017). In the *Drosophila* egg chamber, Collagen IV fibrils are initially

produced and secreted into the intercellular spaces, potentially similar to CIVICs, before being transported and incorporated into the basement membrane (H. Huang et al., 1999). This suggests that Collagen IV undergoes a multi-step process that involves secretion, transport, and integration rather than direct formation at the final site (Dai et al., 2017). In this study I found that both E-Cadherin and Par-3 are localized on the apical and apicolateral domain. However, E-Cadherin exhibits a diffuse signal and was not observed to have a belt like structure, or found as spot adherens junctions, as observed in a classic epithelium. Moreover, though a previous study demonstrated the presence of CIVICs between fat body cells (Dai et al., 2017), whether CIVICs is asymmetrically localized remained unknown. Due to the fact that the fat body tissue exhibits a basement membrane on both surfaces and both surfaces of the basement membrane are thought to be the same, one would suspect CIVICs to be localized symmetrically on both surfaces. However, upon quantifying the number of CIVICs on both sides of the fat body tissue, my results revealed higher levels of CIVICs in the basolateral domain, when compared to the apicolateral domain. This led to a major question which is whether cell-cell adhesion in fat body cells is mediated by E-Cadherin as well as CIVICs or by CIVICs alone. I tested this by knocking down E-Cadherin to observe whether fat body cells would detach from neighboring cells in wandering L3-stage larva. Since E-cadherin has been previously proposed to take part in cell-cell adhesion in fat body cells (Jia et al., 2014), I expected FBCs to undergo detachment or at least partial detachment upon expressing E-Cadherin knockdown. However, in contrast to Collagen IV RNAi and Integrin RNAi, where knockdown led to cell-cell dissociation in the larval fat body (Dai et al., 2017), E-Cadherin knockdown using three different RNAi isoforms was insufficient to induce cell-cell dissociation. Yet, my results alone are still not enough to conclude that cell-cell adhesion in fat body cells are mediated by CIVICs and not E-Cadherin, because

both might contribute. This could be tested through a double knockdown approach of E-Cadherin with Collagen IV or Integrin to see if it may yield stronger dissociation. Overall, these findings highlight the distinct adhesive characteristics of the fat body tissue and the various adhesion mechanisms found across different tissue types. To further elucidate the structural organization of the fat body, it is essential to determine the localization of tight junctions and adherens junction in the fat body tissue of L3-stage larva, which could be done by immunostaining for Armadillo (adherens junction). In contrast to mammalian epithelia, where tight junctions are positioned apically and adherens junctions are present slightly below the apical domain, along the lateral domain; *Drosophila* epithelia display a reversed arrangement (Coopman & Djiane, 2016). However, *Drosophila* adult midgut epithelial cells exhibit an arrangement of intercellular junctions similar to that found in mammals (Chen et al., 2018). Thus, determining whether the fat body follows the conventional *Drosophila* epithelial organization or resembles the mammalian-like arrangement seen in the adult midgut could offer valuable insights.

Consistent with previous reports that revealed that the basement membrane is identical on both surfaces of the fat body tissue (Jia et al., 2014), my results showed that Collagen IV is symmetrically localized between the two opposite sides of the fat body tissue. This was also validated through electron microscopy images which showed that both surfaces of the basement membrane are the same. However, to ensure the accuracy of these quantifications, Collagen IV measurements should be repeated using the optimal settings.

Although Collagen IV in the basement membrane appears to be structurally uniform, I cannot conclude that the basement membranes on opposite sides of the fat body tissue are the same. Firstly, because my results revealed an asymmetrical distribution of Integrin being higher on the basal side, thus distinguishing the two sides of the basement membrane. Second,

because CIVICs function depends on cell attachment via Integrin and Syndecan (Dai et al., 2017), it would be valuable to test whether Syndecan is also localized on the basal side (side b), similar to integrin. These findings raised interesting questions on whether the basement membrane is in fact identical on both surfaces, as indicated in previous studies. It is possible that other basement membrane proteins, such as Laminin, Nidogen, and Perlecan may exhibit asymmetric distribution, potentially influencing structural and functional differences between the two surfaces of the fat body. This could be tested by expressing Laminin (LanB1-GFP), Nidogen (Ndg-GFP), and Perlecan (Trol-YFP) in the fat body then quantifying fluorescence mean intensities on both surfaces of the fat body tissue, similar to the way polarity proteins were quantified.

The discovery that the fat body tissue of wandering L3-stage larva exhibits apicobasal polarity presented intriguing questions about the functional significance of polarity proteins. As mentioned earlier, in a classic epithelium, apicobasal polarity is responsible for the regulation of cell-cell adhesion via E-Cadherin, tissue integrity and cellular behavior (Nistico et al., 2012). To explore the role of polarity in the fat body tissue, I investigated the effects of knocking down several key polarity proteins. Individual knockdowns of aPKC, Scribble, and Lgl led to aberrant cell dissociation with increased tricellular gaps in all knockdowns, while bicellular gaps were significantly increased only in aPKC knockdown. These findings highlight the importance of polarity proteins in maintaining cell-cell adhesion and raised further questions on whether CIVICs numbers are reduced, given that CIVICs mediate cell-cell adhesion in the fat body (Dai et al., 2017). Quantifications of CIVICs revealed that their numbers were disrupted in aPKC, Scribble and Crumbs knockdowns, with a reversed CIVICs localization in Crumbs knockdown. Furthermore, aPKC and Scribble knockdowns reduced Collagen IV levels, whereas Crumbs

knockdown increased Collagen IV levels. This may suggest that Crumbs might play a role in pathways governing CIVICs recruitment. Apart from observing cell detachment and quantifying CIVICs, aPKC knockdown seemed to sometimes have smaller fat body cells when compared to the control and to the other knockdowns. However, this must be repeated with a higher N number and cell size should be quantified to be able to conclude that aPKC knockdown indeed affects fat body cell growth. But before concluding that aPKC knockdown affects cell growth, testing whether autophagy might be taking place is crucial. It is known that integrin mediates adhesion to CIVICs which is essential for Src-Pi3k-AKT signaling pathway to promote normal growth (Britton et al., 2002) and to prevent autophagy (Dai et al., 2017). Testing for autophagy could be done by expressing an autophagy marker (Atg8-mCherry) or by antibody staining using anti-Src. If results show that fat body cells are not undergoing autophagy upon aPKC knockdown, then testing whether Integrin or Syndecan (Sdc-GFP) levels go down, given that CIVICs levels are reduced would be essential. This is because it has been previously shown that Integrin, Collagen IV, and Syndecan are all needed to prevent autophagy, since Integrin or Syndecan knockdown resulted in Atg8a.mCherry-positive autophagosomes (Dai et al., 2017). Moreover, since Pi3K is required to promote fat body growth (Britton et al., 2002) and aPKC knockdown results in smaller cells, it would be interesting to test whether overexpression of Dp110 (Leevers et al., 1996), a pathway component that includes a catalytic subunit of PI3K, rescues the phenotype of aPKC knockdown resulting in enlarged cells. A previous study found that overexpression of Dp110 in *Drosophila* discs enhances cellular growth, thus resulting in bigger cells, while Dp110 mutant animals exhibited smaller cells (H. Huang et al., 1999). Additionally, assessing whether Dlg and Scribble mutants disrupt polarity protein mislocalizations, such as the disrupted aPKC localization observed in *Drosophila* ovariole

(Schmidt & Peifer, 2020) would contribute to a better understanding on whether polarity misregulation follows similar pathways in different *Drosophila* tissues. Additionally, my findings which suggest that polarity in the fat body is needed for cell-cell adhesion raised questions about its broader role in *Drosophila* adipocytes, which are known to regulate lipid storage and release (Liu & Huang, 2013). Investigating the role of polarity proteins in lipid organization by knocking them down and analyzing lipid droplets with BODIPY staining could provide valuable insights on the functional importance of polarity proteins in the fat body.

In *Drosophila* melanogaster, the fat body undergoes a process known as fat body remodeling (FBR) which resembles tissue remodeling and occurs during early metamorphosis. I hypothesized that FBR shares similarities with EMT/EAT, a phenomenon observed in both developmental and pathological conditions, which is initiated by the disruption of apicobasal polarity leading to downregulation of E-Cadherin mediated cell-cell adhesion and the disassembly of adherens junctions (Yang et al., 2020). Because I now found that the larval fat body exhibits apicobasal polarity, which regulates cell-cell adhesion most likely through CIVICs, it suggests that that FBR may follow a distinct mechanism compared to a classic EMT. Thus, I wanted to investigate whether during FBR apicobasal polarity is lost similar to EMT. Using the same approach applied in third instar larva, fat body tissues were dissected from 3hr APF pupa, early during FBR and stained for several polarity proteins (aPKC, Par-3, Par-6, Crumbs, Dlg, and Lgl). My results showed that key polarity proteins (aPKC, Par-6, Par-3, Crumbs, Dlg, and Lgl) are lost by 3hr APF, early during FBR, well before complete tissue dissociation. This shows that similar to EMT, early during FBR, FBCs lose apicobasal polarity which leads to FBCs detachment.

8.2 Fat body remodeling

Similar to EMT, FBR involves the degradation of both cell-cell adhesion proteins and cell-basement membrane components. This degradation is facilitated by MMPs, where MMP1 is thought to cleave E-Cadherin-mediated cell-cell adhesion, while MMP2 cleaves cell-BM interactions, enabling the fat body cells to undergo complete dissociation during FBR (Jia et al., 2014). While previous studies have looked at FBR and changes in cell morphology by dissecting the fat body out of the animal at different timepoints, no one has managed to image the process live. This is because dissecting pupa from its opaque pupal case to allow imaging around 0-13 hours APF is not possible, as attempting to peel the soft pupal case would wound the animal. Live imaging would be crucial to observe detailed morphological changes that take place in the wild type condition. Thus, in this study I decided to try several approaches.

I initially tried to delay FBR by 10 hours to be able to image the entire process of FBR live. However, my results revealed that only a few pupae have successfully delayed FBR. Although this approach could have been successful in imaging the second half of FBR, a major drawback is that it relies on artificially delaying a developmental process which could result in negative side effects. For instance, delaying FBR might affect other tissues within the animal especially that the fat body is a multifunctional tissue that plays a role in energy storage, immune response and acts as a nutritional sensor. Moreover, the fat body regulates energy balance by releasing lipids, carbohydrates and glycogen in response to developmental cues and environmental conditions, thus delaying FBR may impact the function of other tissues or physiological processes such as growth and development (Yongmei Xi, 2015). In parallel, also tried two different *ex vivo* live imaging approaches. Both approaches were limiting since the fat body tissue tends to float in media. However, optimizing the second *ex vivo* approach adapted from the Mao lab, could yield

useful insights into the morphological changes that happen during FBR. Out of all the approaches tested, in my opinion, the *in vivo* live imaging approach was the most effective for studying FBR, as it preserved normal physiological conditions without altering Ecdysone signaling.

Given the limited number of publications that identified genes that regulate FBR, such as Ecdysone (Bond et al., 2011b) and MMPs (MMP1 and MMP2) (Jia et al., 2014), I aimed to uncover the molecular mechanisms driving this process. Through a screening assay, I tested several genes, including epithelial-to-mesenchymal transition (EMT) transcription factors such as Snail**,** Twist and Serpent. This is because EMT transcription factors are normally upregulated in human tumors (Nieto et al., 2016)**.** Moreover, EMT transcription factor, Serpent, has been previously shown to be required for EMT in *Drosophila* midgut (Campbell et al., 2018). In the *Drosophila* fly wing disc, Serpent expression induces loss of apicobasal polarity and impairs tissue organization. In this study I identified that Serpent acts key regulator for FBR. My results revealed that the phenotype of Serpent knockdown mimicked that of animals expressing EcR-DN, which was used as a positive control. Notably, Serpent knockdown impaired cell-cell dissociation during FBR, where FBCs remained closely attached to each other at 16hr APF when FBR is complete and FBCs are expected to be free floating in the hemolymph. Additionally, knocking down broad complex also resulted in no fat body cells in the head of the pupa at 16hr APF, where FBCs would normally be present in the head of the control, which may indicate that fat body cells might still be closely attached to each other. However, acquiring confocal images of FBCs in the dorsal thorax is essential to make a definitive conclusion. It is expected that knocking down broad complex would impair FBR, since broad complex is one of the early response genes where its transcription is induced by Ecdysone signaling (Delanoue et

al., 2010). Early response genes in turn dive the expression of late response genes that are required to regulate the biological responses that result from each Ecdysone pulse (Delanoue et al., 2010). On the other hand, knocking down other genes such as Snail, Twist and Pebble, resulted in the presence of FBCs in the head of the pupa at 16hr APF, similar to the control, suggesting that they are not involved in FBR.

Since Serpent and Ecdysone are now known to be required for cell-cell dissociation during FBR, I wanted to further explore their importance in the process of FBR. Because it is widely known that EMT transcription factors drive a loss of epithelial cell polarity, and I now found that the fat body tissue of wandering 3rd instar larvae is in fact polarized, I wanted to investigate whether blocking Ecdysone signaling or knocking down Serpent would impair loss of apicobasal polarity during FBR. To do this, I quantified the distribution of polarity proteins (Par-3=Baz, Dlg, and Crumbs) at 3hr APF, when polarity is normally lost in the control. I found that disrupting Ecdysone signaling and Serpent in the fat body impairs loss of polarity proteins early during FBR, since polarity proteins Dlg, Par-3, and Crumbs remained asymmetrically localized by 3hr APF, when polarity is normally lost in the control. Dlg remained highly concentrated on side b, while Par-3 and Crumbs were concentrated on the opposite side (side a).

Since Ecdysone signaling and Serpent are required for cell-cell detachment and loss of apicobasal polarity during FBR. I hypothesized that disrupting Ecdysone signaling and Serpent might also disrupt loss of CIVICs early during remodeling, since I previously showed that CIVICs are lost by 3hr APF, early during FBR. Quantification of the number of CIVICs indeed showed that both Ecdysone signaling and Serpent are required for loss of CIVICs early during FBR. In conclusion, Ecdysone signaling and Serpent are both required for loss of apicobasal polarity,

specifically (Dlg, Par-3 and Crumbs) thus leading to cell-cell dissociation and loss of CIVICs, early during FBR, similar to a previous study that reported loss of apicobasal polarity and junction disassembly upon ectopic expression of Serpent in *Drosophila* ectodermal cells (Campbell et al., 2011). While my findings in Chapter V suggest that cell-cell adhesion during FBR is primarily mediated by CIVICs rather than E-Cadherin, a previous study by Jia et al. (2014) reported E-Cadherin loss during FBR. This brings up a crucial question, which is if loss of E-Cadherin observed in Jia et al. (2014) is also regulated by Ecdysone signaling and Serpent, which could be tested by expressing E-Cadherin RNAi in the fat body and repeating the same experiment and quantifications used for Serpent RNAi. In conclusion, fat body remodeling represents a novel EMT-like process, where polarity loss drives the degradation of CIVICs, leading to cell-cell dissociation. A model of FBR is shown in Figure 8.2.

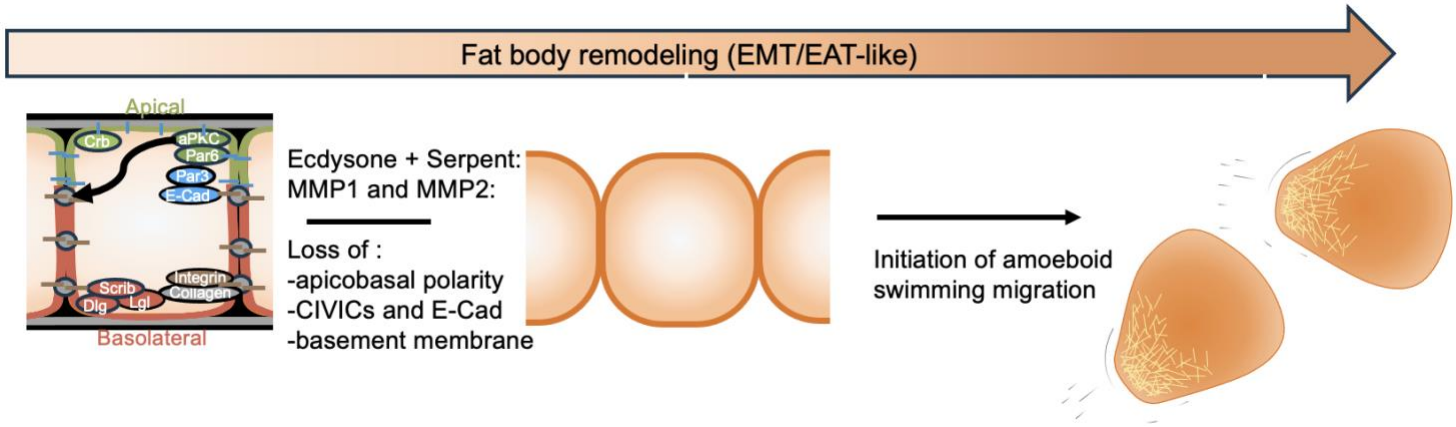

Figure 8.2: A model of the process of FBR (EMT/EAT-like model).

Overall, FBR is a useful, genetically tractable system to study tissue remodeling and potentially even EMT/EAT. It offers easy screening of genes, making it ideal to dissect the molecular mechanism driving FBR. Most importantly, this mechanism might be conserved in humans and could provide valuable insights into the process of tissue remodeling and EMT/EAT in health and disease.

References

Aguila, J. R., Suszko, J., Gibbs, A. G., & Hoshizaki, D. K. (2007). The role of larval fat cells in adult *Drosophila melanogaster*. *Journal of Experimental Biology*, *210*(6), 956–963. https://doi.org/10.1242/jeb.001586

Amălinei, C., Căruntu, I. D., & Bălan, R. A. (2007). Biology of metalloproteinases. *Romanian Journal of Morphology and Embryology = Revue Roumaine de Morphologie et Embryologie*, *48*(4), 323–334.

Ambrosi, D., Ben Amar, M., Cyron, C. J., DeSimone, A., Goriely, A., Humphrey, J. D., & Kuhl, E. (2019). Growth and remodelling of living tissues: perspectives, challenges and opportunities. *Journal of The Royal Society Interface*, *16*(157), 20190233. https://doi.org/10.1098/rsif.2019.0233

Baranwal, S., & Alahari, S. K. (2009). Molecular mechanisms controlling E-cadherin expression in breast cancer. *Biochemical and Biophysical Research Communications*, *384*(1), 6–11. https://doi.org/10.1016/j.bbrc.2009.04.051

Barrallo-Gimeno, A., & Nieto, M. A. (2005). The Snail genes as inducers of cell movement and survival: implications in development and cancer. *Development*, *132*(14), 3151–3161. https://doi.org/10.1242/dev.01907

Betschinger, J., Mechtler, K., & Knoblich, J. A. (2003). The Par complex directs asymmetric cell division by phosphorylating the cytoskeletal protein Lgl. *Nature*, *422*(6929), 326–330. https://doi.org/10.1038/nature01486

Bilder, D. (2004). Epithelial polarity and proliferation control: links from the *Drosophila* neoplastic tumor suppressors. *Genes & Development*, *18*(16), 1909–1925. https://doi.org/10.1101/gad.1211604

Bindhani, B., Maity, S., Chakrabarti, I., & Saha, S. K. (2022). Roles of matrix metalloproteinases in development, immunology, and ovulation in fruit Fly (*Drosophila*). *Archives of Insect Biochemistry and Physiology*, *109*(1). https://doi.org/10.1002/arch.21849

Bond, N. D., Nelliot, A., Bernardo, M. K., Ayerh, M. A., Gorski, K. A., Hoshizaki, D. K., & Woodard, C. T. (2011). ßFTZ-F1 and Matrix metalloproteinase 2 are required for fat-body remodeling in *Drosophila*. *Developmental Biology*, *360*(2), 286–296. https://doi.org/10.1016/j.ydbio.2011.09.015

Bonnans, C., Chou, J., & Werb, Z. (2014). Remodelling the extracellular matrix in development and disease. *Nature Reviews Molecular Cell Biology*, *15*(12). https://doi.org/10.1038/nrm3904

Booth, A., Magnuson, A., Fouts, J., & Foster, M. T. (2016). Adipose tissue: an endocrine organ playing a role in metabolic regulation. *Hormone Molecular Biology and Clinical Investigation*, *26*(1). https://doi.org/10.1515/hmbci-2015-0073

Bracken, C. P., Gregory, P. A., Kolesnikoff, N., Bert, A. G., Wang, J., Shannon, M. F., & Goodall, G. J. (2008). A Double-Negative Feedback Loop between ZEB1-SIP1 and the microRNA-200 Family Regulates Epithelial-Mesenchymal Transition. *Cancer Research*, *68*(19), 7846–7854. https://doi.org/10.1158/0008-5472.CAN-08-1942

Britton, J. S., Lockwood, W. K., Li, L., Cohen, S. M., & Edgar, B. A. (2002). Drosophila's Insulin/PI3-Kinase Pathway Coordinates Cellular Metabolism with Nutritional

Conditions. *Developmental Cell*, *2*(2), 239–249. https://doi.org/10.1016/S1534-5807(02)00117-X

Brown, N. H. (2000). Cell–cell adhesion via the ECM: integrin genetics in fly and worm. *Matrix Biology*, *19*(3), 191–201. https://doi.org/10.1016/S0945-053X(00)00064-0

Campbell, K. (2018). Contribution of epithelial-mesenchymal transitions to organogenesis and cancer metastasis. In *Current Opinion in Cell Biology* (Vol. 55, pp. 30–35). Elsevier Ltd. https://doi.org/10.1016/j.ceb.2018.06.008

Campbell, K., & Casanova, J. (2015). A role for E-cadherin in ensuring cohesive migration of a heterogeneous population of non-epithelial cells. *Nature Communications*, *6*(1), 7998. https://doi.org/10.1038/ncomms8998

Campbell, K., & Casanova, J. (2016). A common framework for EMT and collective cell migration. *Development*, *143*(23), 4291–4300. https://doi.org/10.1242/dev.139071

Campbell, K., Lebreton, G., Franch-Marro, X., & Casanova, J. (2018). Differential roles of the *Drosophila* EMT-inducing transcription factors Snail and Serpent in driving primary tumour growth. *PLOS Genetics*, *14*(2), e1007167. https://doi.org/10.1371/journal.pgen.1007167

Campbell, K., Whissell, G., Franch-Marro, X., Batlle, E., & Casanova, J. (2011). Specific GATA Factors Act as Conserved Inducers of an Endodermal-EMT. *Developmental Cell*, *21*(6), 1051–1061. https://doi.org/10.1016/j.devcel.2011.10.005

CANNON, B., & NEDERGAARD, J. (2004). Brown Adipose Tissue: Function and Physiological Significance. *Physiological Reviews*, *84*(1), 277–359. https://doi.org/10.1152/physrev.00015.2003

Chanson, L., Brownfield, D., Garbe, J. C., Kuhn, I., Stampfer, M. R., Bissell, M. J., & LaBarge, M. A. (2011). Self-organization is a dynamic and lineage-intrinsic property of mammary epithelial cells. *Proceedings of the National Academy of Sciences*, *108*(8), 3264–3269. https://doi.org/10.1073/pnas.1019556108

Chen, J., Sayadian, A.-C., Lowe, N., Lovegrove, H. E., & St Johnston, D. (2018). An alternative mode of epithelial polarity in the *Drosophila* midgut. *PLOS Biology*, *16*(10), e3000041. https://doi.org/10.1371/journal.pbio.3000041

Chiang, C., & Ayyanathan, K. (2013). Snail/Gfi-1 (SNAG) family zinc finger proteins in transcription regulation, chromatin dynamics, cell signaling, development, and disease. *Cytokine & Growth Factor Reviews*, *24*(2), 123–131. https://doi.org/10.1016/j.cytogfr.2012.09.002

Choy, L., & Derynck, R. (2003). Transforming Growth Factor-β Inhibits Adipocyte Differentiation by Smad3 Interacting with CCAAT/Enhancer-binding Protein (C/EBP) and Repressing C/EBP Transactivation Function. *Journal of Biological Chemistry*, *278*(11), 9609–9619. https://doi.org/10.1074/jbc.M212259200

Chuai, M., Hughes, D., & J. Weijer, C. (2012). Collective Epithelial and Mesenchymal Cell Migration During Gastrulation. *Current Genomics*, *13*(4), 267–277. https://doi.org/10.2174/138920212800793357

Coopman, P., & Djiane, A. (2016). Adherens Junction and E-Cadherin complex regulation by epithelial polarity. *Cellular and Molecular Life Sciences*, *73*(18), 3535–3553. https://doi.org/10.1007/s00018-016-2260-8

Cristancho, A. G., & Lazar, M. A. (2011). Forming functional fat: a growing understanding of adipocyte differentiation. *Nature Reviews Molecular Cell Biology*, *12*(11), 722–734. https://doi.org/10.1038/nrm3198

Cui, N., Hu, M., & Khalil, R. A. (2017). *Biochemical and Biological Attributes of Matrix Metalloproteinases* (pp. 1–73). https://doi.org/10.1016/bs.pmbts.2017.02.005

Dai, J., Ma, M., Feng, Z., & Pastor-Pareja, J. C. (2017). Inter-adipocyte Adhesion and Signaling by Collagen IV Intercellular Concentrations in *Drosophila*. *Current Biology*, *27*(18), 2729-2740.e4. https://doi.org/10.1016/j.cub.2017.08.002

Debnath, P., Huirem, R. S., Dutta, P., & Palchaudhuri, S. (2022). Epithelial–mesenchymal transition and its transcription factors. *Bioscience Reports*, *42*(1). https://doi.org/10.1042/BSR20211754

Delanoue, R., Slaidina, M., & Léopold, P. (2010). The Steroid Hormone Ecdysone Controls Systemic Growth by Repressing dMyc Function in *Drosophila* Fat Cells. *Developmental Cell*, *18*(6), 1012–1021. https://doi.org/10.1016/j.devcel.2010.05.007

Ding, X., Li, Z., Peng, K., Zou, R., Wu, C., Lin, G., Li, W., & Xue, L. (2022). Snail regulates Hippo signalling-mediated cell proliferation and tissue growth in *Drosophila*. *Open Biology*, *12*(3). https://doi.org/10.1098/rsob.210357

Dongre, A., & Weinberg, R. A. (2019). New insights into the mechanisms of epithelial–mesenchymal transition and implications for cancer. *Nature Reviews Molecular Cell Biology*, *20*(2), 69–84. https://doi.org/10.1038/s41580-018-0080-4

Ehrhardt, B., El-Merhie, N., Kovacevic, D., Schramm, J., Bossen, J., Roeder, T., & Krauss-Etschmann, S. (2022). Airway remodeling: The *Drosophila* model permits a

purely epithelial perspective. *Frontiers in Allergy*, *3*. https://doi.org/10.3389/falgy.2022.876673

Ellenbroek, S. I. J., Iden, S., & Collard, J. G. (2012). Cell polarity proteins and cancer. *Seminars in Cancer Biology*, *22*(3), 208–215. https://doi.org/10.1016/j.semcancer.2012.02.012

Fischer, K. R., Durrans, A., Lee, S., Sheng, J., Li, F., Wong, S. T. C., Choi, H., El Rayes, T., Ryu, S., Troeger, J., Schwabe, R. F., Vahdat, L. T., Altorki, N. K., Mittal, V., & Gao, D. (2015). Epithelial-to-mesenchymal transition is not required for lung metastasis but contributes to chemoresistance. *Nature*, *527*(7579), 472–476. https://doi.org/10.1038/nature15748

Frantz, C., Stewart, K. M., & Weaver, V. M. (2010). The extracellular matrix at a glance. *Journal of Cell Science*, *123*(24), 4195–4200. https://doi.org/10.1242/jcs.023820

Franz, A., Wood, W., & Martin, P. (2018). Fat Body Cells Are Motile and Actively Migrate to Wounds to Drive Repair and Prevent Infection. *Developmental Cell*, *44*(4). https://doi.org/10.1016/j.devcel.2018.01.026

Gibson, M. C., & Perrimon, N. (2003). Apicobasal polarization: epithelial form and function. *Current Opinion in Cell Biology*, *15*(6), 747–752. https://doi.org/10.1016/j.ceb.2003.10.008

Goldstein, B., & Macara, I. G. (2007). The PAR Proteins: Fundamental Players in Animal Cell Polarization. *Developmental Cell*, *13*(5), 609–622. https://doi.org/10.1016/j.devcel.2007.10.007

Grau, Y., Carteret, C., & Simpson, P. (1984). MUTATIONS AND CHROMOSOMAL REARRANGEMENTS AFFECTING THE EXPRESSION OF SNAIL, A GENE

INVOLVED IN EMBRYONIC PATTERNING IN *DROSOPHILA MELANOGASTER*. *Genetics*, *108*(2), 347–360. https://doi.org/10.1093/genetics/108.2.347

Graziani, V., Rodriguez-Hernandez, I., Maiques, O., & Sanz-Moreno, V. (2022). The amoeboid state as part of the epithelial-to-mesenchymal transition programme. *Trends in Cell Biology*, *32*(3), 228–242. https://doi.org/10.1016/j.tcb.2021.10.004

Harris, T. J. C., & Peifer, M. (2004). Adherens junction-dependent and -independent steps in the establishment of epithelial cell polarity in *Drosophila*. *The Journal of Cell Biology*, *167*(1), 135–147. https://doi.org/10.1083/jcb.200406024

Harris, T. J. C., & Peifer, M. (2005). The positioning and segregation of apical cues during epithelial polarity establishment in *Drosophila*. *The Journal of Cell Biology*, *170*(5), 813–823. https://doi.org/10.1083/jcb.200505127

Harris, T. J. C., & Peifer, M. (2007). aPKC Controls Microtubule Organization to Balance Adherens Junction Symmetry and Planar Polarity during Development. *Developmental Cell*, *12*(5), 727–738. https://doi.org/10.1016/j.devcel.2007.02.011

Hartenstein, V., & Jan, Y. N. (1992). Studying *Drosophila* embryogenesis with P-lacZ enhancer trap lines. *Roux's Archives of Developmental Biology*, *201*(4), 194–220. https://doi.org/10.1007/BF00188752

Herboso, L., Oliveira, M. M., Talamillo, A., Pérez, C., González, M., Martín, D., Sutherland, J. D., Shingleton, A. W., Mirth, C. K., & Barrio, R. (2015). Ecdysone promotes growth of imaginal discs through the regulation of Thor in D. melanogaster. *Scientific Reports*, *5*(1), 12383. https://doi.org/10.1038/srep12383

Hong, Y., Stronach, B., Perrimon, N., Jan, L. Y., & Jan, Y. N. (2001). *Drosophila* Stardust interacts with Crumbs to control polarity of epithelia but not neuroblasts. *Nature*, *414*(6864), 634–638. https://doi.org/10.1038/414634a

Horikoshi, Y., Suzuki, A., Yamanaka, T., Sasaki, K., Mizuno, K., Sawada, H., Yonemura, S., & Ohno, S. (2009). Interaction between PAR-3 and the aPKC–PAR-6 complex is indispensable for apical domain development of epithelial cells. *Journal of Cell Science*, *122*(10), 1595–1606. https://doi.org/10.1242/jcs.043174

Huang, H., Potter, C. J., Tao, W., Li, D.-M., Brogiolo, W., Hafen, E., Sun, H., & Xu, T. (1999). PTEN affects cell size, cell proliferation and apoptosis during *Drosophila* eye development. *Development*, *126*(23), 5365–5372. https://doi.org/10.1242/dev.126.23.5365

Huang, J., Zhang, L., Wan, D., Zhou, L., Zheng, S., Lin, S., & Qiao, Y. (2021). Extracellular matrix and its therapeutic potential for cancer treatment. *Signal Transduction and Targeted Therapy*, *6*(1), 153. https://doi.org/10.1038/s41392-021-00544-0

Hugo, H., Ackland, M. L., Blick, T., Lawrence, M. G., Clements, J. A., Williams, E. D., & Thompson, E. W. (2007). Epithelial—mesenchymal and mesenchymal—epithelial transitions in carcinoma progression. *Journal of Cellular Physiology*, *213*(2), 374–383. https://doi.org/10.1002/jcp.21223

Hutterer, A., Betschinger, J., Petronczki, M., & Knoblich, J. A. (2004). Sequential Roles of Cdc42, Par-6, aPKC, and Lgl in the Establishment of Epithelial Polarity during *Drosophila* Embryogenesis. *Developmental Cell*, *6*(6), 845–854. https://doi.org/10.1016/j.devcel.2004.05.003

Isabella, A. J., & Horne-Badovinac, S. (2015). *Building from the Ground up* (pp. 305–336). https://doi.org/10.1016/bs.ctm.2015.07.001

Isabella, A. J., & Horne-Badovinac, S. (2016). Rab10-Mediated Secretion Synergizes with Tissue Movement to Build a Polarized Basement Membrane Architecture for Organ Morphogenesis. *Developmental Cell*, *38*(1), 47–60. https://doi.org/10.1016/j.devcel.2016.06.009

Ishimoto, H., Sakai, T., & Kitamoto, T. (2009). Ecdysone signaling regulates the formation of long-term courtship memory in adult *Drosophila melanogaster*. *Proceedings of the National Academy of Sciences*, *106*(15), 6381–6386. https://doi.org/10.1073/pnas.0810213106

Jia, Q., Liu, Y., Liu, H., & Li, S. (2014). Mmp1 and Mmp2 cooperatively induce *Drosophila* fat body cell dissociation with distinct roles. *Scientific Reports*, *4*. https://doi.org/10.1038/srep07535

Johnson, M. B., & Butterworth, F. M. (1985). Maturation and aging of adult fat body and oenocytes in *Drosophila* as revealed by light microscopic morphometry. *Journal of Morphology*, *184*(1), 51–59. https://doi.org/10.1002/jmor.1051840106

Kalluri, R., & Weinberg, R. A. (2009). The basics of epithelial-mesenchymal transition. *Journal of Clinical Investigation*, *119*(6), 1420–1428. https://doi.org/10.1172/JCI39104

Karylowski, O., Zeigerer, A., Cohen, A., & McGraw, T. E. (2004). GLUT4 Is Retained by an Intracellular Cycle of Vesicle Formation and Fusion with Endosomes. *Molecular Biology of the Cell*, *15*(2), 870–882. https://doi.org/10.1091/mbc.e03-07-0517

Kemphues, K. J., Priess, J. R., Morton, D. G., & Cheng, N. (1988). Identification of genes required for cytoplasmic localization in early C. elegans embryos. *Cell*, *52*(3), 311–320. https://doi.org/10.1016/S0092-8674(88)80024-2

Kershaw, E. E., & Flier, J. S. (2004). Adipose Tissue as an Endocrine Organ. *The Journal of Clinical Endocrinology & Metabolism*, *89*(6), 2548–2556. https://doi.org/10.1210/jc.2004-0395

Kiger, J. A., Natzle, J. E., Kimbrell, D. A., Paddy, M. R., Kleinhesselink, K., & Green, M. M. (2007). Tissue remodeling during maturation of the *Drosophila* wing. *Developmental Biology*, *301*(1), 178–191. https://doi.org/10.1016/j.ydbio.2006.08.011

Krahn, M. P., Bückers, J., Kastrup, L., & Wodarz, A. (2010). Formation of a Bazooka–Stardust complex is essential for plasma membrane polarity in epithelia. *Journal of Cell Biology*, *190*(5), 751–760. https://doi.org/10.1083/jcb.201006029

Kuchinke, U., Grawe, F., & Knust, E. (1998). Control of spindle orientation in *Drosophila* by the Par-3-related PDZ-domain protein Bazooka. *Current Biology*, *8*(25), 1357–1365. https://doi.org/10.1016/S0960-9822(98)00016-5

LaBarge, M. A., Nelson, C. M., Villadsen, R., Fridriksdottir, A., Ruth, J. R., Stampfer, M. R., Petersen, O. W., & Bissell, M. J. (2009). Human mammary progenitor cell fate decisions are products of interactions with combinatorial microenvironments. *Integr. Biol.*, *1*(1), 70–79. https://doi.org/10.1039/B816472J

Leevers, S. J., Weinkove, D., MacDougall, L. K., Hafen, E., & Waterfield, M. D. (1996). The *Drosophila* phosphoinositide 3-kinase Dp110 promotes cell growth. *The EMBO Journal*, *15*(23), 6584–6594.

Leptin, M. (1991). twist and snail as positive and negative regulators during *Drosophila* mesoderm development. *Genes & Development*, *5*(9), 1568–1576. https://doi.org/10.1101/gad.5.9.1568

Lim, J., & Thiery, J. P. (2011). Alternative Path to EMT: Regulation of Apicobasal Polarity in *Drosophila*. *Developmental Cell*, *21*(6), 983–984. https://doi.org/10.1016/j.devcel.2011.11.017

Lin, B., Luo, J., & Lehmann, R. (2021). *A phosphoregulated RhoGEF feedback loop tunes cortical flow driven amoeboid migration* in vivo. https://doi.org/10.1101/2021.10.29.466358

Liu, Z., & Huang, X. (2013). Lipid metabolism in <italic>*Drosophila*</italic>: development and disease. *Acta Biochimica et Biophysica Sinica*, *45*(1), 44–50. https://doi.org/10.1093/abbs/gms105

Llano, E., Adam, G., Pendás, A. M., Quesada, V., Sánchez, L. M., Santamaría, I., Noselli, S., & López-Otín, C. (2002). Structural and Enzymatic Characterization of *Drosophila* Dm2-MMP, a Membrane-bound Matrix Metalloproteinase with Tissue-specific Expression. *Journal of Biological Chemistry*, *277*(26), 23321–23329. https://doi.org/10.1074/jbc.M200121200

Lorentzen, A., Bamber, J., Sadok, A., Elson-Schwab, I., & Marshall, C. J. (2011). An ezrin-rich, rigid uropod-like structure directs movement of amoeboid blebbing cells. *Journal of Cell Science*, *124*(8), 1256–1267. https://doi.org/10.1242/jcs.074849

Lu, P., Takai, K., Weaver, V. M., & Werb, Z. (2011). Extracellular Matrix Degradation and Remodeling in Development and Disease. *Cold Spring Harbor Perspectives in Biology*, *3*(12), a005058–a005058. https://doi.org/10.1101/cshperspect.a005058

Lu, P., Weaver, V. M., & Werb, Z. (2012). The extracellular matrix: A dynamic niche in cancer progression. *Journal of Cell Biology*, *196*(4), 395–406. https://doi.org/10.1083/jcb.201102147

Lumeng, C. N., & Saltiel, A. R. (2011). Inflammatory links between obesity and metabolic disease. *Journal of Clinical Investigation*, *121*(6), 2111–2117. https://doi.org/10.1172/JCI57132

Marchetti, M., Fanti, L., Berloco, M., & Pimpinelli, S. (2003). Differential expression of the *Drosophila* BX-C in polytene chromosomes in cells of larval fat bodies: a cytological approach to identifying *in vivo* targets of the homeotic Ubx, Abd-A and Abd-B proteins. *Development*, *130*(16), 3683–3689. https://doi.org/10.1242/dev.00587

Mavrakis, M., Rikhy, R., & Lippincott-Schwartz, J. (2009). Plasma Membrane Polarity and Compartmentalization Are Established before Cellularization in the Fly Embryo. *Developmental Cell*, *16*(1), 93–104. https://doi.org/10.1016/j.devcel.2008.11.003

McGill, M. A., McKinley, R. F. A., & Harris, T. J. C. (2009). Independent cadherin–catenin and Bazooka clusters interact to assemble adherens junctions. *Journal of Cell Biology*, *185*(5), 787–796. https://doi.org/10.1083/jcb.200812146

Morais-de-Sá, E., Mirouse, V., & St Johnston, D. (2010). aPKC Phosphorylation of Bazooka Defines the Apical/Lateral Border in *Drosophila* Epithelial Cells. *Cell*, *141*(3), 509–523. https://doi.org/10.1016/j.cell.2010.02.040

Muqbil, I., Wu, J., Aboukameel, A., Mohammad, R. M., & Azmi, A. S. (2014). Snail nuclear transport: The gateways regulating epithelial-to-mesenchymal transition? *Seminars in Cancer Biology*, *27*, 39–45. https://doi.org/10.1016/j.semcancer.2014.06.003

Nelliot, A., Bond, N., & Hoshizaki, D. K. (2006). Fat-body remodeling in *Drosophila* melanogaster. *Genesis*, *44*(8), 396–400. https://doi.org/10.1002/dvg.20229

Nelson, W. J. (2003). Adaptation of core mechanisms to generate cell polarity. *Nature*, *422*(6933), 766–774. https://doi.org/10.1038/nature01602

Nieto, M. A. (2009). Epithelial-Mesenchymal Transitions in development and disease: old views and new perspectives. *The International Journal of Developmental Biology*, *53*(8-9–10), 1541–1547. https://doi.org/10.1387/ijdb.072410mn

Nieto, M. A., Huang, R. Y.-J., Jackson, R. A., & Thiery, J. P. (2016). EMT: 2016. *Cell*, *166*(1), 21–45. https://doi.org/10.1016/j.cell.2016.06.028

Nistico, P., Bissell, M. J., & Radisky, D. C. (2012). Epithelial-Mesenchymal Transition: General Principles and Pathological Relevance with Special Emphasis on the Role of Matrix Metalloproteinases. *Cold Spring Harbor Perspectives in Biology*, *4*(2), a011908–a011908. https://doi.org/10.1101/cshperspect.a011908

Oda, H., Tsukita, S., & Takeichi, M. (1998). Dynamic Behavior of the Cadherin-Based Cell–Cell Adhesion System during*Drosophila*Gastrulation. *Developmental Biology*, *203*(2), 435–450. https://doi.org/10.1006/dbio.1998.9047

Page-McCaw, A., Serano, J., Santé, J. M., & Rubin, G. M. (2003). *Drosophila* Matrix Metalloproteinases Are Required for Tissue Remodeling, but Not Embryonic Development. *Developmental Cell*, *4*(1), 95–106. https://doi.org/10.1016/S1534-5807(02)00400-8

Paniagua, A. E., Segurado, A., Dolón, J. F., Esteve-Rudd, J., Velasco, A., Williams, D. S., & Lillo, C. (2021). Key Role for CRB2 in the Maintenance of Apicobasal Polarity in Retinal Pigment Epithelial Cells. *Frontiers in Cell and Developmental Biology*, *9*. https://doi.org/10.3389/fcell.2021.701853

Parra-Peralbo, E., Talamillo, A., & Barrio, R. (2021). Origin and Development of the Adipose Tissue, a Key Organ in Physiology and Disease. *Frontiers in Cell and Developmental Biology*, *9*. https://doi.org/10.3389/fcell.2021.786129

Pasquier, N., Jaulin, F., & Peglion, F. (2024). Inverted apicobasal polarity in health and disease. *Journal of Cell Science*, *137*(5). https://doi.org/10.1242/jcs.261659

Pastor-Pareja, J. C., & Xu, T. (2011). Shaping Cells and Organs in *Drosophila* by Opposing Roles of Fat Body-Secreted Collagen IV and Perlecan. *Developmental Cell*, *21*(2), 245–256. https://doi.org/10.1016/j.devcel.2011.06.026

Pellikka, M., Tanentzapf, G., Pinto, M., Smith, C., McGlade, C. J., Ready, D. F., & Tepass, U. (2002). Crumbs, the *Drosophila* homologue of human CRB1/RP12, is essential for photoreceptor morphogenesis. *Nature*, *416*(6877), 143–149. https://doi.org/10.1038/nature721

Perez-Moreno, M., & Fuchs, E. (2006). Catenins: Keeping Cells from Getting Their Signals Crossed. *Developmental Cell*, *11*(5), 601–612. https://doi.org/10.1016/j.devcel.2006.10.010

Pinet, K., & McLaughlin, K. A. (2019). Mechanisms of physiological tissue remodeling in animals: Manipulating tissue, organ, and organism morphology. *Developmental Biology*, *451*(2). https://doi.org/10.1016/j.ydbio.2019.04.001

Ramos-Lewis, W., & Page-McCaw, A. (2019). Basement membrane mechanics shape development: Lessons from the fly. *Matrix Biology*, *75–76*, 72–81. https://doi.org/10.1016/j.matbio.2018.04.004

Raza, Q. S., Vanderploeg, J. L., & Jacobs, J. R. (2017). Matrix Metalloproteinases are required for membrane motility and lumenogenesis during *Drosophila* heart development. *PLOS ONE*, *12*(2), e0171905. https://doi.org/10.1371/journal.pone.0171905

Rehorn, K.-P., Thelen, H., Michelson, A. M., & Reuter, R. (1996). A molecular aspect of hematopoiesis and endoderm development common to vertebrates and *Drosophila*. *Development*, *122*(12), 4023–4031. https://doi.org/10.1242/dev.122.12.4023

Rembold, M., Ciglar, L., Yáñez-Cuna, J. O., Zinzen, R. P., Girardot, C., Jain, A., Welte, M. A., Stark, A., Leptin, M., & Furlong, E. E. M. (2014). A conserved role for Snail as a potentiator of active transcription. *Genes & Development*, *28*(2), 167–181. https://doi.org/10.1101/gad.230953.113

Reuter, R., & Leptin, M. (1994). Interacting functions of *snail, twist* and *huckebein* during the early development of germ layers in *Drosophila*. *Development*, *120*(5), 1137–1150. https://doi.org/10.1242/dev.120.5.1137

Ribatti, D., Tamma, R., & Annese, T. (2020). Epithelial-Mesenchymal Transition in Cancer: A Historical Overview. *Translational Oncology*, *13*(6), 100773. https://doi.org/10.1016/j.tranon.2020.100773

Richardson, E. C. N., & Pichaud, F. (2010). Crumbs is required to achieve proper organ size control during *Drosophila* head development. *Development*, *137*(4), 641–650. https://doi.org/10.1242/dev.041913

Rosen, E. D., & Spiegelman, B. M. (2006). Adipocytes as regulators of energy balance and glucose homeostasis. *Nature*, *444*(7121), 847–853. https://doi.org/10.1038/nature05483

Ruprecht, V., Wieser, S., Callan-Jones, A., Smutny, M., Morita, H., Sako, K., Barone, V., Ritsch-Marte, M., Sixt, M., Voituriez, R., & Heisenberg, C.-P. (2015). Cortical Contractility Triggers a Stochastic Switch to Fast Amoeboid Cell Motility. *Cell*, *160*(4), 673–685. https://doi.org/10.1016/j.cell.2015.01.008

Saitoh, M. (2018). Involvement of partial EMT in cancer progression. *The Journal of Biochemistry*, *164*(4), 257–264. https://doi.org/10.1093/jb/mvy047

Sam, S., Leise, W., & Keiko Hoshizaki, D. (1996). The serpent gene is necessary for progression through the early stages of fat-body development. *Mechanisms of Development*, *60*(2), 197–205. https://doi.org/10.1016/S0925-4773(96)00615-6

Sandmann, T., Girardot, C., Brehme, M., Tongprasit, W., Stolc, V., & Furlong, E. E. M. (2007). A core transcriptional network for early mesoderm development in *Drosophila melanogaster*. *Genes & Development*, *21*(4), 436–449. https://doi.org/10.1101/gad.1509007

Schindelin, J., Arganda-Carreras, I., Frise, E., Kaynig, V., Longair, M., Pietzsch, T., Preibisch, S., Rueden, C., Saalfeld, S., Schmid, B., Tinevez, J.-Y., White, D. J., Hartenstein, V., Eliceiri, K., Tomancak, P., & Cardona, A. (2012). Fiji: an open-source platform for biological-image analysis. *Nature Methods*, *9*(7), 676–682. https://doi.org/10.1038/nmeth.2019

Schmidt, A., & Peifer, M. (2020). Scribble and Dlg organize a protection racket to ensure apical–basal polarity. *Proceedings of the National Academy of Sciences*, *117*(24), 13188–13190. https://doi.org/10.1073/pnas.2007739117

Seifert, J. R. K., & Lehmann, R. (2012). *Drosophila* primordial germ cell migration requires epithelial remodeling of the endoderm. *Development*, *139*(12), 2101–2106. https://doi.org/10.1242/dev.078949

Sharifkhodaei, Z., Padash-Barmchi, M., Gilbert, M. M., Samarasekera, G., Fulga, T. A., Van Vactor, D., & Auld, V. J. (2016). The *Drosophila* tricellular junction protein Gliotactin regulates its own mRNA levels through BMP-mediated induction of miR-184. *Journal of Cell Science*, *129*(7), 1477–1489. https://doi.org/10.1242/jcs.178608

Shin, K., Fogg, V. C., & Margolis, B. (2006). Tight Junctions and Cell Polarity. *Annual Review of Cell and Developmental Biology*, *22*(1), 207–235. https://doi.org/10.1146/annurev.cellbio.22.010305.104219

Simpson, P. (1983). MATERNAL-ZYGOTIC GENE INTERACTIONS DURING FORMATION OF THE DORSOVENTRAL PATTERN IN DROSOPHILA EMBRYOS. *Genetics*, *105*(3), 615–632. https://doi.org/10.1093/genetics/105.3.615

Smallhorn, M., Murray, M. J., & Saint, R. (2004). The epithelial-mesenchymal transition of the *Drosophila* mesoderm requires the Rho GTP exchange factor Pebble. *Development*, *131*(11), 2641–2651. https://doi.org/10.1242/dev.01150

Soo, K., O'Rourke, M. P., Khoo, P.-L., Steiner, K. A., Wong, N., Behringer, R. R., & Tam, P. P. L. (2002). Twist Function Is Required for the Morphogenesis of the Cephalic Neural Tube and the Differentiation of the Cranial Neural Crest Cells in the Mouse Embryo. *Developmental Biology*, *247*(2), 251–270. https://doi.org/10.1006/dbio.2002.0699

Spokony, R. F., & Restifo, L. L. (2007). Anciently duplicated Broad Complex exons have distinct temporal functions during tissue morphogenesis. *Development Genes and Evolution*, *217*(7), 499–513. https://doi.org/10.1007/s00427-007-0159-y

St Johnston, D., & Ahringer, J. (2010). Cell Polarity in Eggs and Epithelia: Parallels and Diversity. *Cell*, *141*(5), 757–774. https://doi.org/10.1016/j.cell.2010.05.011

Stevens, L. J., & Page-McCaw, A. (2012). A secreted MMP is required for reepithelialization during wound healing. *Molecular Biology of the Cell*, *23*(6), 1068–1079. https://doi.org/10.1091/mbc.e11-09-0745

Suzuki, A., & Ohno, S. (2006). The PAR-aPKC system: lessons in polarity. *Journal of Cell Science*, *119*(6), 979–987. https://doi.org/10.1242/jcs.02898

Tal Rousso, Annette M Shewan, Keith E Mostov, Eyal D Schejter, & Ben-Zion Shilo. (2013). Apical targeting of the forming Diaphanous in *Drosophila* tubular epithelia. *Cell Biology Developmental Biology*. https://doi.org/10.7554/eLife.00666.001

Tanentzapf, G., & Tepass, U. (2003). Interactions between the crumbs, lethal giant larvae and bazooka pathways in epithelial polarization. *Nature Cell Biology*, *5*(1), 46–52. https://doi.org/10.1038/ncb896

Tang, Y., Feinberg, T., Keller, E. T., Li, X.-Y., & Weiss, S. J. (2016). Snail/Slug binding interactions with YAP/TAZ control skeletal stem cell self-renewal and differentiation. *Nature Cell Biology*, *18*(9), 917–929. https://doi.org/10.1038/ncb3394

Tepass, U. (1997). Epithelial differentiation in *Drosophila*. *BioEssays*, *19*(8), 673–682. https://doi.org/10.1002/bies.950190807

Tepass, U., & Hartenstein, V. (1994). Epithelium formation in the *Drosophila* midgut depends on the interaction of endoderm and mesoderm. *Development*, *120*(3), 579–590. https://doi.org/10.1242/dev.120.3.579

Tepass, U., & Hartenstein, V. (1994). The Development of Cellular Junctions in the *Drosophila* Embryo. *Developmental Biology*, *161*(2), 563–596. https://doi.org/10.1006/dbio.1994.1054

Tepaß, U., & Knust, E. (1990). Phenotypic and developmental analysis of mutations at thecrumbs locus, a gene required for the development of epithelia in*Drosophila* melanogaster. *Roux's Archives of Developmental Biology*, *199*(4), 189–206. https://doi.org/10.1007/BF01682078

Tepass, U., Tanentzapf, G., Ward, R., & Fehon, R. (2001). Epithelial Cell Polarity and Cell Junctions in *Drosophila*. *Annual Review of Genetics*, *35*(1), 747–784. https://doi.org/10.1146/annurev.genet.35.102401.091415

Tepass, U., Theres, C., & Knust, E. (1990). crumbs encodes an EGF-like protein expressed on apical membranes of *Drosophila* epithelial cells and required for organization of epithelia. *Cell*, *61*(5), 787–799. https://doi.org/10.1016/0092-8674(90)90189-L

Thiery, J. P., Acloque, H., Huang, R. Y. J., & Nieto, M. A. (2009). Epithelial-Mesenchymal Transitions in Development and Disease. *Cell*, *139*(5), 871–890. https://doi.org/10.1016/j.cell.2009.11.007

Thompson, L., Chang, B., & Barsky, S. (1996). Monoclonal Origins of Malignant Mixed Tumors (Carcinosarcomas) Evidence for a Divergent Histogenesis. *The American Journal of Surgical Pathology*, *20*(3), 277–285.

Tracy, E., Rowe, G., & LeBlanc, A. J. (2020). Cardiac tissue remodeling in healthy aging: the road to pathology. *American Journal of Physiology-Cell Physiology*, *319*(1), C166–C182. https://doi.org/10.1152/ajpcell.00021.2020

Tsai, J. H., & Yang, J. (2013). Epithelial–mesenchymal plasticity in carcinoma metastasis. *Genes & Development*, *27*(20), 2192–2206. https://doi.org/10.1101/gad.225334.113

Vandewalle, C. (2005). SIP1/ZEB2 induces EMT by repressing genes of different epithelial cell-cell junctions. *Nucleic Acids Research*, *33*(20), 6566–6578. https://doi.org/10.1093/nar/gki965

Vandewalle, C., Van Roy, F., & Berx, G. (2009). The role of the ZEB family of transcription factors in development and disease. *Cellular and Molecular Life Sciences*, *66*(5), 773–787. https://doi.org/10.1007/s00018-008-8465-8

Vasquez, C. G., de la Serna, E. L., & Dunn, A. R. (2021). How cells tell up from down and stick together to construct multicellular tissues – interplay between apicobasal polarity and cell–cell adhesion. *Journal of Cell Science*, *134*(21). https://doi.org/10.1242/jcs.248757

Vega, S., Morales, A. V., Ocaña, O. H., Valdés, F., Fabregat, I., & Nieto, M. A. (2004). Snail blocks the cell cycle and confers resistance to cell death. *Genes & Development*, *18*(10), 1131–1143. https://doi.org/10.1101/gad.294104

Verma, R. P., & Hansch, C. (2007). Matrix metalloproteinases (MMPs): Chemical–biological functions and (Q)SARs. *Bioorganic & Medicinal Chemistry*, *15*(6), 2223–2268. https://doi.org/10.1016/j.bmc.2007.01.011

Verma, S. K., Nagashima, K., Yaligar, J., Michael, N., Lee, S. S., Xianfeng, T., Gopalan, V., Sadananthan, S. A., Anantharaj, R., & Velan, S. S. (2017). Differentiating brown and white adipose tissues by high-resolution diffusion NMR spectroscopy. *Journal of Lipid Research*, *58*(1), 289–298. https://doi.org/10.1194/jlr.D072298

Wickman, G. R., Julian, L., Mardilovich, K., Schumacher, S., Munro, J., Rath, N., Zander, S. AL, Mleczak, A., Sumpton, D., Morrice, N., Bienvenut, W. V, & Olson, M. F. (2013). Blebs produced by actin–myosin contraction during apoptosis release damage-associated molecular pattern proteins before secondary necrosis occurs. *Cell Death & Differentiation*, *20*(10), 1293–1305. https://doi.org/10.1038/cdd.2013.69

Woichansky, I., Beretta, C. A., Berns, N., & Riechmann, V. (2016). Three mechanisms control E-cadherin localization to the zonula adherens. *Nature Communications*, *7*(1), 10834. https://doi.org/10.1038/ncomms10834

Woods, D. F., & Bryant, P. J. (1991). The discs-large tumor suppressor gene of *Drosophila* encodes a guanylate kinase homolog localized at septate junctions. *Cell*, *66*(3), 451–464. https://doi.org/10.1016/0092-8674(81)90009-X

Wu, C., Li, Z., Ding, X., Guo, X., Sun, Y., Wang, X., Hu, Y., Li, T., La, X., Li, J., Li, J., Li, W., & Xue, L. (2019). Snail modulates JNK-mediated cell death in *Drosophila*. *Cell Death & Disease*, *10*(12), 893. https://doi.org/10.1038/s41419-019-2135-7

Wu, J., Jiang, J., Chen, B., Wang, K., Tang, Y., & Liang, X. (2021). Plasticity of cancer cell invasion: Patterns and mechanisms. *Translational Oncology*, *14*(1), 100899. https://doi.org/10.1016/j.tranon.2020.100899

Yang, J., Antin, P., Berx, G., Blanpain, C., Brabletz, T., Bronner, M., Campbell, K., Cano, A., Casanova, J., Christofori, G., Dedhar, S., Derynck, R., Ford, H. L., Fuxe, J., García de Herreros, A., Goodall, G. J., Hadjantonakis, A.-K., Huang, R. Y. J., Kalcheim, C., … Sheng, G. (2020). Guidelines and definitions for research on epithelial–mesenchymal transition. *Nature Reviews Molecular Cell Biology*, *21*(6), 341–352. https://doi.org/10.1038/s41580-020-0237-9

Yang, J., Mani, S. A., & Weinberg, R. A. (2006). Exploring a New Twist on Tumor Metastasis. *Cancer Research*, *66*(9), 4549–4552. https://doi.org/10.1158/0008-5472.CAN-05-3850

Yongmei Xi, Y. Z. (2015). Fat Body Development and its Function in Energy Storage and Nutrient Sensing in *Drosophila* melanogaster. *Journal of Tissue Science & Engineering*, *06*(01). https://doi.org/10.4172/2157-7552.1000141

Zajac, A. L., & Horne-Badovinac, S. (2022). Kinesin-directed secretion of basement membrane proteins to a subdomain of the basolateral surface in *Drosophila*

epithelial cells. *Current Biology*, *32*(4), 735-748.e10. https://doi.org/10.1016/j.cub.2021.12.025

Zeigerer, A., Lampson, M. A., Karylowski, O., Sabatini, D. D., Adesnik, M., Ren, M., & McGraw, T. E. (2002). GLUT4 Retention in Adipocytes Requires Two Intracellular Insulin-regulated Transport Steps. *Molecular Biology of the Cell*, *13*(7), 2421–2435. https://doi.org/10.1091/mbc.e02-02-0071

Zeng, J., Huynh, N., Phelps, B., & King-Jones, K. (2020). Snail synchronizes endocycling in a TOR-dependent manner to coordinate entry and escape from endoreplication pausing during the *Drosophila* critical weight checkpoint. *PLOS Biology*, *18*(2), e3000609. https://doi.org/10.1371/journal.pbio.3000609

Zhang, Y., & Weinberg, R. A. (2018). Epithelial-to-mesenchymal transition in cancer: complexity and opportunities. *Frontiers of Medicine*, *12*(4), 361–373. https://doi.org/10.1007/s11684-018-0656-6

Zheng, H., Wang, X., Guo, P., Ge, W., Yan, Q., Gao, W., Xi, Y., & Yang, X. (2017). Premature remodeling of fat body and fat mobilization triggered by platelet-derived growth factor/VEGF receptor in *Drosophila*. *The FASEB Journal*, *31*(5), 1964–1975. https://doi.org/10.1096/fj.201601127R

Zheng, X., Carstens, J. L., Kim, J., Scheible, M., Kaye, J., Sugimoto, H., Wu, C.-C., LeBleu, V. S., & Kalluri, R. (2015). Epithelial-to-mesenchymal transition is dispensable for metastasis but induces chemoresistance in pancreatic cancer. *Nature*, *527*(7579), 525–530. https://doi.org/10.1038/nature16064